IMPI's 53rd Annual Microwave Power Symposium (IMPI 53)

2019 PROCEEDINGS

June 18-20, 2019

Caesars Palace
Las Vegas, Nevada, USA

ISSN 1070-0129

Presented by the
International Microwave Power Institute
PO Box 1140, Mechanicsville, VA 23111
Phone: +1 (804) 559 6667 • Email: info@impi.org
www.impi.org

Welcome to Las Vegas for the 53rd IMPI Symposium

Each year, IMPI brings together researchers from across the globe to share the latest findings in microwave and RF heating theories and applications, and this year we have an outstanding array of researchers in attendance. If you are not yet a member of IMPI, we strongly encourage you to consider joining onsite. IMPI membership connects you to microwave and RF academia, researchers, developers and practitioners across the globe. Talk to an IMPI member today to learn more about the value of joining our outstanding organization!

Thank you for joining us. We hope you learn from the technical presentations, interact with your colleagues, and enjoy the atmosphere of the Symposium. And do take the opportunity to visit the many interesting sites in and around Las Vegas.

Special thanks to Shanghai Ocean University for sponsorsing the printed Proceedings:

IMPI wishes to express its gratitude to the following individuals:

TECHNICAL PROGRAM COMMITTEE

Chairmen

Graham Brodie, University of Melbourne, Australia
Roger Williams, 3D RF Energy Corp, USA

Members

Kostiantyn Achkasov, SAIREM, France
Raymond Boxman, Tel Aviv University, Israel
Sumeet Dhawan, Nestle, USA
John F. Gerling, Gerling Consulting Inc., USA
Klaus Werner, pinkRF, The Netherlands
Satoshi Horikoshi, Sophia University, Japan
Vadim V. Yakovlev, Worcester Polytechnic Institute, USA
Marilena Radoiu, RTI Health + Wellness Solutions, Canada
Kama Huang, Sichuan University, China

FOOD SCIENCE AND TECHNOLOGY COMMITTEE

Chairman

Ulrich Erle, Nestle R&D, USA

Members

Jean-Paul Bernard, SAIREM, France
Yang Jaio, Shanghai Ocean University, China
Marie Jirsa, Tyson Foods, USA
Jennipher Marshall-Jenkinson, MTA, United Kingdom
Pranjali Muley, Louisiana State University, USA
Jeyamkondan Subbiah, University of Nebraska- Lincoln, USA
Juming Tang, Washington State University, USA
Mark Watts, Campbell Soup Company, USA

Purchasing Information: Copies of the Proceedings of the 53rd Annual Microwave Power Symposium, as well as back issues from prior years, are available for purchase. Contact Molly Poisant, Executive Director of IMPI, at +1 804 559 6667 or molly.poisant@impi.org for details.

Table of Contents

Solid State II

Industrial & RF Drying

Microwave Ovens

INDUSTRIAL PROCESSING II & BIOMASS

MODELLING & DIELECTRIC PROPERTIES

LABORATORY & DIELECTRIC MEASUREMENTS

Posters

Notes

Notes

Notes

Notes

Notes

What's New in the Microwave Debate?

Kenneth R. Foster[1]

[1]Department of Bioengineering, University of Pennsylvania, Philadelphia PA 19106 USA

Keywords: Microwave energy, bioeffects, safety standards, cancer, electromagnetic hypersensitivity, 5G wireless communications

The possible health and safety hazards of radiofrequency (RF) and microwave energy have been debated for many years, and exposure limits have been in place since the 1960s without major change in their rationale. Within the past year, two major international exposure limits, those of the Institute of Electrical and Electronics Engineers (IEEE) and International Commission on Nonionizing Radiation Protection (ICNIRP) have had major revisions. The fundamental assumptions behind the limits (that hazards above about 100 kHz are chiefly thermal in nature) are unchanged, although the limits have been revised considerably above a "transition frequency" of 6 GHz on the basis of thermal modeling studies.

The scientific and public nature of the "microwave debate" has been changing over the years, as new technologies and research methodologies have emerged.

1. Increased use of the millimeter-wave (30-300 GHz) band for communications, including Internet of Things devices and 5G wireless communications systems. We will soon be awash with millimeter wave signals from a multitude of devices: mm-wave handsets, "small cells" mounted on light poles and other low structures, mm-wave power transfer systems, and a vast multitude of IoT devices. High powered mm-wave sources are appearing, and industrial applications are bound to follow.

2. The scientific and technological landscape for setting exposure limits is changing:

- Technology for exposure assessment is rapidly improving. Numerical dosimetry studies using image-based models have provided an extraordinarily detailed understanding of RF absorption by the body, and these, coupled with detained thermal modeling of RF-exposed tissue, provide a detailed picture of the thermal response of tissue to RF exposure.
- The RF/microwave bioeffects literature continues to expand rapidly. According to one database (EMF-Portal) there are now approximately 3700 laboratory and epidemiology studies related to bioeffects or health effects of RF/microwave fields, together with dozens of health-agency reviews completed within the past decade. However, in part due to the rapid increase in number of online journals,

many with weak standards of peer review, the overall quality of the literature appears to be declining. Many studies have significant risk of bias or otherwise are of poor quality. Health agencies in their reviews of the literature have started to complain about the poor quality of many RF bioeffects studies and openly complain that many such studies should not have been published. This has led to increased emphasis on systematic reviews, risk-of-bias evaluations, and meta-analyses in reviews of the scientific literature – which has increased dramatically the amount of effort need to do acceptable reviews.

3. New health issues are emerging, in particular "electrical hypersensitivity" (EHS, referring to self-reported symptoms that some individuals consider to be caused by exposure to low-level electromagnetic fields in the environment). Numerous well controlled studies have failed to link the symptoms that EHS individuals report with actual exposure, but the condition has become an important factor in some political and legal disputes related to RF/microwave exposures from commonplace technologies such as cell telephones and Wi-Fi.

In short, despite important technical advances, particularly in dosimetry and exposure assessment, there remains a need for more research as well as careful scientific reviews of the evidence. Standardized risk studies remain in short supply, particularly at millimeter wave frequencies due to emerging 5G communications technology. There is a growing awareness of the need for systematic reviews of the literature to replace more traditional narrative reviews – but these are far more demanding to produce. The possible health risks of RF/microwave energy remain a public issue, possibly declining somewhat, but nevertheless one that requires sensitivity on the part of industry that uses this form of radiant energy.

Microwave Plasma Sterilization at Low and Atmospheric Pressures

Klaus Martin Baumgaertner[1], Joachim Schneider[1], Andreas Schulz[2], Matthias Walker[2]

[1]Muegge GmbH, Reichelsheim (Odenwald), Germany
[2]Institute of Interfacial Process Engineering and Plasma Technology (IGVP), University of Stuttgart, Stuttgart, Germany

Keywords: Microwave Plasma, Duo-Plasmaline, Sterilization

INTRODUCTION

The efficiency of plasma sterilization was already proved to be comparable to standard sterilization processes based on dry heat, hot steam or chemicals (e.g. hydrogen peroxide or peracetic acid)[1],[2]. In addition, plasma sterilization does not rely on dangerous or even toxic substances, and the process time can be limited even to only some seconds as no post-treatment is necessary[3],[4]. Therefore, plasma sterilization processes are well suited for food packaging applications. Microwave plasma efficiently sterilizes without damaging the packaging material. Microwave plasma sources can be designed for applications at both low pressure and atmospheric pressure.

STERILIZATION TESTS AND RESULTS AT LOW PRESSURE

Plasma sterilization tests were performed on Bacillus subtilis, Bacillus atrophaeus and Aspergillus niger spores. 10^6-10^7 spores were spread by pipetting on PE/PET multi-layer foil samples, each approximately 30 cm^2 in area. Some spores were stacked. At low pressure (10 Pa - ~ 500 Pa), two different plasma sources were applied, both operated with 2.45 GHz microwaves: a Duo-Plasmaline [5], which produced an axially homogeneous plasma, and the Planartron, which produced a 2-dimensional homogeneous plasma area. These plasmas sterilize by a combination of radicals and UV radiation acting on the spores. As illustrated in the schematic diagram of the Planartron plasma source (Figure 1a), the spores on top of the PE/PET multi-layer foil samples were directly exposed to the plasma. After the plasma sterilization tests, the spores were rinsed off the surface of the samples and applied to agar plates. This procedure allowed counting the number of spores that were able to form colonies (i.e. the colony forming units) and for comparing them to the number of colony forming units from untreated reference samples. Despite partial stacking of the spores (seen by optical microscopy), the results of low-pressure plasma sterilization with the Planartron (Figure 1b) demonstrated successful inactivation of spores by more than 5 orders of magnitude after 10 s of plasma treatment.

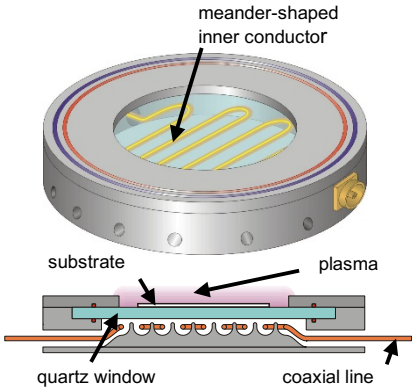

Figure 1a. Schematic diagram of the Planartron plasma source: perspective view (top) and cross section (bottom).

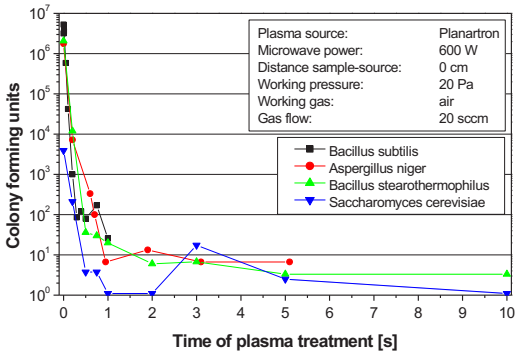

Figure 1b. Results of fast spore inactivation in the low-pressure air plasma of the Planartron plasma source.

Additional plasma sterilization tests at low pressure by application of the Planartron and a Duo-Plasmaline type of plasma source, respectively, were aimed at maximizing the sterilization effect. Different working gas mixtures were tested by varying the working gas pressure from 10 Pa up to several hundred Pa as well as the settings of the microwave power applied in the pulse mode and in the continuous wave mode, respectively. The microwave power was varied in the range from some hundred W up to 4 kW.

STERILIZATION TESTS AND RESULTS AT ATMOSPHERIC PRESSURE

A Duo-Plasmaline type of plasma source was adapted for plasma sterilization at atmospheric pressure. Figure 2a shows the schematic diagram of the Duo-Plasmaline plasma source. The plasma electrons, ions and neutrals (radicals in particular) were kept inside the vacuum chamber, while only plasma UV radiation was able to pass through the quartz window in the top plate of the vacuum chamber. Because of the transmissivity of the quartz window, only plasma UV radiation with wavelengths $\lambda>170$ nm irradiated the spores on top of the PE/PET multi-layer foil samples at atmospheric pressure. The samples were fixed to the inside bottom of the Petri dishes and the Petri dishes were turned upside down. Thus, the spore-contaminated top of the PE/PET multi-layer foil samples was facing the window, and plasma UV radiation provided the only sterilizing effect accordingly. Many microorganisms, particularly spores, are protected by different pigments (with different absorption spectra) against the inactivating effect of energetic light. Generation of a continuous UV emission spectrum by the plasma can thus inactivate different microorganisms simultaneously. Moreover, the inactivation effectiveness increases with decreasing UV wavelength. Therefore, the plasma sterilization tests, using the Duo-Plasmaline plasma source, aimed at optimizing the process gas mixture for continuous emission over a wide range of the UV and maximizing the intensity of the plasma UV radiation close to 170 nm wavelength, i.e. at the threshold of transmissivity of the quartz

window. Gas mixtures of nitrogen (N_2) and carbon dioxide (CO_2) were very effective in inactivating spores protected by pigments like Bacillus atrophaeus, even when they were stacked in a single spot (see Figure 2b).

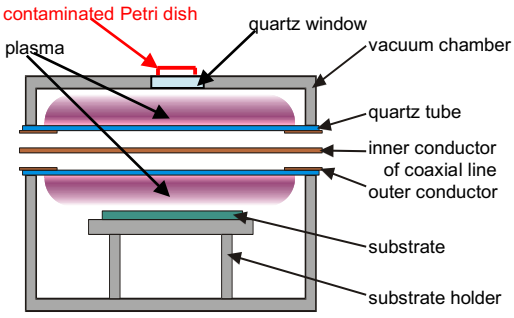

Figure 2a. Schematic diagram of a Duo-Plasmaline type of plasma source for plasma sterilization at atmospheric pressure.

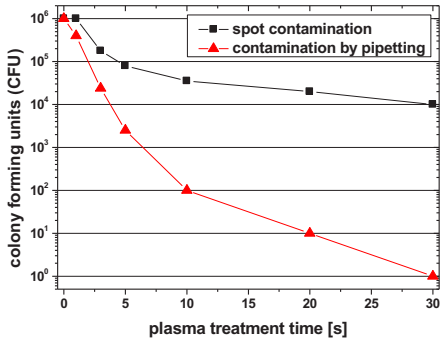

Figure 2b. Results of plasma sterilization tests on Bacillus atrophaeus spores with the Duo-Plasmaline type of plasma source at atmospheric pressure; a gas mixture of N_2 and CO_2 was applied.

Additional plasma sterilization tests were performed with the Duo-Plasmaline plasma source at atmospheric pressure on spores much better protected by pigmentation, like Aspergillus niger spores. These tests showed inactivation of partly stacked Aspergillus niger spores by more than 4 orders of magnitude after 30 s of treatment.

CONCLUSION

Microwave plasma sterilization efficiently inactivated relevant spores within only tens of seconds at atmospheric pressure and even in the sub-second range at low pressure. Despite the lack of radicals, i.e. using only plasma generated UV radiation, sterilization at atmospheric pressure even showed substantial inactivation of stacked pigmented spores.

REFERENCES

[1] J. Pollak, M. Moisan, D. Kéroack and M.K. Boudam, *J. Phys. D: Appl. Phys.* 41 (2008) 135212.
[2] F. Rossi, O. Kylián and M. Hasiwa, *Plasma Process. Polym.* 3 (2006) 431.
[3] J. Feichtinger, A. Schulz, M. Walker and U. Schumacher, *Surf. Coat. Technol.* 174-175 (2003) 564.
[4] J. Schneider, K.-M. Baumgärtner, J. Feichtinger, J. Krüger, P. Muranyi, A. Schulz, M. Walker, J. Wunderlich and U. Schumacher, *Surf. Coat. Technol.* 200 (2005) 962.
[5] W. Petasch, E. Räuchle, H. Muegge, K. Muegge, *Surf. Coat. Technol.* 93 (1997) 112.

Functional Coatings Deposited from Low-pressure Microwave Plasmas

Robert Mueller[1], Klaus-Martin Baumgaertner[1], Monika Balk[1], Joachim Schneider[1], Stefan Merli[2], Andreas Schulz[2], Matthias Walker[2] and Guenter Tovar[2]

[1]Muegge GmbH, Reichelsheim (Odenwald), Germany
[2]Institute of Interfacial Process Engineering and Plasma Technology (IGVP), University of Stuttgart, Stuttgart, Germany

Keywords: Microwave Plasmas, Low-pressure Plasmas, Barrier Coatings, Anti-scratch Coatings, High-rate Applications.

INTRODUCTION

Coatings are used in industry to enhance the functionality of materials. Low-pressure microwave plasmas can conveniently deposit multi-functional coatings. Due to their high electron densities, which induce high densities of chemically reactive species, particularly radicals, microwave plasmas are suitable for high-rate deposition applications even at low-pressure. This paper overviews multi-functional coatings deposited from low-pressure microwave plasmas for industrial applications.

GAS BARRIERS FOR POLYMER FOOD PACKAGING

Polymer materials are commonly used for food packaging. There is a demand for novel, high performance barriers for this type of materials, because the current generation of barriers either does not fulfil the required performance or is not economically feasible. A Duo-Plasmaline microwave plasma source forming a homogeneous plasma area and an electron cyclotron resonance (ECR) microwave plasma source forming a three-dimensional plasma were used for plasma deposition of gas diffusion layers on polymer foils and on complex three-dimensional polymer packaging materials, respectively. Gradient layers were designed starting with a polymer-like layer and ending in a hard silicon oxide (SiO_x) barrier film. The polymer-like layer improves adhesion to the surface of the polymer packaging material and offers high mechanical flexibility, whereas the hard SiO_x film optimally blocks oxygen permeation.

ELECTRICAL INSULATION BARRIERS FOR FLEXIBLE THIN-FILM SOLAR CELLS

Microwave plasma is used to deposit insulating SiO_x layers on metal foils. The task of the layer is to insulate electrically the metal foil, and to protect the sensitive absorber layer, e.g. consisting of copper indium gallium di-selenide (CIGS), against the diffusion of

iron from the substrate, while maintaining the full flexibility of the solar module. In addition, the layers must withstand process temperatures of up to 650°C during the subsequent CIGS deposition process.

The insulating SiO_x layers were deposited from hexamethyldisiloxane (HMDSO) via low-pressure chemical vapor deposition fed by a microwave plasma. A Duo-Plasmaline plasma source generated a homogeneous plasma within an array configuration. A deposition rate of up to 60 µm/min provided for very short process times and is therefore suited for industrial applications.

An additional challenge was using metal foils made of cheap construction steel. In general, the surface of an uncoated sheet of construction steel was characterized by flakes, rifts and trenches (Figure 1a). These cannot be completely covered by an electrical insulation layer deposited by a low-pressure plasma process without bias (Figure 1b). Application of an additional bipolar bias voltage covered every surface deformity on the substrate (Figure 1c), and prevented the formation of pinholes between the construction steel foil and the back contact of the flexible thin film solar module.

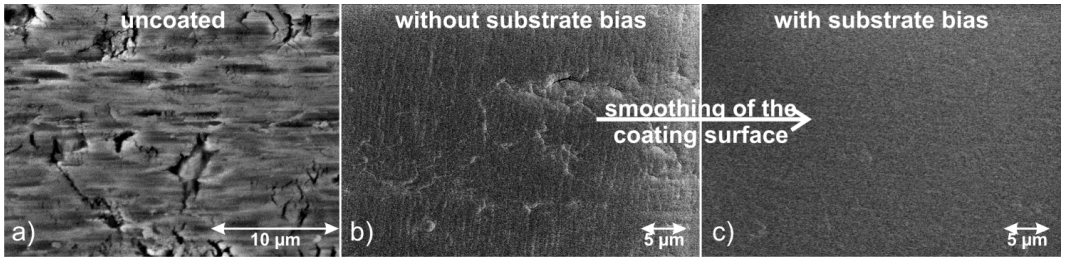

Figure 1. Surface of a metal foil made of cheap construction steel: a) uncoated, b) coated with an insulating SiO_x layer deposited in a low-pressure microwave plasma process without application of substrate bias, and c) coated with an insulating SiO_x layer deposited in a low-pressure microwave plasma process with additional substrate bias.

HIGH-RATE DEPOSITION OF SCRATCH-RESISTANT AND ANTI-ABRASIVE COATINGS

Industrial-scale plasma deposition of scratch-resistant coatings on polymers, e.g. polycarbonate (PC), has to provide homogeneous coating thickness over a large area as well as high deposition rates. A scalable Duo-Plasmaline-based plasma source provides a deposition rate ≥ 20 µm/min with a high coating quality of quartz-like layers. This is due to the high plasma density in the Duo-Plasmaline low-pressure microwave plasma source. Tests performed on plasma-deposited quartz-like protection layers on polycarbonate material show that scratch resistance values comparable to window glass can be achieved with this kind of coatings. The 5.4 µm quartz-like protection layer on the 10x15 cm^2 polycarbonate test sample in Figure 2 was deposited in a low-pressure microwave plasma process with the deposition rate of 50 µm/min.

Figure 2. Polycarbonate plate with additional quartz-like protection layer deposited in a low-pressure microwave plasma process showing almost 100% transparency.

Apart from their anti-abrasive properties, diamond and diamond-like layers provide excellent heat transfer. This is due to the by far highest thermal conductivity of diamond compared to other mineral materials. It is feasible to industrially deposit diamond layers using low-pressure microwave plasma sources. In view of long process times of up to several hundreds of hours without interruption for zero defect production of diamond layers and artificial diamonds, these microwave plasma sources have to be reliable in terms of long uptime, fast restart and persistence of the microwave plasma system in order to guarantee stable process parameters.

CONCLUSION

The large parameter space as well as the flexibility in design of low-pressure microwave plasma sources are essential prerequisites for satisfying industrial demands for deposition of multi-functional coatings for a large variety of applications.

FREEZEWAVE or Microwave Assisted Freezing; the NITOM and the NIMIW Effects May Explain the Reduction of the Size of Ice Crystals

A. Le-BAIL[1], P.K. JHA[1], M. SADOT[1], S. CHEVALLIER[1], S. CURET[1], C. COUEDEL[1], M. HAVET[1], V JURY[1], O. ROUAUD[1], J.P. BERNARD[2]

[1]ONIRIS-GEPEA UMR CNRS 6144, Nantes FRANCE
[2]SAIREM, Lyon, FRANCE

Keywords: freezing; Microwave; Radio frequency; microstructure; modelling

INTRODUCTION

Several innovative freezing technologies assisted by external fields (magnetic, electric, electromagnetic) have been developed with the objective of reducing the size of ice crystals and the freeze damage. This presentation will propose a summary of the FREEZEWAVE collaborative project on freezing assisted by low power microwave (MAF) (2450 MHz) applied to different types of foods. Results related to apple, potato and a methyl cellulose gel will be presented, considering different techniques that have been used to assess the size of ice crystals and freeze damage (NMR, CRYO-SEM, X-ray MicroCT, Mass diffusion, etc.).

METHODOLOGY

In the PhD project of P.K. JHA[1], MAF of apples and potatoes was performed by applying constant MW power (CMAF = 167 W/kg) and pulsed MW power (P1MAF and P2MAF = 500 and 667 W/kg with 10 s pulse width and 20 s pulse interval) during freezing. A custom-built MW freezer which consisted of a domestic MW cavity installed in a blast freezer was used for MAF. The impact of MAF conditions on freezing parameters and quality attributes (for e.g. microstructure, texture, drip loss, etc.) of apples and potatoes were studied using several analytical techniques. In the PhD project of M. Sadot[2], methylcellulose gel was considered. A rectangular waveguide WR 340 (section 86 mm x 43 mm) was blown by gaseous Nitrogen at -45°C. A solid state generator (GMS200, SAIREM, France) was used for both setups, and MW pulses were generated thanks to a switch. The size of ice crystals was analyzed by cryo-SEM for apple and potato and also after freeze-drying of the sample of frozen gel as well as apple and potato.

RESULTS

MW use during freezing of apple did not affect importantly the time – temperature evolution, and no supercooling was observed; besides, tiny temperature oscillations were observed in the case of pulsed MW. The application of MWs during the freezing process produced a superior microstructure (homogenous pore size distribution with a larger population of small pores) than the control process. Moreover, MAF of apple resulted in a lower drip loss, meanwhile, it also led to a lower reduction in firmness/hardness compared to the reference sample. The MW form (constant mode or pulsed mode) and power level were found as critical parameters that controlled the quality attributes of the apple sample. For instance, average pore size, texture loss, and drip loss significantly ($p < 0.05$) decreased with the introduction of pulsed MW conditions and with the increase in MW power level. P2MAF condition gave the best result in terms of microstructure and other quality attributes such as drip loss and texture.

The MAF potato samples exhibited microstructure with more small size pores that were distributed uniformly throughout the sample, while no MAF condition resulted in a product having relatively larger pores and a wider pore size distribution range. The texture loss and drip loss were lower for MAF sample than the control sample. Quality preservation was better when MW intensity was increased. Among all freezing conditions, P2MAF condition yielded the best result in terms of microstructure and other quality attributes such as drip loss and texture.

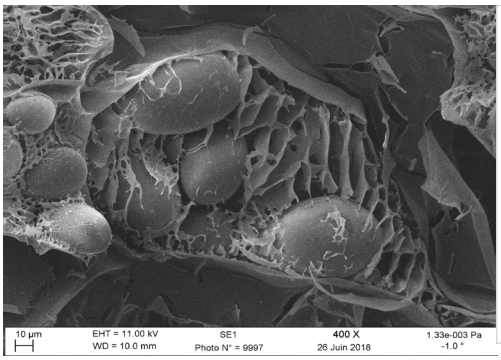

Figure 1. Cryo-SEM image of potato frozen under MAF. Starch granules are surrounded by intracellular ice crystals.

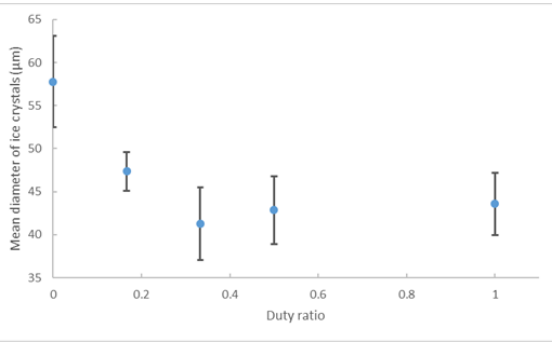

Figure 2. Impact of the duty ratio of emitted MW power on the ice crystals mean diameters for methyl cellulose gel at equal MW energy brought (except for control freezing).

For the methylcellulose gels, the use of MW during freezing induced a reduction of the ice crystal mean diameter. The values decreased from 57.8 µm for the control freezing without MW to 41.3 for MW assisted freezing with a duty ratio of 0.333 (28.6% reduction). The reduction obtained with a low duty ratio of 0.167 is less than the one resulting from higher duty cycles. From a duty ratio of 0.333, there seems to be no significant difference between the experiments. Results obtained for the duty ratio of 0.167 could be explained by a too short exposure duration to MWs or by a too long duration without MW.

DISCUSSION

Two concepts are proposed to explain the observed ice crystal size reduction in frozen systems by using microwaves. The "NITOM" concept (Nucleation Induced by Temperature Oscillation caused by Microwaves) is based on the fact that under specific duty ratio, the temperature of the sample undergoing freezing will oscillate (Xanthakis et al., 2014). The fluctuating temperature is expected to favour secondary nucleation, which, in turn, suppresses the crystal growth. This concept is illustrated in figures 3 & 4 below.

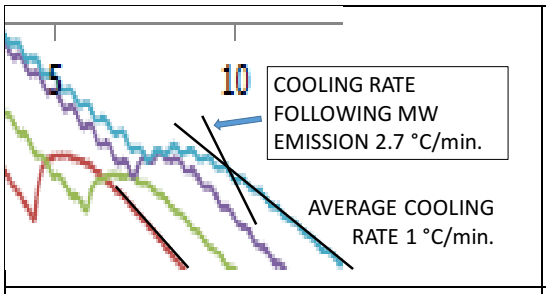

Figure 3: Zoom on cooling rates during the tests done by Xanthakis et al (2014). A much faster cooling was observed during temperature drop following MW emission.

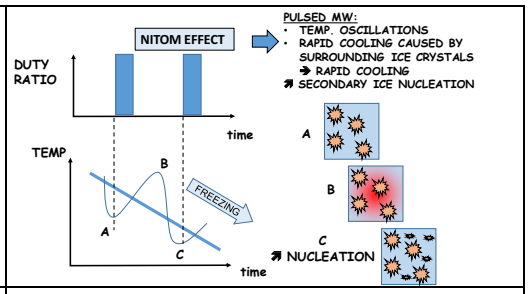

Figure 4 Scheme presenting the "NITOM" effect; Following MW emission, a faster cooling promotes the apparition of new ice nuclei, resulting in a refined ice crystals population.

The second concept is called "NIMIW" (Nucleation Induced by constant or pulsed MWs power), and it is based on constant or pulsed (short time) emission. NIMIW can be explained by the impact of MW on the hydrogen bonds between water molecules, which may affect the water cluster structures during freezing. It is expected that MWs could exert a torque and displace the water molecules from their equilibrium relationships in the ice cluster, resulting in fragmentation of existing ice crystals when ice crystals are in the form of nuclei (a nuclei being a small but stable ice crystal). The fragmented ice crystal nuclei may act as new nucleation sites and promote the secondary nucleation, thus, causing ice crystal size reduction thanks to the duplication of ice crystals nuclei during MAF.

CONCLUSION

The precise impact of MW on freezing is still under debate. Two concepts that have been proposed to explain MW freezing can be considered. One of the challenges is to be able to measure the temperature oscillation related to the NITOM effect, which is very small in some cases. Radio frequency (RF) assisted freezing has also been successfully used to reduce the size of ice crystals, also with a pulsed mode. Further research is needed to unravel the situation.

REFERENCES

[1] P.K. Jha, Thèse Univ. Nantes, "Study on the effect of electromagnetic radiations during freezing on ice structure and quality of fruit and vegetable tissues", ED SPI 602, 9/11/2018

[2] M. Sadot, Thèse Univ. Nantes, "Etude numérique et expérimentale d'un procédé de congélation assistée par micro-ondes", ED SPI 602, 24/09/2018

Development of an Innovative Process for Microwave Volume Expansion of Snacks

B. Wäppling Raaholt[1]

[1]RISE Research Institutes of Sweden, Agrifood and Bioscience, Göteborg, Sweden

Keywords: microwave volume expansion, microwave puffing, processing, production, snacks.

INTRODUCTION

Microwave volume expansion, or microwave puffing, is commonly known for puffing of corn into popcorn. In this paper, an innovative microwave process for volume expansion of a snack formulation of relatively high protein content will be briefly presented and discussed. The work combines process design and use of microwave processing as a means to achieve the desired product quality, in terms of texture, porosity, colour and shelf-life stability of the snacks. Microwave puffing offers intensification of the process for production of snacks. The volume expansion achieved is related to volumetric processing by microwaves, combined with pressure being built up in the product during processing. Industrial examples are found in literature [1].

METHODOLOGY

The microwave process was designed to achieve volume expansion of a snack formulation. The microwave oven used is an institutional microwave combination oven (Panasonic NEC1453, with power output measured to 89% of the selected specified power level, according to the IEC 60705 standard test [2]). Temperatures were measured in the product samples using fibre-optic probes (FOT-L, Fiso) which were placed in the centre of 3-4 different samples during each process run. Product temperatures were measured during microwave processing, in 3 replicates, in order to get accurate temperature profiles. The microwave treatment was followed by a final step of drying, in order to adjust the moisture content of the produced snacks. The quality of the puffed snacks was evaluated in terms of texture, using an Instron texture analyzer (Instron 5542 universal testing machine, Norwood, MA, USA), expansion degree (in terms of thickness, measured using a caliper), density of the puffed samples (using a pycnometer Micromeritics, AccuPyc II 1340), and colour (using DigiEye system v 2.43, Verivide).

Water content was measured as follows. Two hours after processing, the snack was mashed, weighted and dried in a vacuum oven at 80°C and 100 mmHg overnight and weighted again in the morning. From the weight, the moisture content was calculated. Samples were measured in triplicates. Water activity was measured with a dew point water activity meter (AquaLab 4TE, Decagon Devices Inc., Pullman, WA, USA) on 3 puffed crisps in each sample group. *Dimensions* were measured with a Vernier caliper as follows: a) the *thickness* was measured on 5 samples in the same sample group and 4 times at different angles over the cross section of the crisp. b) The *diameter* was measured twice on 5 samples in the same sample group

and twice on each crisp. c) The *apparent volume*, $V_{apparent}$, was calculated using the measured thickness and diameter for the same 5 crisps within a sample group. The crisp was approximated to have a cylindrical shape, hence the apparent volume is $V_{apparent} = \left(\frac{d}{2}\right)^2 \pi h$, where d is the diameter and h is the thickness. d) The *apparent density* $\rho_{apparent}$ was calculated using the apparent volume and weight of the same 5 crisps within a sample group, and by taking the average value for these crisps:

$$\rho_{apparent} = \frac{m}{V_{apparent}}\Big|_{average} \quad \text{(Equation 1)}$$

Moreover, *true density* was measured with a gas pycnometer (AccuPyc II 1340, Micro-meritics, Norcross, GA, USA). The true density is the density of the solids in a sample including closed pores. Each crisp was split into 2 pieces and one of the halves was analyzed in the pycnometer. The same 5 crisps used in the dimension analysis were used. From the true density, the true volume, V_{true}, was calculated: $V_{true} = \frac{\rho_{true}}{m}$, where ρ_{true} is the true density and m is the mass of the half cheese crisp. *Porosity (void fraction)* is the fraction of the volume of voids, V_{voids}, over the total volume of the cheese snack. In our case $V_{apparent}$ is used as the "total volume". The true volume, V_{true}, is the volume of solid matter including closed pores in a sample gained from the pycnometer.

$$\varepsilon_{void\ fraction} = \frac{V_{voids}}{V_{apparent}} = \frac{V_{apparent} - V_{true}}{V_{apparent}} = 1 - \frac{V_{true}}{V_{apparent}}$$

The porosity, $\varepsilon_{void\ fraction}$, is between 0 and 1, where a higher fraction means a more porous crisp.

Colour measurements were made by taking photos in the DigiEye system [3], and evaluating *ΔE** and the *degree of lightness L* [4]. DigiEye photos were taken of snacks in 6 replicates. One photo was taken of the top sides and one of the back sides. The CIELAB values were collected from fixed circles of 160 pixels of each snack. The photos were taken 4 days after baking since the snacks look darker directly after baking. After a few days they were stabilized to achieve a lighter colour. The CIELAB values were collected from the surface area of 6 snacks. From these, the value of *ΔE** were calculated:

$$\Delta E^* = \sqrt{\left(L^* - L^*_{ref}\right)^2 + \left(a^* - a^*_{ref}\right)^2 + \left(b^* - b^*_{ref}\right)^2},$$

where L^*_{ref}, a^*_{ref} and b^*_{ref} are the L*a*b* values of a white chart which are compared to the L^*, a^*, and b^* values of the snack. The higher ΔE*, the more different is the crisp colour from the white chart, i.e. the darker the crisp is. The L* value was analysed as well. The maximum degree of whiteness (white) is at L*=100 and minimum whiteness (black) at L*=0. The higher the L* value, the lighter the colour of the snacks.

Texture was analyzed in a 3-point bending test which gives three values: 1) *modulus:* the fraction of stress through strain. The higher modulus, the stiffer and less rubbery is the material, 2) *flexure stress* and 3) *flexure strain*. Maximum flexure stress is the stress at which the crisp breaks. A low

stress means that the snack is crispy. Flexure strain at maximum flexure stress: the strain by which the cheese crisp breaks. The lower the strain, at which the crisp breaks, the more crispy the crisp.

RESULTS & DISCUSSION

Pre-dried samples had a slightly improved expansion degree. However, the appearance was much different compared to the reference samples. Therefore, pre-drying was used only in the screening trials and not for the optimisation step. The optimal microwave processing conditions for the snacks were found when the target temperature (145-150°C) was reached in as short a time as possible, while avoiding browning. The process settings selected were microwave processing at the 'high power level' (75 W/g) to a target temperature of 145-150°C, followed by a post-drying step to reach the desired final moisture content (approximately 2.4% ±0.5%). When selecting the microwave process time, important criteria to consider were the resulting generation of snacks with enough expansion, a solid structure, crispiness close to the reference snacks, and as little browning as possible. Moreover, a shorter processing time was preferable. Results showed that the process settings which meet these requirements are: 'very high' microwave power level (75 W/g) for 50 seconds. This power level resulted in good quality of the snacks in terms of expansion, structure, crispiness and colour (avoidance of browning), and also a process time shorter than for 'high power' (37.5 W/g). In order to reach a final moisture content (2.4%) and a shelf-stable product, a post-drying step (convective drying at 110°C for 25 minutes) was designed.

It is possible to achieve the quality parameters of the snacks within the desired range of values for each of the quality parameters: colour, density, expansion degree and texture. The desired values were achieved from measurements of conventionally baked reference samples. The appropriate process design was found by combining innovative design and tailor-making of the microwave volume expansion process with experimental design of experiments.

CONCLUSION

The resulting process for microwave volume expansion of snacks offers an efficient way to produce snacks of desired quality. Microwave volume expansion of snacks, followed by a final drying step, can be used to produce snacks of relatively high protein content. The resulting quality parameters were able to set very close to the conventionally baked reference samples. The potential in using the method for different types of snack formulations is promising.

REFERENCES

[1] B. Wäppling Raaholt, *Applications of Microwave Heating of Foods*, Chalmers University of Technology, ISBN 978-91-7597-239-8, 2015, pp. 46-48.
[2] IEC Standard 60705, Household microwave ovens – methods for measuring performance, 4th ed. Geneva, Switzerland, 2018 (2010, AMD1:2014, AMD2:2018 Consolidated version).
[3] CanonD90, DigiEye, v 2.43.
[4] The Hunter L•a•b colour space (http://www.hunterlab.com/appnotes/an08_96a.pdf)

N-BREAD Process; A New Process Based on Low Pressure-low Vacuum Processing to Develop the Next Generation of Snacks

Patricia Le-BAIL[1], Olivier PAURD[2], Laure VILLACEQUE[2],

Manon CHEMIN[2]

[1] INRA, UR1268 Biopolymers Interactions Assemblies, BP 71627, F44316 Nantes, France

[2]Nbread Process, 41700 Contres, Frances

Keywords: microwave; fruit; vegetable; cellular structure; snacking.

INTRODUCTION

This presentation is related to an innovative process, the N-bread process, which is based on combining a vacuum assisted mixing with a thermal setting obtained thanks to microwaves. This innovative and disruptive food processing process permits to create new structure and new texture, starting from several kinds of ingredients, food by-products etc. This process can transform any type of food - or almost - into a compact food, having the texture and appearance of sponge cake or bread, melting or crunchy, while maintaining the taste and organoleptic properties of staple foods. This process, which has been twice awarded, contributes to the development of new types of foods which are easier to consume, cheaper to produce, opening up immense possibilities for fast food and "nutraceuticals".

METHODOLOGY

The method is based on the use of gas to pressurize and aerate the raw ingredient, followed by thermal coagulation by microwaves. Different concepts and patents have been filed on this technology [1], [2]. The equipment is shown in Figure 1 below.

Figure 1: NBREAD equipment

During this study, a method of kneading under pressure followed by baking in a microwave oven has been used. Such method of pressure-vacuum kneading has been used in bread making for a few decades to improve the quality of sandwich breads. This process makes it possible to develop very aerated breads with low-protein flours. The conventional ones like the 1962 Chorleywood Bread Process (CBP) is the best known ("TWEEDY" kneader). It combines both a fast kneading speed with a vacuum and pressure application.

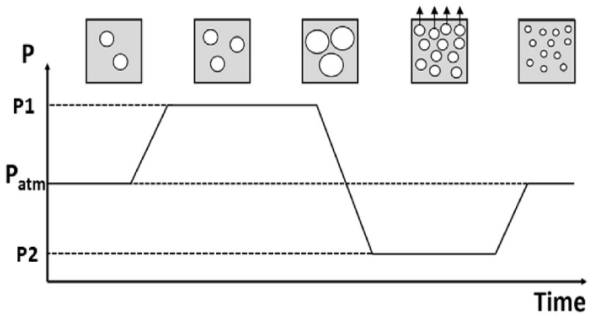

Figure 2: Schematic representation of the effect of pressure evolution during kneading with pressure and vacuum that can be applied to bread dough to improve aeration of the dough during kneading[4]

The N-Bread process is different from the processes presented in the previous section. The dough is first blended at slow speed at atmospheric pressure and then at a faster rate under pressure to incorporate more gas into the pulp. At the end of kneading, a partial vacuum can be applied in order to induce a finer and homogeneous cellular aeration. In the case of microwaved cellular structure, the kinetics of baking are very fast of the order of a few minutes. Different tests have been done to develop a model system in order to better understand the impact of the processing parameters; some results will be presented. A food is an association of raw materials and constituents, transformed to varying degrees by different treatments (mixing, baking, shaping, etc.) whose objective is to confer the desired use functions. The process requires specific formulations which have been developed for specific applications.

Figure 3: Example of peanut by-product bread, using NBREAD process

Figure 4: Example of raspberry bread, using NBREAD process

Figure 5: Example of pea bread, using NBREAD process

DISCUSSION

This technology offers a new field of application of microwave processing of foods. Food by products and food wastes may be processed to deliver high value snacks and food products. The precise control of the pressure during the process is the key to success. Further applications may be envisaged to build new sweet or salty specialties.

CONCLUSION

Low pressure vacuum processing of hydrated matrices provides access to new possibilities in terms of food processing. Micro wave thanks to its capability to bake quickly a foamy structure which is minimally absorbing the micro waves power.

REFERENCES

[1] Cauvain, S. P. & Young, L. S. (2006) The Chorleywood Bread Process. A volume in Woodhead.Cereal Chemistry. 58(3),158–64

[2] Sadot, M., Cheio, J., & Le-Bail, A. (2017) Impact of dough aeration of pressure change during mixing. Journal of Food Engineering. 195, 150-157.

O_2 Dissociation Produced by a Compact Collisional Plasma Source

K. Achkasov[1], L. Latrasse[1], F. Zoubian[1] and N. Britun[2]

[1]Sairem, Neyron, France
[2]Université de Mons, Mons, Belgium

Keywords: microwave plasma, collisional plasma, solid-state generator, laser spectroscopy, optical emission spectroscopy, O_2 dissociation.

INTRODUCTION

Oxygen plasmas are used in surface cleaning, etching, functionalization, etc. mainly due to their high chemical reactivity. One of the parameters characterizing plasma reactivity is the molecular dissociation degree. In oxygen plasmas, O_2 dissociation indicates that reactive O-atoms are available to react with other elements on the sample surface and hence modify surface properties. The goal of the present study was to measure the O_2 dissociation in plasmas produced by a "Hi-Wave" microwave (MW) plasma source [1]. The O_2 dissociation was studied by optical emission and laser spectroscopy in pure O_2, as well as in Ar-O_2 and N_2-O_2 gas mixtures. The relative density of the O-atoms obtained by two photon absorption laser-induced fluorescence (TALIF) was calibrated by optical actinometry. The O-atom number density was calculated for all the studied conditions, whereas the O_2 number density was determined by the ideal gas state equation. The electron temperature, gas temperature and the density of Ar metastables were determined experimentally by optical emission and absorption spectroscopy, respectively. The measurements were performed as a function of the applied MW power, working pressure and the distance from the "Hi-Wave" plasma source.

EQUIPMENT, DIAGNOSTICS TOOLS AND PLASMA CONDITIONS

The relative density of O-atoms was detected with the TALIF method [2], using a Sirah Cobra Stretch dye laser working at 10 Hz pulse repetition frequency and 5 ns pulse duration. The O-atoms were excited at the wavelength of ~225.6 nm. The relative density of the O-atoms obtained by TALIF was calibrated by optical actinometry, using Ar as an actinometer and assuming corona excitation [2]. For the actinometry, the electron temperature (T_e), gas temperature (T_{gas}), and density of Ar metastables were determined using optical emission and absorption spectroscopy, respectively. An Andor iStar 740 ICCD camera (TALIF image registration), and an Andor SR750 monochromator (spectra acquisition) with a resolution of about 0.05 nm were employed.

The "Hi-Wave" plasma source, powered by a Sairem GMS450W solid-state MW generator, was characterized with various gases and their mixtures. The plasma was ignited in a ~30 L vacuum chamber with a base pressure of ~10^{-7} Torr. The MW plasma source

was mounted on a custom-designed vacuum flange protruding inside the chamber, which allowed varying the distance between the plasma source and the diagnostic laser beam. The laser beam position was fixed during the measurements. Most of the data were obtained at a distance D = 56 mm between the plasma source and the laser beam. The plasma stability was considered when choosing the plasma conditions -- specifically the applied MW power, working pressure, and the distance from the plasma source. Sometimes the gas mixture was changed as well, and in addition to pure O_2, Ar-O_2 or N_2-O_2 gas mixtures were used. The minimum pressure for a stable discharge was about 20 mTorr [2.6 Pa], whereas the maximum pressure was limited to 200 mTorr [26 Pa]. Discharge sustainability determined the minimum MW power; the difference of the nominal generator power (450 W) and reflected power (i.e. P_{max} = 450W - $P_{reflected}$) determined the maximum power.

RESULTS: GAS TEMPERATURE

Gas temperature is important for TALIF signal calibration. We determined T_{gas} as a function of the applied MW power and gas pressure, using the rotational band from the first negative ro-vibrational system of N_2^+ [3]. T_{gas} at 40 mTorr [5.3 Pa] stayed around 880 K for N_2 admixture percentages from 5 % to 50 %. However, T_{gas} was typically a step function of either the MW power or the discharge pressure, as can be seen in Figure 1 for an admixture of O_2 + 25 % N_2. The T_{gas} error bars (Fig. 1(b)), corresponding to the Boltzmann fit errors used for rotational temperature determination, did not exceed 5 %.

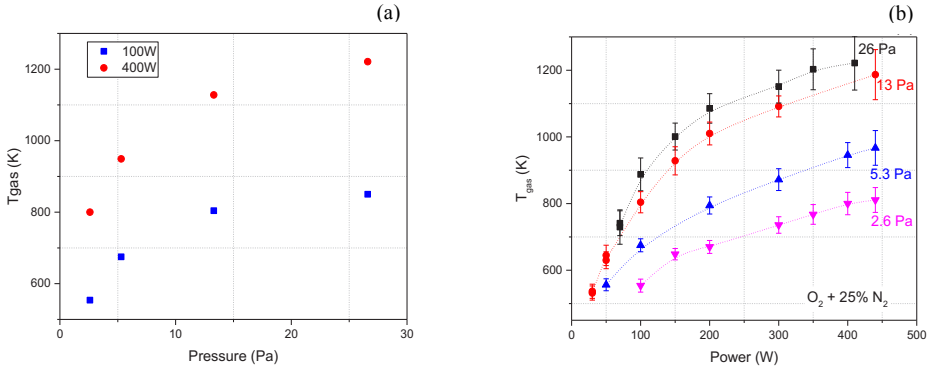

Figure 1. Gas temperature for the admixture of O_2 + 25% N_2 as a function (a) of the working pressure for a MW power of 100 and 400 W; (b) of the MW power for 4 working pressures.

The total span of T_{gas} corresponding to the examined MW power range (30 – 450 W) was from about 400 to 1300 K. Both temperature as functions both of pressure and power initially increased quickly, and then saturated. At high gas pressure, the collision rate increase enhanced the collisional heat transfer from the electrons. This is suggested to be the main reason for such significant gas heating (see Figure 1(a)).

RESULTS: O_2 DISSOCIATION

The O-atom number density was calculated for all the studied conditions (based on the available calibration data), and the O_2 number density was determined for the same

conditions by the ideal gas state equation (using the available values of pressure, O_2 content, and T_{gas}).

The O-atom density and the O_2 dissociation degree are shown in Fig. 2 as a function of the MW power for 4 working pressures. The O density increased considerably with pressure. For all the pressures, it increased rapidly with the discharge power until 100 W; beyond 100 W the variation became less pronounced (Fig. 2(a)). A slightly different behavior is exhibited in Fig. 2(b) for the O_2 dissociation degree where its saturation with the discharge power was less pronounced. However, increasing the pressure from 20 to 200 mTorr [2.6 to 26 Pa] decreased the dissociation degree by ~1.5 times. This is most likely related to the electron cooling at high pressure from collisional energy transfer.

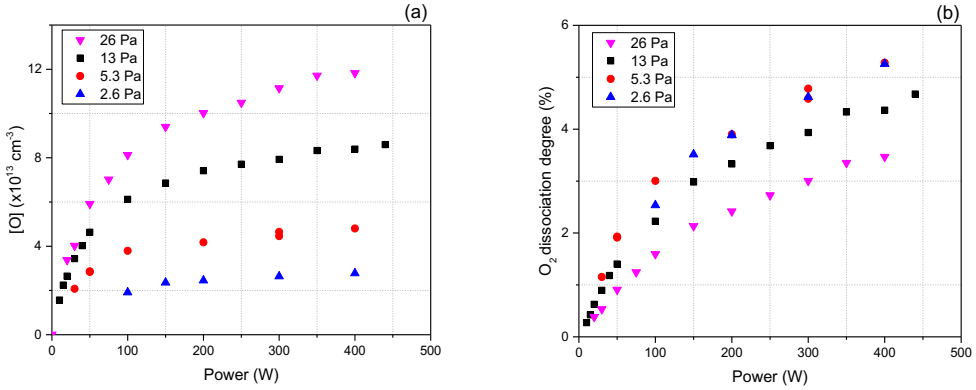

Figure 2. O atom density (a) and O_2 dissociation degree (b) as a function of applied MW power and working pressure in a pure O_2 discharge, measured at 56mm from the plasma source.

Dissociation was also determined at D = 86, 116 and 146 mm (not shown). It decreased with distance from the source, roughly a by factor of 10% each 3 cm at 40 mTorr [5.3 Pa].

CONCLUSION

The MW plasma source characterization performed by optical emission and laser spectroscopy showed that the gas temperature ranged from 400 to 1300 K at a distance of 56 mm from the "Hi-Wave" plasma source. The O_2 dissociation reached 5.3 % in a pure O_2 discharge (at 5.3 Pa [40 mTorr], 400 W power).

REFERENCES

[1] L Latrasse, M Radoiu, J Lo, P Guillot, *J Microw Power Electromagn Energy*. 2017, 51:1, 43–58.
[2] N. Britun, et al. *J. Phys. D: Appl. Phys.* 50 (2017) 075204
[3] N. Britun, et al. *J. Appl. Phys.* 114 (2013) 013301

Microwave Plasma Sources for High-rate Applications

Monika Balk[1], Jiehong Jin[1], Markus Endermann[1], Joachim Schneider[1], Klaus-Martin Baumgaertner[1], Steffen Pauly[2], Stefan Merli[2], Andreas Schulz[2], Matthias Walker[2] and Guenter Tovar[2]

[1]Muegge GmbH, Reichelsheim (Odenwald), Germany
[2]Institute of Interfacial Process Engineering and Plasma Technology (IGVP), University of Stuttgart, Stuttgart, Germany

Keywords: Microwave Plasma, Remote Plasma Source, Downstream Plasma Source, Waste Gas Abatement, Pyrolysis, Plasma Etching, High Rate Applications.

INTRODUCTION

High-quality results in combination with high-rate output are major requirements for many plasma processes on industrial level. Microwave-induced plasma sources can meet these requirements. Under low-pressure conditions, plasma excitation by microwaves can easily generate non-equilibrium plasmas, characterized by high-energy or "hot" electrons, while the low-energy heavy ions and neutral particles in the plasma stay almost at room temperature. Therefore, plasma surface treatment of even thermally sensitive materials is feasible. Sterilization of food and food packaging are prominent industrial examples of this kind of "cold" plasma treatment. In addition, high electron densities inducing high densities of chemically reactive radicals are achievable by microwave plasmas both at low pressure and atmospheric pressures. This property is essential for achieving high-rate output, e.g. high etching rates.

This paper will present different examples of microwave plasma sources for high-rate applications, focusing on downstream plasma sources flexibly applicable over a large parameter range, e.g. from low-pressures up to even atmospheric pressure, as well as on remote plasma sources (RPS).

DOWNSTREAM MICROWAVE PLASMA SOURCES

The basic setup of a downstream microwave plasma source consists of a process chamber (i.e. vacuum chamber at low-pressure) with a gas supply on one side and a gas outlet (i.e. connection to the vacuum pump at low-pressure conditions) on the opposite side. The microwave is injected perpendicular to the direction of the gas flow (see Figure 1a)). In a favorable downstream microwave plasma source setup, resonant coupling of the microwave leads to a local peak of the electric field intensity inside the process chamber. Thus, a local plasma at the spot of the maximum electric field intensity is formed. Depending on the resonant cavity, the pressure inside the process chamber and the injected microwave power, it is possible to adjust the extension of the plasma inside the

process chamber. Resonance conditions are essential for achieving very high plasma densities, which is particularly important for hydrogen activation in diamond deposition processes.

Under low-pressure conditions (0.1 to 60 mbar), industrial applications of the downstream microwave plasma source like plasma cleaning, surface activation or functionalization are performed with microwave power in the range between 100 W and 3000 W. Diamond deposition will require more power. This paper will present several downstream microwave plasma source setups suitable for different industrial applications from low-pressure up to atmospheric pressure. The latter is important for high-rate waste gas abatement and for high-rate pyrolysis, respectively (cf. Figure 1b)).

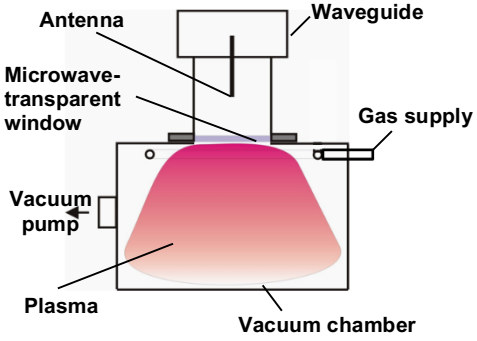

Figure 1a). Schematic of a downstream microwave plasma source operated at low-pressure conditions.

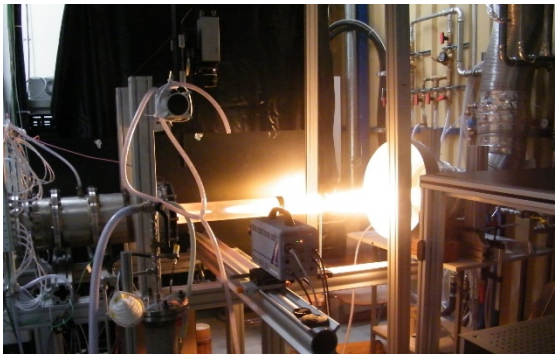

Figure 1b). Downstream microwave plasma source operated at atmospheric pressure for high-rate waste gas abatement or for high-rate pyrolysis.

REMOTE MICROWAVE PLASMA SOURCES

Remote plasma sources (RPS) operated by microwave power are widely used for industrial etching applications, e.g. decapsulation of semiconductor chips for failure analysis, cleaning of plasma deposition chambers in the semiconductor industry and production of micro-components.

The special feature of an RPS is limitation of the plasma to the RPS plasma chamber. This means, only radicals produced in the plasma will migrate from the plasma chamber into the process chamber and act on the surface of the substrate to be treated. Thus, any impact of bombardment by charged particles is avoided, and only chemical etching by radicals will occur in the process chamber.

Fundamental understanding of the process inside the RPS plasma chamber is necessary for improving process parameters, particularly the etching rate. Therefore, microwave coupling and microwave distribution inside the plasma chamber are modeled by the finite element method (FEM). This facilitated developing a new RPS and analyzing the effect of different experimental parameters. As proof of principle, the experimentally obtained plasma pattern and simulation results of the electric field are compared in Figure 2. As expected, the plasma distribution matches the electric field

pattern. Further improvements achieved with the newly developed RPS are evaluated by plasma etching tests on standardized samples.

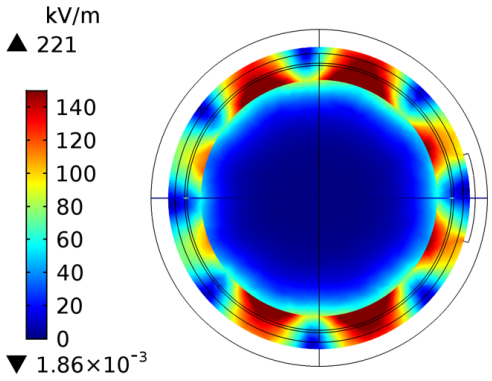

Figure 2a). Simulation of the electric field distribution inside the RPS.

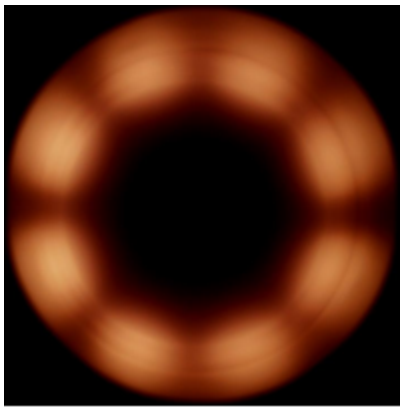

Figure 2b). Photograph of Argon plasma inside the RPS plasma chamber.

CONCLUSION

Microwave-induced plasma sources, e.g. downstream plasma sources and remote plasma sources in particular, offer a wide parameter range for a large variety of high-rate industrial applications. Fundamental understanding of the respective plasma process assisted by computer simulation is essential for targeted design of the plasma source.

Effectiveness of Selective Heating Using Semiconductor Microwave Generator in Food and Meal Field

Satoshi Horikoshi

Sophia University, 7-1 Kioi-cho, Chiyoda-ku, Tokyo, 102-8554, Japan

Keywords: Semiconductor microwave generator, Selective heating, Ripening of meat, Hospital food

INTRODUCTION

We have conducted microwave heating applications using semiconductor (solid-sate) microwave generators since the beginning of 2000. The use of semiconductor-based generators in chemical reactions offers various advantages, such as, the reactions using solid catalysts and chemistry free reactions [1-2]. On the other hand, when the semiconductor generator is used as a generation source for in-liquid plasma and it is generated by controlled pulse microwave irradiation, the life of the device (electrode antenna) can be extended to a practical level [3]. In this presentation, we will introduce the application to the food field, utilizing the features of such semiconductor generators.

RESULTS & DISCUSSION

Aging and quality improvement of meat: Microwaves are a kind of electromagnetic waves, so they have very high exergy energy. Traditionally, the combination of microwave and meat have been used for thawing and cooking (such as bacon heating) of meat. However, of the various types of energy, thermal energy is the lowest exergy, so using microwave energy for bulk heating is a waste of exergy. Our research strategy is an attempt to discover phenomena that other energies cannot imitate and apply them to the food sector. Because of the need for precise control, semiconductor-based generators are very effective microwave sources. One experimental example of direct heating of a substance by microwaves and an electromagnetic wave effect is shown below. The papain enzyme was used as a model enzyme. It is a cysteine protease enzyme largely used as a meat tenderizer via the breakdown of tough meat fibers, thereby rendering the meat easier to cook. This enzyme is extensively used in the textile, pharmaceutical, and cosmetic industries. If the enzymatic activity of papain could be enhanced by the microwaves' electromagnetic fields, it would lead to significant industrial benefits.

Possible changes in the degree of enzymatic activity in the papain-assisted hydrolysis of proteins in beef samples were examined by comparing microwave heating relative to conventional heating [4]. The hydrolysis in beef samples, whose surface was covered with the papain enzyme, was used as the model process (20×20×50 mm

rectangularly-shaped specimens). The papain-treated beef samples were subjected to pulsed microwave irradiation (PMI; 20-millisecond pulses; Fig. 1b) and to continuous microwave irradiation (CMI; Fig. 1c). Under microwave heating, the papain-treated samples of Fig. 1b-i and Fig. 1c-i softened in a manner suggestive of liquefied jelly when compared with the non-irradiated papain-free initial sample (Fig. 1a). This shows that exposing the papain-coated beef specimens to microwave heating enhanced the decomposition of the protein(s) on the beef surface. The degree of softness of the beef surface under PMI conditions was, to some extent, greater than under CMI. By contrast, by heating in an electric furnace at 45 °C for 10 min, the papain-treated beef sample of Fig. 1d softened much less than under microwave irradiation. Moreover, after the conventional heat treatment, the specimen's surface was unlike the jelly-like surface displayed by the samples of Fig. 1b and Fig. 1c. Experiments were also conducted at 50 °C (+5 °C) and 40 °C (–5 °C) in the electric furnace to examine whether errors in temperature measurements could explain this difference. There were no differences at both these temperatures. Accordingly, despite the same temperature conditions (45 °C), the microwaves promoted the activity of papain on the beef surface that we attribute to the microwaves' electromagnetic fields.

The results afford two possible mechanistic considerations. In the first instance, the hydrolysis of the beef protein(s) by the papain enzyme was enhanced under PMI compared to CMI conditions, as the applied microwaves power for PMI was 1.8 times higher than for CMI (11 W). The microwave power level influences the papain's activity and by the instantaneous electric and magnetic field enhancement under microwave pulsed irradiation. In the second instance, microwave heating occurred first in the inner core of the beef samples, and the surface temperature was that of the surrounding atmosphere, thus being cooler than the inner core, a temperature gradient was established under microwave heating. Consequently, some of the moisture contained within the bulk moved to the surface, thus causing the enzymatic hydrolysis reaction to occur mostly at the specimens' surface, as the extent of diffusion of the papain enzyme into the beef was limited. Thus, migration of the water in the bulk of the specimens to the surface had little consequence on any reaction occurring in the bulk. For the conventionally heated specimen, because the temperature inside the electric furnace was high, any moisture on the surface of the beef sample tended to evaporate, thereby causing the hydrolysis reaction at the surface to be inhibited, as evidenced by the results shown in Fig. 1d relative to Figs. 1b and c. In summary, compared to conventional heating, microwave heating presents certain features that promote the activity of the papain enzyme in the in vivo case that we attribute to the accelerating effect of the electromagnetic fields of the microwave radiation.

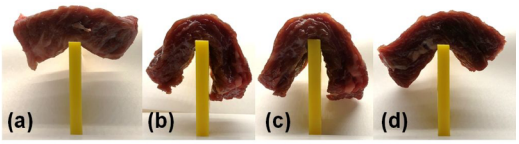

Fig. 1. Observations of the surface changes and the degree of beef samples after applying papain to the beef: (a) control experiment with no papain used on the beef, (b) papain-treated beef sample after heating with pulsed microwave irradiation (PMI) and maintaining it at 45 °C for 10 min (c) papain-treated beef sample subjected to continuous microwave irradiation (CMI) under otherwise identical conditions as in (b), and (d) papain-treated beef sample subjected to heating in an electric furnace at 45 °C for 10 min [4].

How can we commercialize such enzyme activities? There are many obstacles before it can be put to practical use. We tried to induce enzyme activity by microwaves into make aged meat in order to improve the added value of microwaves. Ripened meat improves the flavor and taste of the meat. For example, aged meat sold in American supermarkets is twice as expensive as untreated meat. This price difference requires a period (3 weeks to 2 months) to make aged meat and requires strict control of temperature and humidity. If it tries to activate enzymes in the meat and try to improve the concentration of amino acids that are the source of umami, the surface of the meat will be covered with mold. On the other hand, in conditions where mold does not grow, enzyme activity in meat does not improve. In order to solve this problem, we prototyped a device incorporating a semiconductor microwave generator.

Intelligent microwave cooker: Currently, eating habits take advantage of individual personality, food of various kinds and form in which it is being sold. On the other hand, the method of food heating is not added to most meals. The microwave oven is convenient to heat cooked food such as from supermarkets and convenience stores. However, it is impossible for individuals to set the temperature, and heating of the microwave oven is adjusted by the arrangement on the food, water concentration and salt concentration. In order to practice this innovation, we switched the microwave source of the microwave oven to the RF high power semiconductor generator (semiconductor type generator). There have been attempts to utilize semiconductor type generator for microwave ovens from long ago, but there was no one available with the size and price of the device, and it could not be put into practical use. However, in recent years we succeeded in ultra-miniaturization of the generator, and it is estimated that selling price will be sold at the same price as the current price if mass-produced. In this presentation we will introduce “intrigant microwave cooker” such as a new microwave cooking oven and new warm catering cart that the partial heating of foods for a lunch box and hospital plate meal using a semiconductor type generator. Furthermore, it also shows that in combination with the internet of things (IoT) can be effective when implementing and for sale at a market.

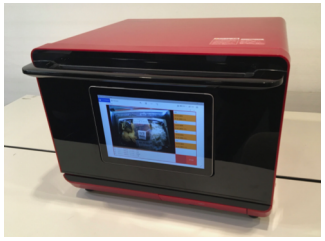

Fig. 2. Picture of intelligent microwave cooker

CONCLUSION

“Why do we need to use microwaves?” and “Why do we need a semiconductor generator?” This presentation will suggest this point with examples.

REFERENCES

[1] S. Horikoshi, N. Serpone (Eds) *RF power semiconductor generator application in heating and energy utilization*, Springer, Japan, 2019 will be published.
[2] S. Horikoshi, T. Watanabe, A. Narita, Y. Suzuki, N. Serpone, Sci. Rep. 8:5151 DOI:10.1038/s41598-018-23465-5 2018) 2019.
[3] S. Horikoshi, S. Sawada, S. Sato, N. Serpone, *Plasma Chem. Plasma Process.*, vol. 39 pp. 51–62 2019.
[4] S. Horikoshi, K. Nakamura, M. Yashiro, K. Kadomatsu, N. Serpone, *Sci. Rep.*, submitted 2019.

Microwave-assisted Regeneration of Zeolite 13X for CO_2 Capture

Candice Ellison[1,2], Dushyant Shekhawat[1]

[1]National Energy Technology Laboratory, Morgantown, WV, USA
[2] Leidos Research Support Team, Morgantown, WV, USA

Keywords: Carbon capture, sorbent, zeolite, microwave regeneration

INTRODUCTION

As sorbent regeneration imparts a significant energy penalty in conventional CO_2 capture systems, this study aims to accelerate desorption kinetics by application of microwaves. Microwaves are expected to increase regeneration rates by rapidly and volumetrically heating the sorbent. In addition, microwaves may promote CO_2 desorption by selective excitation of molecular bonds between CO_2 and adsorption sites, enabling regeneration at lower temperatures than would be required otherwise by conventional thermal methods [1].

METHODOLOGY

A fixed bed of zeolite 13X sorbent was supported in a quartz tube and placed inside a microwave waveguide applicator supplied by 2.45 GHz, 300 W continuous wave. The sorbent bed was pretreated under CO_2 gas flow until adsorption capacity was reached as indicated by online mass spectrometry. Desorption was initiated under N_2 flow by heating the sorbent to 200°C by microwaves and sustained until outlet CO_2 concentration returned to zero, indicating complete desorption. Parallel desorption experiments were conducted in an electric furnace to compare microwave with conventional heating.

RESULTS

Microwave and conventional heating were compared for their effect on CO_2 desorption rates from zeolite 13X sorbent. Sorbent regeneration by microwaves required only 5 minutes for complete desorption, compared to 10 minutes by conventional heating.

DISCUSSION

Microwaves were demonstrated to reduce sorbent regeneration times by half compared to conventional heating. Conventional heating is limited by conventional heat transfer mechanisms, resulting in slow temperature response in sorbents with low thermal conductivity. Under microwaves, heat transfer by dielectric loss enables rapid, volumetric heating of zeolite 13X, which exhibits good coupling with the applied electric field.

CONCLUSION

Microwaves proved advantageous for rapid regeneration of zeolite 13X, which was realized in half the time required by conventional heating. Consequently, microwaves could substantially reduce the energy penalty of sorbent regeneration compared to conventional systems.

REFERENCES

[1] T. Chronopoulos, Y. Fernandez-Diez, M. M. Maroto-Valer, R. Ocone, and D. A. Reay, *Micropor. Mesopor. Mat.*, vol. 197, pp. 288-290, 2014.

The Ecosystem of RF Energy: Design, Manufacture and Commercial Availability of High-Power Solid-State Microwave Generator Systems

Enver Krvavac and John Mastela

PrecisePower, Schaumburg, Illinois, USA

Kenneth Kaplan

Cellencor, Inc., Ankeny, Iowa, USA

Keywords: RF semiconductor device, Solid state microwave generator, RF Energy Ecosystem, Microwave applicator, System Design, System Manufacturing, System Integration

INTRODUCTION AND SCOPE

A large number of studies and experiments with Solid-State RF Energy have been published and demonstrated to date. The reasons for this are obvious, since the movement for Solid-State is gaining strength as part of reducing the cost of ownership, by offering better overall reliability and longer lifetime than incumbent magnetron-based RF energy systems. Solid state RF energy also has greater operating efficiency, field distribution, and precision control than is possible with conventional magnetron tubes, and additionally features graceful degradation (soft-failure).

The initial focus, and understandably so, of development of the solid state RF Energy generation has been on the basic technology enabler, the RF semiconductor device; and its manufacturability. The next milestone was the first successful prototype of the generator. To enable the commercial availability of dependable solid state microwave generators, the overall RF Energy ecosystem must be achieved with the disciplines of Design for Manufacturability (DFM), Design for Test (DFT), Design for Cost (DFC), and Design for Reliability (DFR). To complete the ecosystem, customer specific application and end-user system integration should be understood upfront with early engagement. Specific application and system integration include the necessary generator RF power output requirements and the selection of either individual high-power waveguide outputs, or multiple coaxial RF outputs and final integration with the microwave applicator.

This paper discusses the specifics of the solid state RF Energy ecosystem pyramid (Fig. 1) to achieve the widespread commercial success of high-power solid-state generators.

THE CONCEPT OF AN ECOSYSTEM

An ecosystem is defined (Dictionary by Merriam-Webster) as the complex of a community of organisms and its environment functioning as an ecological unit. It can also be defined as something (such as a network of businesses) considered to resemble an ecological ecosystem especially because of its complex interdependent parts.

With respect to the emerging Solid-State RF Energy, we can envision a type of ecosystem emerging. In this system, collaboration between multiple key participants will be required to create a design, manufacture, and supply chain pyramid.

1. Semiconductor device manufacturers are in the middle of the pyramid as this is the technology enabler and is the heart of the Solid-State RF Energy concept.

The best Solid-State, RF energy generators, especially those for industrial applications, such as food processing, drying, agriculture, medical care, and automotive ignition, will have to start with the right choice of discrete or integrated (pallet or module) transistors. Several semiconductor device technologies are available today to amplify both continuous-wave and pulsed signals to be used in these RF generators: LDMOS and gallium nitride, both on silicon carbide (GaN/SiC) and silicon (GaN/Si). Each technology offers its own set of characteristics in terms of power, efficiency, and gain.

Careful evaluation of performance tradeoffs related to cost should be undertaken. However, one must not overlook key attributes of reliability and ruggedness of the transistor that will be used for industrial applications. Close and upfront collaboration must be taken up with the semiconductor manufacturers to ensure the reliability and ruggedness are met for each specific end-use application. For example, in addition to high temperature life time DC cycling, traditionally done by the manufacturers, reliability must be demonstrated, both for discrete and integrated transistors, under RF power cycling for various duty cycles, fast and slow or high and low.

2. System Design and Manufacturing are to the bottom left and right of the pyramid and both are fed down by the semiconductor device.

Obviously, the advancement of solid state generators has been tied to the improvements in the RF semiconductors. However, it should not be limited in scope and vision. Beyond the transistor, the system designer within the ecosystem, must use robust design approaches with respect to electronic, mechanical, cooling, software/firmware, and reliability to achieve performance goals and to ensure that the product will have a long life in the field. Software/firmware is integral to the design and performance of the Solid-State RF generator. The generator's ability to function in the end-user system, with varying loads, can only be accomplished with embedded software/firmware (Fig. 2). The software's capability includes rapidly sweeping frequency, pulsing power, and phase adjustment, features not available with magnetron-based generator.

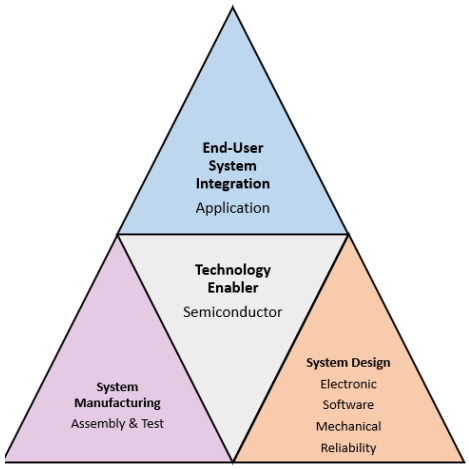

Figure 1. Solid-State RF Energy Ecosystem

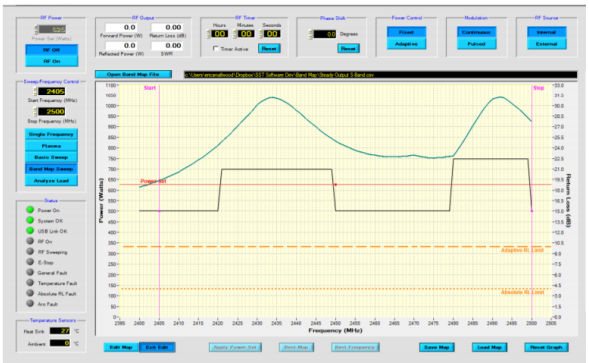

Figure 2. Software for Solid-State RF Generators

To ensure long life and high reliability of the product, the system designer should incorporate all proper design methodologies, including (and not limited to): active and all passive component thermal analysis under standard and extreme conditions; thorough performance characterization and analysis at all standard and extreme test conditions; long term RF signal and thermal cycling test; MTTF calculations and active device junction and passive components temperature measurements (Fig. 3).

Ideally, the system designer and the manufacturing facility should be the same entity to ensure a good overall design. With proper protocols and processes for assembly, as well as reliability check points, overall robust design can be achieved. For example, x-ray inspection of RF device attachment (Fig. 4) may be part of the reliability test process.

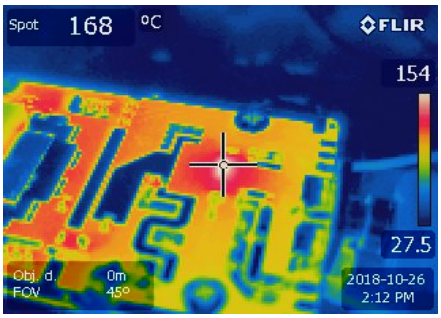

Figure 3. IR scan of active and passive components

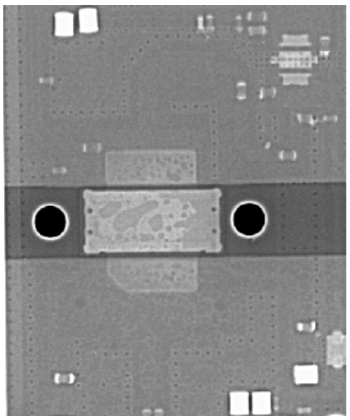

Figure 4. X-ray of pallet showing undesirable voiding under RF

3. End-User System Integration is at the top of the pyramid and is fed by system design and manufacturing.

Integration is where the concept becomes a reality, where the end-user can use the product after it has been fully developed. It starts with a definition of performance requirements that specifies each component and how they are integrated. This involves top down planning and bottom up engineering (semiconductor device, system design and manufacturing). In collaboration with the end-user, a unique design for the applicator/chamber may be developed at the same time. The end result will be a system that fully meets the user's requirement.

CONCLUSION

The adoption of solid state RF Energy technology resides in multi-layered ecosystem building. The ultimate industrial adoption of solid state RF generators requires seamless coupling between multiple entities: semiconductor device manufactures, system design and manufacturing, and end-user system integration.

The solid state RF technology/design that can gain the most momentum in this ever-changing ecosystem will survive and eventually thrive.

REFERENCES

[1] Mark Murphy, Electronic Design Magazine, "Here Comes the Solid-State RF Energy Evolution", March 10, 2018
[2] Norm Dye and Helge Granberg, Radio Frequency Transistors: Principles and Practical Applications, Butterworth-Heinemann, Newton, MA, 1993, pp. 71-81

Design of a Trailer Mounted Microwave Weed Control System

Graham Brodie and Paul Prater

[1]Dookie Campus, University of Melbourne, Nalinga Rd., Dookie, Victoria, 3647, Australia

Keywords: Microwave weed control, field demonstration, trailer system.

INTRODUCTION

Modern no-till cropping depends on herbicides for weed management; therefore, herbicide applications are an important system input. Unfortunately, herbicide resistance in many weed species is becoming wide spread [1] and multiple herbicide resistances in several economically important weed species has also been widely reported. In time, herbicide resistant weeds will ultimately result in significant crop yield reductions and grain contamination [2]. Davis et al. [3, 4] were among the first to study the lethal effect of microwave heating on seeds and emerged weed plants; however, herbicide treatments were far cheaper than microwave treatment at the time of their experiments and herbicide resistance was not an evident problem. Since then herbicide resistance has become a significant problem and the International Agency for Research on Cancer (IARC), which is part of the World Health Organization (WHO), concluded that glyphosate is probably carcinogenic to humans. Therefore, alternative weed control strategies, like microwave treatment, need to be revisited; however, practical field demonstration was needed for conservative industries, like the agricultural sector, to consider technology adoption. This paper presents the design of a trailer mounted microwave weed killing system for field demonstration purposes.

METHODOLOGY

To facilitate relatively close, safe observation of the microwave weed killing process during field demonstrations, a trailer mounted system was built around four independently controlled, 2 kW, fixed power, water cooled microwave generators, operating at 2.45 GHz. The trailer is a dual axel, 2.4 m by 1.8 m (8’ by 6’) metal trailer. The magnetron heads are supplied via switch-mode power supplies and the electrical power for the system is provided by two 3-phase, 7 kVA, gasoline generators, mounted on the trailer (Figure 1). Industry standard switch gear and the switch-mode power supplies for each magnetron head are housed in a weather resistant cabinet, at the front of the trailer. Operator controls are located on the outside of this cabinet, for easy access. Wave guides and horn antennae channel the microwave energy from the magnetron heads to the soil surface. The antennae are spaced apart, across the width of the trailer, to demonstrate that inter-row microwave treatment could be used to kill weeds emerging between the rows of

a standing crop without damaging the crop plants themselves. A metal chain is dragged along the ground to provide an electrical earth, when the trailer is in operation. Microwave field strength was measured at the operator's point near the front of the trailer, the hitching point for the trailer, and in the various directions from the horn antenna, using a Tenmars TM-194 microwave leakage detector. Initially, coolant was circulated through a large radiator; however, this was found to be inadequate on hot days and a refrigerated cooler has been installed to provide more stable coolant temperatures for prolonged operation. The choice of 2 kW fixed power microwave generators was based on allowing close observation of processes under experimental conditions, while still allowing small scale field demonstrations to be conducted for agriculturalists.

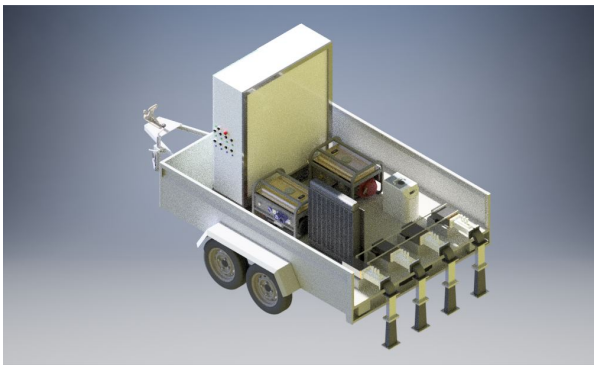

Figure 1. Rendered image of the original trailer design.

RESULTS

The trailer system has been used over much of the south east portion of Australia (New South Wales, Victoria, and South Australia). It has performed over 1000 hours of experimental and demonstration work, without major concern. Initially, there was an over-heating problem, when the ambient temperature was above 30 °C; however, this has since been overcome by using a refrigerated water cooler to provide a more stable coolant temperature. The time average field strength at the location of the operator for the trailer system was measured at 13.2 V m^{-1}. This is well below the allowable exposure for both the operator and for the public (i.e. 61.4 V m^{-1}). Safe approach was determined to be at 2.5 m from the unshielded antenna, so close quarters public demonstrations are made with mesh shielding over the antennae and having the public at least 3 – 4 m from the antennae. Antenna height above the ground profoundly affects the weed and soil heating ability of the system (Figure 2). With the antennae positioned at about 1 cm above the ground, the trailer system is effective at killing weeds at an operating speed of about 1 – 2 km hr^{-1} (Figure 3a). Three-stub tuners allow impedance matching between the antenna to the plants and soil. Matching is based on power monitoring at the circulators of the microwave generators, which include probe points for measuring forward and reflected power, with a -57 dB power coupling factor. In the future, increasing the microwave generators' power will allow much faster operating speeds. The trailer has been successfully demonstrated in a wide range of weather conditions from hot days (> 37 °C) to cold, drizzly, windy winter conditions. In all cases, weed destruction and soil heating efficacy was evident, with no

threat of fire. Based on knowledge gained from this trailer and development of evanescent field applicators, a more commercial four by 20 kW system, powered from the PTO of a tractor, is being developed (Figure 3b).

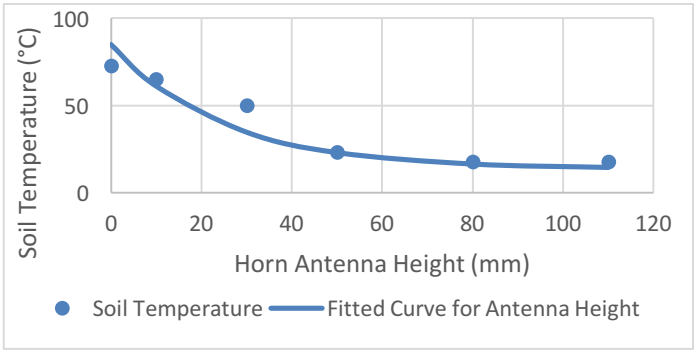

Figure 2. Effect of antenna height above ground on soil temperature, after 15 seconds of heating.

(a) (b)

Figure 3. (a) Microwave treatment of kikuyu grass – equivalent to approximately 1 km hr^{-1} and (b) proposed new weed killer system

CONCLUSION

Development of the trailer mounted system has allowed the industry to better understand the technology and has therefore generated considerable interest in microwave weed control.

REFERENCES

[1] I. M. Heap, The occurrence of herbicide-resistant weeds worldwide, *Pesticide Science,* vol. 51, no 3, pp. 235-243, 1997.

[2] G. Brodie, Derivation of a Cropping System Transfer Function for Weed Management: Part 1 – Herbicide Weed Management, *Global Journal of Agricultural Innovation, Research & Development,* vol. 1, no 1, pp. 11-16, 2014.

[3] F. S. Davis, J. R. Wayland and M. G. Merkle, Ultrahigh-Frequency Electromagnetic Fields for Weed Control: Phytotoxicity and Selectivity, *Science,* vol. 173, no 3996, pp. 535-537, 1971.

[4] F. S. Davis, Wayland, J. R. and Merkle, M. G., Phytotoxicity of a UHF Electromagnetic Field, *Nature,* vol. 241, no 5387, pp. 291-292, 1973.

Design Approach for High Power Solid State Generator

M. Garuti[1], F. Braghiroli[1] and F. Garuti [1]

[1]MKS Instruments Alter Products, Reggio Emilia, Italy

Keywords: Solid State Microwave generator, High Power Generators, RF Power Amplifier.

INTRODUCTION

We have witnessed a constant and greater dissemination of deposition processes and growth of pure materials through PE-CVD processes in the past few years. A clear example is the dynamic market of synthetic ornamental gems, such as diamonds.

In said processes, synthesis gas is brought to its ionised state (plasma) through microwaves with significantly high power between 10 kW and 50 kW, depending on the design of the system, in the frequencies of 2450 MHz for power less than 15 kW and 915 MHz for power greater than 15 kW.

Said processes are distinctive because they are discontinuous and extremely long; in some cases they reach 1,000 hours of continued operation and any interruption jeopardises the result.

Today, all the applications use classical microwave generators with magnetron and sophisticated power systems capable of guaranteeing the best possible control of the magnetron and its uptime.

Nevertheless, magnetron is by design a component subject to wear and requires replacement after a few thousand hours. It is common to reach 10,000 hours of operation, but in the above-mentioned applications it is preferable to use a maintenance plan and replace magnetron before is worn out.

Solid state microwave generators potentially offer an excellent solution for the life limitations of magnetron, as they have a much higher estimated life and greater output power stability, all benefits of great value for the above-mentioned processes.

In addition to these benefits, there is frequency control within the allowed range, a characteristic that is not allowed with the magnetron and a narrow-band emission that is better than any magnetron in terms of quality.

The purpose of this project is to describe the concepts adopted in designing an industrial solid state power generator 8 kW @915 MHz that allows the identification of the necessary scale-up in order to offer multi-kilowatt solutions.

CONCEPT CRITERIA

As known, solid state generators are essentially power amplifiers with different cascade amplification stages. The amplification ratio normally adopted on each stage is between 12 and 18 dB which means that the input signal is multiplied 30 through 60 times for each stage.

As the initial reference signal that defines the operating frequency of the entire amplifier has a power of the order of 50 mW, as previously mentioned there is a need of at least 3 or 4 series amplifiers in order to obtain the power of the order of several hundred of Watt.

The power transistor market capable of operating at microwave frequencies is huge, especially at low continuous power, while it is significantly smaller if we look for components capable of delivering power of the order of several hundred of Watt in continuous mode, namely power that has a meaning to those who intend to develop solutions for industrial applications.

In particular, at the frequency of 2450 MHz, the market offers transistors with a unit power of about 300 W, while at 915 MHz (another frequency in the ISM band) there are transistors available at 750W and more.

Therefore, the topology adopted to make a solid state amplifier with continuous power with value ranging from 1 to 2 kW, a significant range to hypothesise an industrial application, is a topology that relies on cascade amplification stages for low power and parallel amplification stages to reach the above-mentioned values.

The diagram below gives a better understanding of the concept. The first three amplification stages A1-A3 raise the input signal to a major level for the last A4 stages which have unit power of several hundred of Watt each. These last amplification stages are used in the "parallel" configuration and their outputs are then joined with a final device called combiner whose purpose is to add said values and bring it to the output.[1]

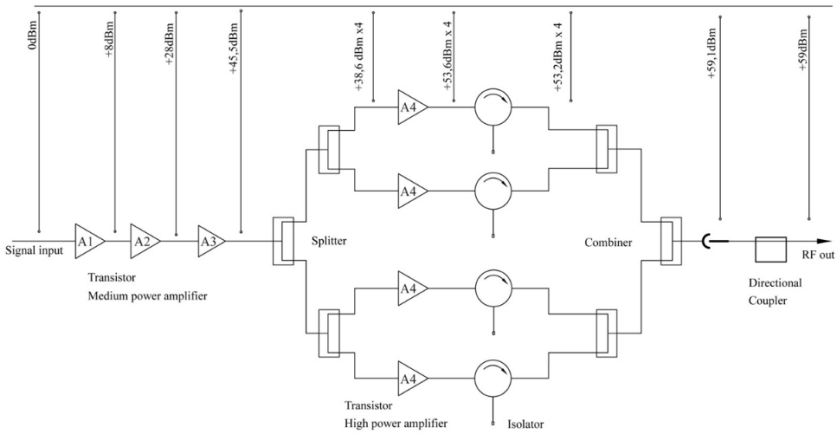

Figure 1. Schematic diagram of a solid state microwave power amplifier>1 kW

DISCUSSION

In the proposed diagram, the end amplifiers are protected each with an isolator. In some topologies, the isolation is made at the end after the combiner with a single isolator of proper power. With this topology, the output power for each amplifier is of the order of 1.5-2 kW at 915 MHz.

In order to offer solutions that allow for a significantly higher power, there are two possible ways. Either develop an end applicator that allows the input of an "n" sources of single power like above, or the develop a generator that "combines" all the sources and offers a single output with power that is the sum of the contributions of each source.

The first case, many sources that deliver the power in the same cavity, obviously require a proper analysis of the interference that each source can cause to the other (cross-coupling) and will impose some building compromises. On the other hand, it gives the possibility to distribute power on each source with phase, frequency and power, regardless of the others, if the generator of the reference signal allows it. It is a configuration hypothesis that opens the possibility to control the distribution of energy in the cavity in an unthinkable manner with conventional magnetron sources. This is an application field to be explored.

The second type of generator, that combines several sources and that has only one output, allows the direct replacement of an existing conventional magnetron generator and offers, in addition, control of phase and frequency (obviously within the allowed range).

This configuration requires a project effort on the power combiner that receives a plurality of sources as input and presents the sum of the previous in single power output. Said combiner requires a proper electromagnetic design capable of optimising the geometry to reduce the inevitable loss of energy.

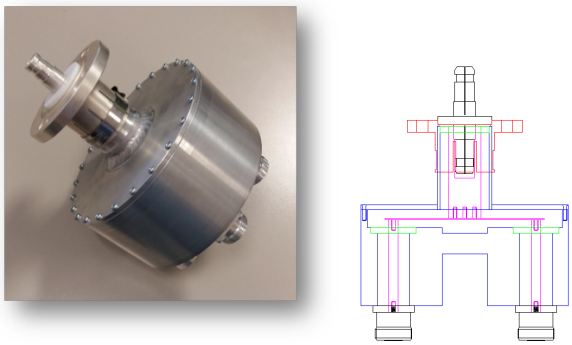

Figure 1. Power combiner 6 to 1 and initial EM design

CONCLUSION

This project focuses on a concept design of a solid state generator with a single power output of 8 kW @915 MHz, consisting of six unit power sources of 1.5 kW each, with a combiner device with 6 inputs and 1 output.

REFERENCES

[1] US Patent 9,595,930 B2 – Garuti et al., MKS Instruments Inc.

Investigation into Dielectric Sample Heating using Active Load Techniques with Coherent Dual Channel Microwave Solid State Generators

R. Wesson

MACOM, Nijmegen, Netherlands

Keywords: IQ Correction, Coupler Directivity, Calibration, RF Energy System Measurement Accuracy, Dielectric Sample Heating, Phase Substitution Technique.

INTRODUCTION

Dielectric sample heating is a field of interest in biochemistry, chemistry and medicine. Solid state technology is gradually being applied to fields of science and industry where poorly controlled valve based technologies have long held sway due to the high power levels or efficiencies required. In this paper we apply MACOM's RF Energy heating system-in-a-box to a dielectric heating challenge, on a small scale such as might be beneficial in a research lab rather than a production line. The paper takes a first look at how to achieve the measurement accuracy required for this application and proposes correction techniques that improve the precision of measurement and hence of energy delivery to the load.

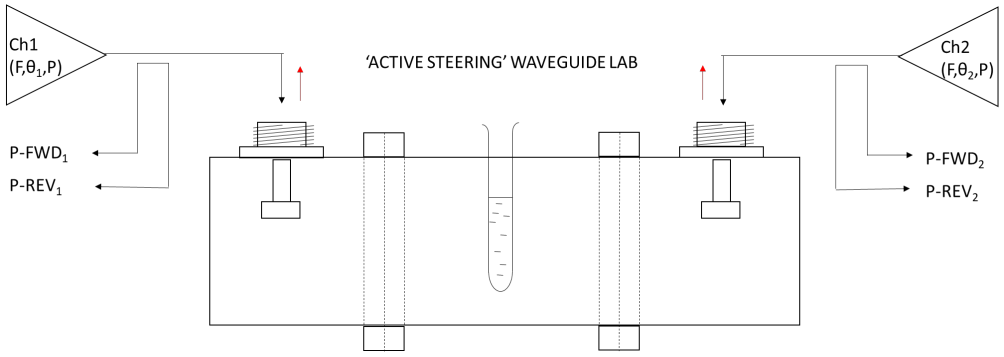

Figure 1: Active Load Waveguide Lab Concept

The prototype actively steered 'waveguide lab' dielectric sample heating system shown in Figure 1 and Figure 2 can be tested with the sample tube empty with a 360 degree phase sweep. The expected result is that there should be very little power dissipated and the channel 2 receive power should be the same as the channel 1 forward power across all angles. Rather, large variations are measured in FWD and REV power levels (Figure 3).

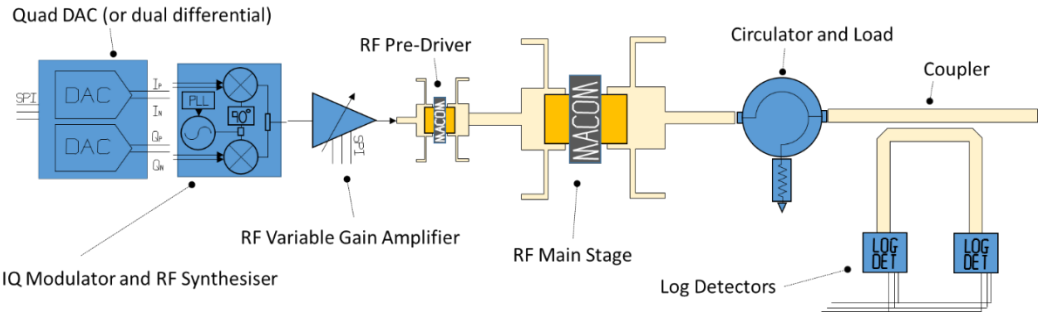

Figure 2: Elements of Typical RF Energy Power Module

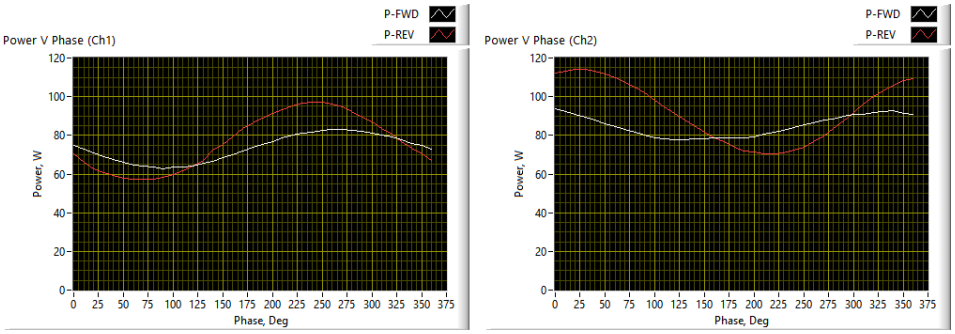

Figure 3: Baseline performance plots of 'waveguide lab' system.

With such large variations, it is tricky to determine exactly what is going on. Are the observed power variations genuine, or artefacts? In fact, we have a mix for both.

IQ ARCHITECTURE & COUPLER RELATED MEASUREMENT ERRORS

RF Energy Systems typically make use of an IQ architecture for generation of precise phase and amplitude signals. In communication systems these signals are modulated, but in RF Energy systems they are used pseudo-statically to provide precise phase and amplitude control. IQ DC offsets and gains should be corrected to mitigate power variation over phase angle, with 1dB variation measured in the uncalibrated test system.

Stable forward power over phase angle is one prerequisite for accurate dielectric heating, but is only one of the mechanisms involved in the initial observations of Figure 3. The accuracy of a multichannel RF Energy measurement system can be evaluated by connecting two channels together and transmitting directly from one into the other.

The directivity equations in

Figure 4: Directivity Correction Math can be used to give us S1 and S2 as a function of M1 and M2 and the (symmetric) directivity D. Knowing that the forward power should be flat we can optimise D for flatness of S1 from M1 and M2, and the same correction applied to S2. Scalar systems lack the phase measurement needed to fully implement this correction so a phase substitution technique is proposed that uses the only phase information that is known in typical RF Energy use cases, the set phase. This value is substituted into the

scalar measurements to give an indication of the phase relationship between the wanted and parasitic components, from which a complex vector is 'best fitted' for flat responses.

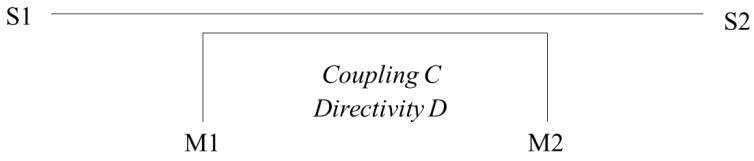

$M1 = S1.C + S2.C.D$ $M2 = S2.C + S1.C.D$

$M1/C = S1 + S2.D$ $M2/C = S2 + S1.D$

For simplicity we assume C = 1 (we're only interested in getting clean, proportional results)

$M1 = S1 + S2.D$ $M2 = S2 + S1.D$

$S1 = M1-S2.D$ $S2 = M2-S1.D$

Bringing S2 into S1…

$S1 = M1-(M2-S1.D).D$

NOTE: S1,S2,M1 and M2 are complex values with phase as well as magnitude

$S1 = M1-M2.D-S1.D^2$

$S1+S1.D^2 = M1-M2.D$

$S1(1+D^2) = M1-M2.D$

$S1 = (M1-M2.D)/(1+D^2)$

… and by symmetry…

$S2 = (M2-M1.D)/(1+D^2)$

Figure 4: Directivity Correction Math

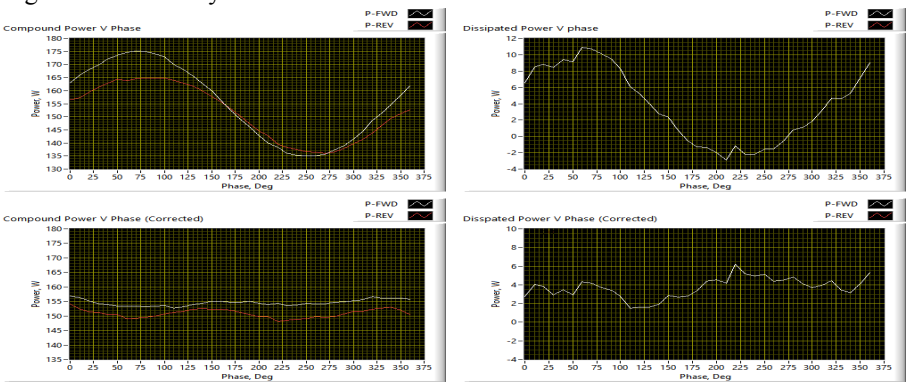

Figure 5: Raw and Corrected FWD and REV power measurements using Phase Substitution

CONCLUSIONS

The transition to solid state power generation for heating applications can be motivated by the ability to control signals precisely and to measure power delivery to RF loads by accurately assessing forward and reflected power. The following steps are recommended to ensure systems operate as intended: IQ DC offset and gain imbalance correction should be incorporated. All couplers should be of type 'symmetric' and placed on the 'hot' side of the circulator. Systems should incorporate phase measurement as well as amplitude to facilitate calibration that generalises to complex loads.

Utilizing Independent Parallel Outputs from High Power Solid State Microwave Generators

Kenneth Kaplan

Cellencor, Inc., Ankeny, Iowa, USA

Keywords: Solid state microwave generator, microwave applicator, circularly polarized patch antenna, high power microwaves

INTRODUCTION

High power solid state microwave generators are now commercially available. Some microwave generators, such as the PrecisePower family, optionally offer multiple coaxial RF outputs instead of a single waveguide output. Using multiple outputs and antennas allows the development of radically new kinds of applicators with finely controllable and superior energy distribution characteristics. The purpose of this study is to compare this new configuration with traditional magnetron-style waveguide feeds.

EXPERIMENTAL APPARATUS AND PROCEDURE

The notional design of a high power solid state microwave generator comprises a number of lower power amplifier modules operated in parallel, with outputs combined to provide a single high power waveguide output, analogous to the output of a magnetron power head. For example, an 8 kilowatt generator utilizes eight 1 kilowatt power modules. Usually the outputs are combined to provide a single waveguide output. The PrecisePower solid state generator architecture optionally allows each power module to feed an independent RF output which can be connected to multiple antennas using convenient coaxial cable feedlines. Each RF output can be independently controlled with respect to frequency, phase, power output, and modulation. The user software supports this alternative configuration and allows control of each module independently or all modules as a group.

A new type of high power planar patch antenna (Fig. 1a) was developed for use as a basic feed element. The antenna is constructed of thick, extremely low loss, and highly thermally conductive substrate material with heavy copper cladding. The coaxial connector is a 7/16 DIN type. The antenna is capable of handling over 1 kilowatt of continuous power at 2450 MHz. The design produces a circularly polarized wave with an optimal balloon-shaped pattern (Fig. 1b) [1]. When a circularly polarized wave is reflected from a surface (such as from the load or the bottom of the applicator), the

direction of rotation reverses. The reflected wave does not couple with the incident wave. Therefore, the "hot spots" and "cold spots" typical of multimode applicators with typical linearly polarized feeds do not develop [3].

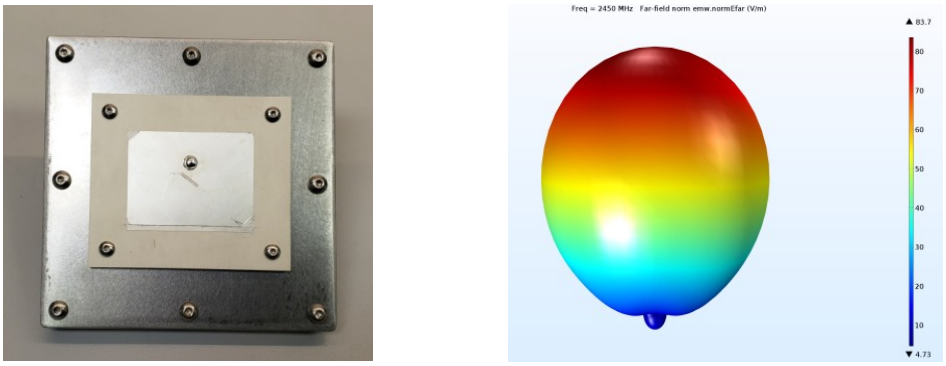

Figure 1. (a) Circularly polarized high power patch antenna, and (b) far field plot of same antenna

A COMSOL Multiphysics model of a loaded applicator with four such antennas was created (Fig. 2). A model with identical dimensions and load with a single waveguide feed was also created for comparison.

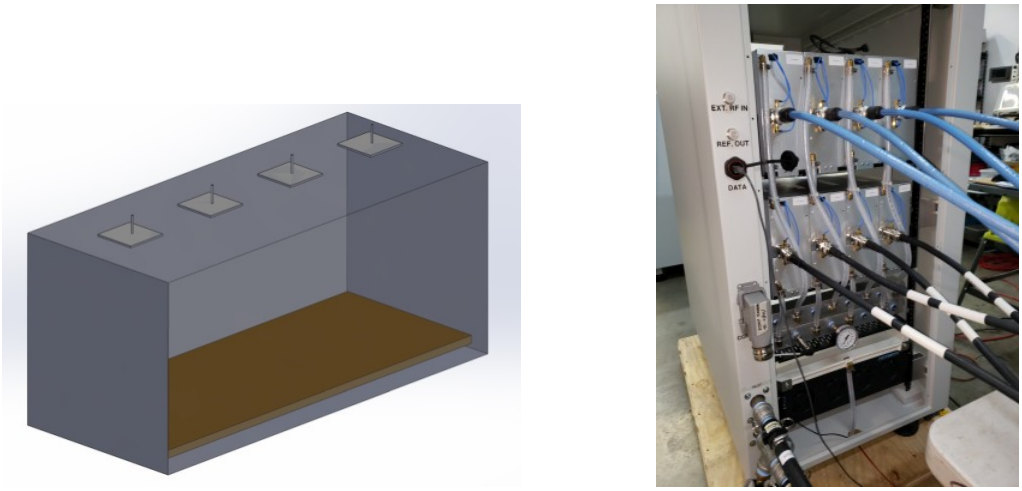

Figure 2. (a) 3D rendering of applicator used in the COMSOL model. Four patch antennas are on the top surface. The brown slab is the load which has a moderate dielectric constant of 7. (b) An 8 kilowatt PrecisePower generator (with rear covers off) showing the power modules and their individual coaxial RF outputs.

RESULTS AND DISCUSSION

COMSOL 3D simulations of the two applicator configurations show dramatic differences in the electromagnetic energy distribution within the applicators. Figure 3a

shows the waveguide fed version, which has an energy distribution with scattered nodes typical of a single feed to a multimode cavity. The field is strongest in the central region under the feed, and there are multiple hot and cold nodes distributed through the cavity. In contrast, the multiple antenna versions (Fig. 3b) shows strong linear vertical fields evenly distributed throughout the cavity on both the X and Y axes. This clearly illustrates the elimination of nodes due to the circular polarization of the waves. As a result, heating of the load will be much more uniform than the waveguide fed version.

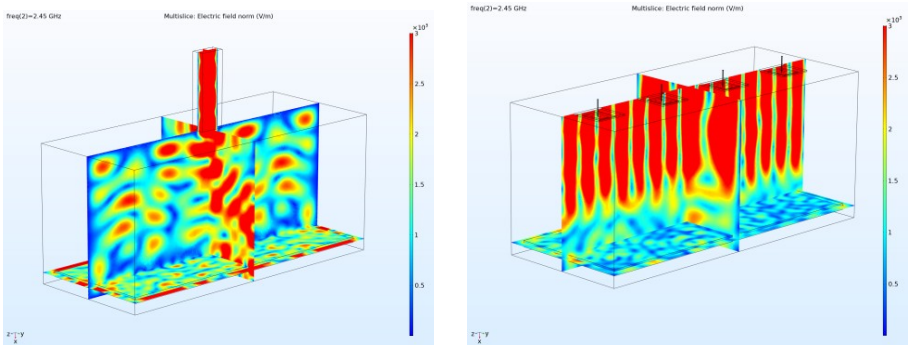

(a) (b)

Figure 3. COMSOL model results of (a) applicator fed top center with WR-340 waveguide, and (b) top fed with four circularly polarized patch antennas. The patch antennas are fed in phase. Both models are excited at the same input power levels.

Antenna placement is very important. Other arrangements, especially rows of antennas at right angles, can produce other highly useful patterns including energy concentration in well-defined areas. Circularly polarized antennas are especially suitable for beam forming applications where the relative phases of the antenna feeds are shifted [2]. Mechanically, these antennas are highly compatible with applicators operating at high pressures and/or temperatures.

CONCLUSION

High power microwave generators with multiple outputs driving circularly polarized patch antennas offer microwave system designers a new and highly effective means to build finely tuned and effective applicators for a wide variety of applications. There are many other aspects of this technique which are ripe for future investigation.

REFERENCES

[1] C. A., Balanis, Antenna Theory, Analysis and Design, 4th ed., Wiley, N.Y. 2016, pp.784-815.
[2] R .J. Mailloux Phased Array Antenna Handbook, 3rd ed., Artech House, Norwood MA, 2018 pp. 280-294
[3] M. S. Miller, Microwave Oven Cavity Excitation Employing Circularly Polarized Beam Steering for Uniformity of Energy Distribution and Improved Impedance Matching, U.S. Patent 4,336,434, 1982

Design of a Microwave Cavity for an Atypical Commercial Application

John F Gerling

Gerling Consulting, Inc., Modesto, CA, USA

Keywords: Microwave cavity, microwave heating, electromagnetic modeling, commercial microwave oven

INTRODUCTION

Microwave ovens (MWO) designed for commercial applications typically resemble those for residential use. That is, both oven types employ large multimode cavities that satisfactorily heat a variety of food articles having different shapes, sizes and types. A major difference between them is that most residential MWOs feature a turntable to enhance microwave coupling and heating uniformity while commercial MWOs instead use a mode stirrer in an attempt to achieve similar performance. However, such features may not be practical in small cavities designed to meet unusual geometric constraints. This limitation may lead to a design challenge depending on the variety of food articles for which the MWO is intended.

METHODOLOGY

The application in this study involves a custom-designed commercial MWO to heat various substances contained in a cylindrical product package of various sizes. Dielectric properties of each of five samples were measured within the nominal heating temperature range (Figure 1).

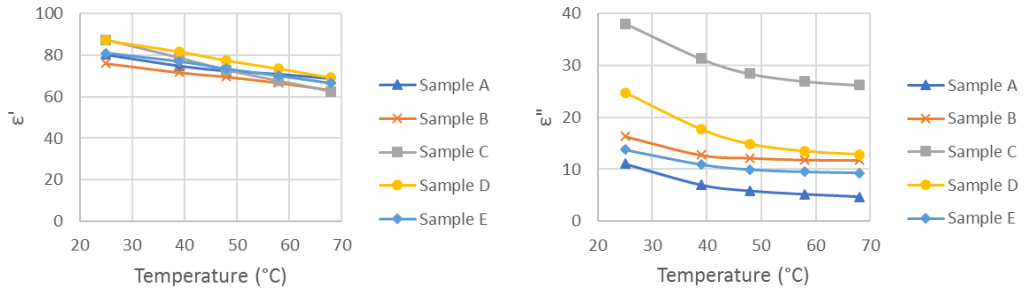

(a) (b)

Figure 1. Measured dielectric constant (a) and loss factor (b) for five product samples.

The cylindrical packages were the same diameter but varied in length, in some cases different lengths for the same material. The design criteria included a desired heating rate that, assuming a minimum microwave coupling efficiency of 80%, yielded a

calorimetrically determined minimum input power requirement of approximately 2 kW for the largest volume package. Cost factors favored a microwave power delivery configuration using two identical 1 kW magnetrons. Other design criteria were the height and footprint of the MWO which were limited due to operator height and available counter area. These criteria, along with considerations for manufacturing and maintenance costs, yielded an upright cavity geometry as shown in Figure 2. Design criteria for handling the product resulted in its location close to one wall.

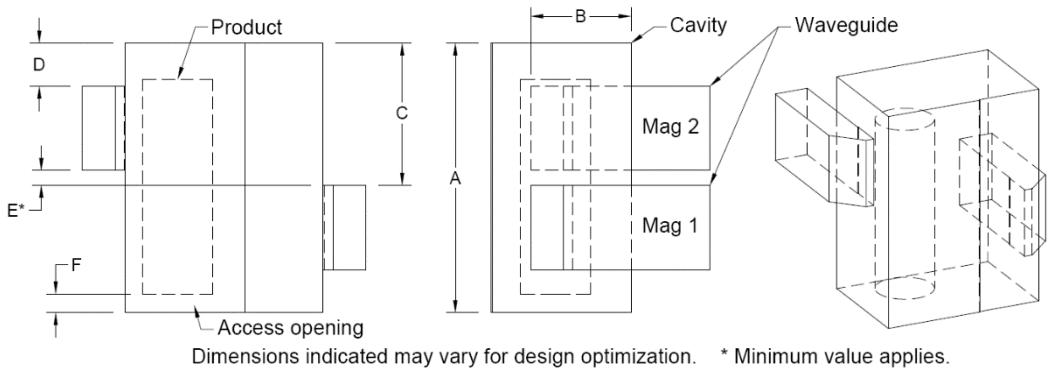

Figure 2. Cavity outline and product location showing variable dimensions for optimization.

For cavities that are small relative to the load size, it is often possible to find a geometry that maximizes microwave coupling efficiency and heating uniformity for a given load. However, when optimizing for multiple load types, a single cavity geometry rarely achieves the best possible performance for each individual load. Consequently, performance compromises are made for some loads to achieve the best possible overall performance for all loads.

The optimized cavity geometry is found using computational techniques to simulate the electromagnetic fields in and reflections from the cavity. The frequency characteristics of the reflection coefficient were computed for the electromagnetic field absorbed for each load material, geometry and values of complex permittivity. Cavity dimensions indicated in Figure 2 were varied between iterative computations for each set of five product samples. Variables B, C and D were found to have the most influence in overall performance.

RESULTS

It was found that variations in material parameters had less influence on performance than sample size. As shown in Figure 3, larger samples generally coupled well to microwave energy from both sources while smaller samples coupled better to one source than the other. Conveniently, temperature also had minimal influence on performance for all samples as suggested by the similarity between curves at the temperature extremes.

Heating uniformity within each volume varied between different product package sizes. In some cases the heating profile indicated concentrations of heat absorption, suggesting that product substances lacking the ability to rapidly diffuse the heat may not yield favorable results. However, liquid substances in this study were of low viscosity

which facilitated heat dissipation and temperature uniformity by the presence of convective flows within the volume.

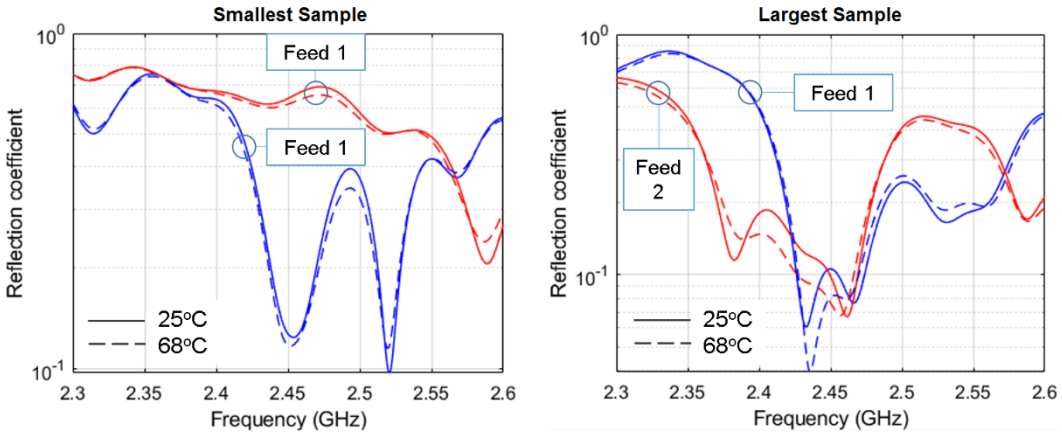

Figure 3. Computed reflections from the design cavity for small and large samples.

DISCUSSION

As expected, a cavity geometry that maximizes performance for all samples could not be found. Good coupling was achieved for large samples with both microwave sources while small samples performed well with only one source. However, noting that small samples require less power to achieve the desired heating rate, good coupling with only one source or marginal coupling with both sources was deemed acceptable. Additionally, sample materials having a high capacity for heat dissipation (e.g. due to convective flows in low viscosity liquids) can achieve satisfactory overall heating uniformity.

CONCLUSION

A microwave cavity was designed for a commercial application to heat various liquids in containers of various sizes. The cavity geometry was determined using computational techniques to optimize overall performance for all articles to be heated. Results indicate sufficient coupling efficiency and heating uniformity to achieve the desired outcome of the design effort.

The RFEA is Dead – Long Live the RFEA within IMPI

Dr. Klaus Werner

pinkRF, RFEA *(formerly),* The Netherlands

Keywords: solid state RF energy, RF Energy Alliance, IMPI, microwave technology

INTRODUCTION

The Radio Frequency Energy Alliance (RFEA) was founded in October 2014 to promote and facilitate the introduction of a revolutionary technology into consumer and commercial cooking appliances. This solid-state RF technology is able to generate powerful microwaves from semiconductor devices (hence the "solid state") and puts those to very finely controlled use inside a novel RF powered oven to perfectly cook our food in a minimum amount of time. Driven by the whitegoods companies, the organization has worked on technologies and standardization to bring cost down swiftly and increase the speed of adoption.

Forward 4 years, we need to conclude that the technology has not seen the intended mass-market uptake, yet. The developments to reduce the cost have taken longer than anticipated and certainly the consumer-oriented companies have delayed or paused the development efforts all together with only a few exceptions.

The delay of the commercialization of RF Energy applications has clearly impacted the RFEA organization; members resigned and the financial backing as well as the overall mandate eroded. Finding new members in more "classical" industry realms proved to be difficult in view of differentiation and IP. The leadtime to develop and market industrial machines is typically much longer than for consumer devices. In short, the "appetite" for industrial users to join was limited.

The RFEA organization has reviewed the situation and found that the reasons to work on this technology as an industry consortium have not changed. Those are as valid as they were during the inception of the RFEA, so it was clear to continue the work, but also that the organizational structure had to change as well.

In short, this led to a review of possible partner organizations. IMPI clearly stood out with respect to membership diversity, mandate and volume, scientific backing and legacy. Fortunately, the IMPI Board was very willing to cooperate and accepted

the idea to act as "safe haven" for the RFEA heritage. We're currently in the process of ramping up solid state RF-focused activities within IMPI.

The panel discussion will give further details of this new "working environment"; the way it functions, the topics and routine at hand and the ways to join the team that continues to work on various aspects of solid state RF technology. Objectives for the team are amongst others to promote the solid state RF technology and to establish a globally important community and platform for solid state RF Energy powered systems, with all roles along the value chain eco system are represented. Typical activities encompass training sessions internal and external to IMPI, and representation of the team and the work at trade shows and conferences. Furthermore, workgroups will be created to discuss and align on overarching value chain topics like hardware and software standards to enhance user experience and reduce the design-in burden of system engineers.

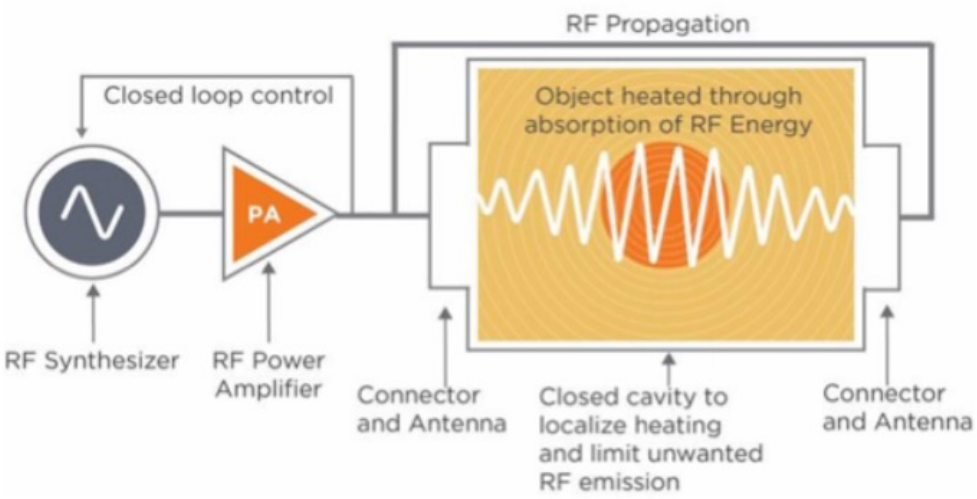

Figure 1. Schematic diagram of an RF energy system.

Sublethal Stress on *Salmonella* Typhimurium in Red Pepper Powders by Radio Frequency Heating

Hangjin Zhang[1], Chuting Gong[1], Yanyun Zhao[2], Shunshan Jiao[1*]
[1]SJTU-OSU Innovation Center for Environmental Sustainability and Food Control, Key Laboratory of Urban Agriculture, Ministry of Agriculture, School of Agriculture and Biology, Shanghai Jiao Tong University, 800 Dongchuan Rd., Shanghai 200240, China
[2]Department of Food Science and Technology, 100 Wiegand Hall, Oregon State University, OR, USA

Keywords: *Salmonella* Typhimurium, Sublethal injury, Heat stress, Radio frequency (RF), Low-moisture foods (LWFs)

INTRODUCTION

Radio Frequency (RF) heating had been proposed to be a new pasteurization method for the low-moisture foods[1, 2]. Conventional thermal treatment could result in sublethal injured cells, which can repair to be normal under a favorite environment[3]. There are some literatures on the resuscitation or repair of sublethally injured microorganisms in liquid media but lack of the effect of food matrix on the sublethal injury cells[4, 5]. The objective of the present study was to determine repair conditions by Overlay (OV) method firstly, then investigate the effect of RF heating on the subdamage rates of *Salmonella* Typhimurium in red pepper powder with different mediums. This would be helpful for better understanding of the sublethal injury of *Salmonella* Typhimurium in low-moisture foods (LMFs) by RF treatments.

METHED

A RF heating unit (12 kW, 27.12 MHz) was used in this study. About 25 g of inoculated red pepper powders filled in a round polypropylene (PP) container (8.9 cm Dia. × 4.3 cm H) was placed in the middle of a big rectangular PP container (13.5 L×10.2 W×5.2 H cm^3) which held un-inoculated samples, then they were put on the bottom electrode for RF treatments. The fiber optic temperature sensor was directly inserted at the center of the treated red pepper powder. Electrode gap was fixed to 8.0 cm and the samples were heated to 90°C and holding for 3 min [1]. Overlay method (OV) was used for the enumeration of heat-injured cells according to the method described by Kang, & Fung (1999) [6] with some modifications.. Briefly, RF-treated samples were serially diluted and 1 mL solution was poured into tryptose soya agar (TSA) by pour plate method, incubated at specific conditions to allow injured cells to recover. Then 7-10 mL of SS Agar was overlaid on the plates. After solidification, plates were incubated for an additional time at 37°C, and typical black colonies were enumerated. The percentage of sublethally injured cells after thermal treatment was estimated by the following equation:

RESULTS

Previous study indicated that 3-log reduction of *Salmonella* Typhimurim in red pepper powders was achieved after RF heating to 90°C and holding for 3 min[1]. According to Fig. 1, repair time and culture temperatures had no significant ($p>0.05$) influence on numbers of heat injured cells after the RF treatment. The bacteria under thermal stress suffered from injuries on both outer and cytoplasmic membrane which consequently led to cell death. Different repair time and culture temperatures had no significance on the total bacterial colonies in the TSA and NASA culture mediums, respectively. It was estimated that the sublethal injury ratio was 32-54%, while the ratio in NASA medium was relatively lower, which indicated most active cells were injured in sites of cytoplasmic membrane in varying degrees during RF heating. As temperature increased, the log survivors of *Salmonella* Typhimurium in the powders decreased gradually among the three medium, with maximum 4.29-log reduction at 100°C for 3 min holding time. However, there was no significant differences among the three medium under each temperature level ($p>0.05$).

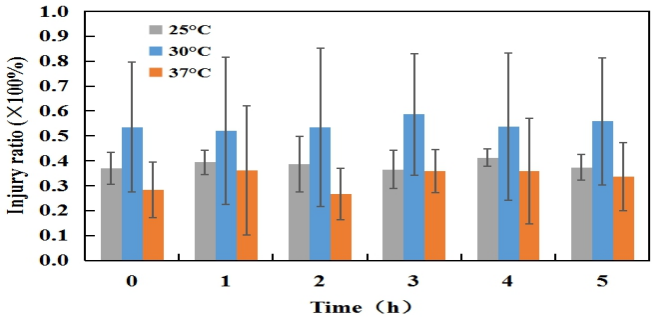

Figure 1. Effect of repair conditions on injury ratio of *Salmonella* Typhimurium in red pepper powders.

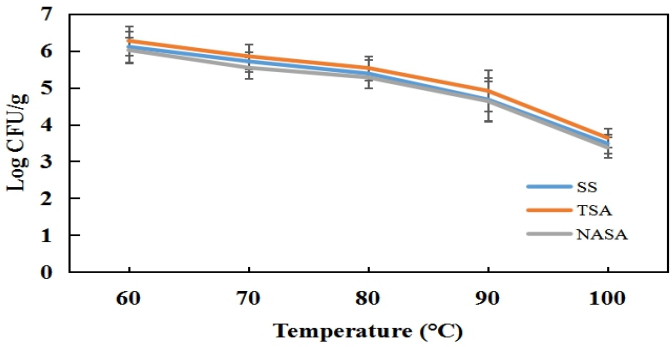

Figure 2. Effect of RF heating temperatures on the sublethal cells of *Salmonella* Typhimurium in red pepper powders.

DISCUSSION

RF heating achieved good pasteurization effect with small numbers of sublethal injured cells, the cells can suffer from injures in different sites including outer and cytoplasmic membrane. NASA medium contained high concentration of NaCl, thus cells with damaged cytoplasmic membrane are sensitive due to the decrease or loss of osmotic regulation function, while the bile salts in SS agar were resistant for the damaged outer membrane cells. The presence of sublethal injured cells present a potential threat to food safety, since in pathogen diagnostics they may repair under a favor environment and result in underestimation of survivors or even false negative results due to the selective media used, thus causing secondary pollution on the food matrix.

CONCLUSION

This study demonstrated that the repair temperature and repair time did not significantly influence enumeration of heat injured cells. RF heating inactivated *Salmonella* Typhimurium with small numbers of heat-injured cells, and they were suffered from different parts injuries. Different RF pasteurizing temperatures (60-100°C) had no significant influence on heat injured cells.

REFERENCES

[1] Hu, S., Zhao, Y., Hayouka, Z., Wang, D., & Jiao, S. (2018). Inactivation kinetics for *Salmonella* Typhimurium in red pepper powders treated by radio frequency heating. *Food Control,* 85, 437-442.

[2] Jeong, S. G., & Kang, D. H. (2014). Influence of moisture content on inactivation of Escherichia coli O157: H7 and *Salmonella enterica* serovar Typhimurium in powdered red and black pepper spices by radio-frequency heating. *International Journal of Food Microbiology,* 176, 15-22.

[3] Wu, V. C. H. (2008). A review of microbial injury and recovery methods in food. *Food Microbiology,* 25(6), 735-744.

[4] Wang, X., Devlieghere, F., Geeraerd, A., & Uyttendaele, M. (2017). Thermal inactivation and sublethal injury kinetics of *Salmonella enterica* and *Listeria monocytogenes* in broth versus agar surface. *International Journal of Food Microbiology,* 243, 70-77.

[5] Suo, B., Shi, C., & Shi, X. (2012). Inactivation and occurrence of sublethal injury of *Salmonella* Typhimurium under mild heat stress in broth. *Journal of Consumer Protection and Food Safety,* 7(2), 125-131.

[6] Kang, D. H., & Fung, D. Y. (1999). Thin agar layer method for recovery of heat-injured *Listeria monocytogenes*. *Journal of Food Protection,* 62(11), 1346-1349.

Investigation of Hot Air-assisted Radio Frequency Heating as a Simultaneously Dry-blanching and Pre-dewatering Method for Carrot Cubes

Chuting Gong[1], Hangjin Zhang[1], Yanyun Zhao[2], Yubin Miao[3], Shunshan Jiao[1*]

[1]SJTU-OSU Innovation Center for Environmental Sustainability and Food Control, Key Laboratory of Urban Agriculture, Ministry of Agriculture, School of Agriculture and Biology, Shanghai Jiao Tong University, 800 Dongchuan Rd., Shanghai 200240, China
[2]Department of Food Science and Technology, 100 Wiegand Hall, Oregon State University, OR, USA
[3]School of Mechanical Engineering, Shanghai Jiao Tong University, 800 Dongchuan Rd., Shanghai 200240, China

Keywords: Hot air-assisted radio frequency (HA-RF), Ultrasound-assisted osmotic dehydration (UOD), Pre-dewatering, Blanching, Carrots

INTRODUCTION

Blanching and pre-dewatering are critical steps in dehydration process of vegetables for protecting quality and improving drying efficiency. Hot water/steam are commonly used for conventional blanching, and osmotic dehydration (OD) or hot air drying are used for pre-dewatering. Those conventional methods exist some disadvantages, such as low retention rate of water-soluble nutrient, long treatment time and serious water pollution, etc. RF heating has been proposed as dry-blanching method for potato cubes [1] and carrots cubes [2], and hot air-assisted RF (HA-RF) has also been studied as a roasting method for nuts [3-4]. However, there are only few studies on simultaneous blanching and pre-dewatering process. Infrared heating has been used as a simultaneous dry-blanching and dehydration method for longan, apple slices, carrots and potatoes, enzymatic reaction was reduced and water was removed at the same time [5]. This study investigated HA-RF heating as a simultaneously dry-blanching and pre-dewatering method for carrot cubes. HA-RF dry-blanching and pre-dewatering treatment and associated microstructure and quality (texture, vitamin C, color, etc.) change were evaluated by comparing with improved ultrasound-assisted osmotic dehydration (40 % Sucrose, 10% NaCl, 1:4 Solid-to-liquid ratio).

METHODOLOGY

RF heating unit (12 kW, 27.12 MHz) was used in this study. Fresh carrot cubes with 86.8% initial water content ($5.0 \times 5.0 \times 5.0$ mm^3) were placed in polypropylene container (13.5 L×10.2 W×6.8 H cm^3) and treated by HA-RF heating for 10.0-15.0 min with electrode gap of 8.0-8.6 cm. Carrot cubes were treated by hot air for further pre-dewatering. Temperature profile during HA-RF heating was recorded by fiber optic sensors, microstructure was evaluated by scanning electron microscopy, vitamin C content was measured by spectrophotometric method. Texture and color were determined by texture analyzer and colorimeter, respectively. Data were analyzed using analysis of variance (ANOVA) at $p<0.05$ by SPSS software.

RESULTS

HA-RF carried out simultaneous blanching and pre-dewatering and it reduced POD activity to less than 5%. Moisture content of carrot cubes was reduced by 25.9% after 45 min HA-RF treatment with the electrode gap of 8.3 cm, and it was 29.3 % after 45.0 min UOD treatment. Samples after UOD had higher lightness and redness than HA-RF. Vitamin C content of samples treated by HA-RF (61.9%) was higher than that treated by UOD (51.6%). HA-RF obtained better hardness and cell puffiness. Besides, energy consumption of blanching and pre-dewatering by simultaneous HA-RF pre-treatment (0.10-0.30 kWh/kg) was lower than that of hot water blanching plus UOD pre-dewatering (0.79 kWh/kg).

Table 1. The moisture content, water activity, color (lightness & redness), hardness and vitamin C content of carrot cubes treated by UOD and HA-RF at different electrode gap.

Treatments	Moisture content	Water activity	L*(Lightness)	a* (redness)	Hardness	Vitamin C (mg/100g)
UOD	57.5±0.0^c	0.63±0.03^c	46.70±0.37^b	37.62±0.41^b	49.9±2.7^b	6.70±0.14^d
HA-RF (8.0 cm)	60.9±0.5^b	0.82±0.01^a	45.91±0.84^c	32.63±0.66^d	53.0±5.8^b	8.07±0.13^a
HA-RF (8.3 cm)	61.4±0.7^b	0.77±0.01^b	46.69±0.52^{bc}	32.02±0.07^d	68.5±4.0^a	7.91±0.13^c
HA-RF (8 6 cm)	71.9±0.2^a	0.81±0.01^a	45.24±0.24^d	35.33±0.40^c	52.0±4.9^b	7.76±0.13^b

The superscripts in the same column with different alphabet are significantly different ($p<0.05$)

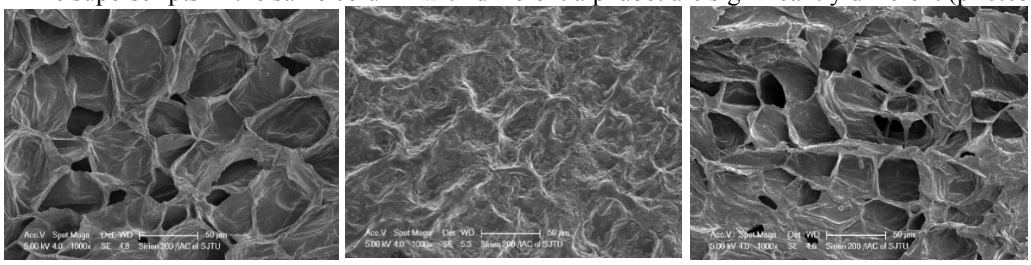

(a) (b) (c)

Figure 1. SEM micrographs of untreated carrot cubes (a) and samples after UOD (b)and HA-RF (8.3 cm) pre-treatment (c).

DISCUSSION

The results indicated that HA-RF treatment obtained desired blanching effect along with the pre-dewatering process which is more efficient than hot water blanching plus UOD pre-dewatering treatment. Owing to dielectric and volumetric heating characteristics of RF treatment, carrots treated by HA-RF preserved good cell puffiness and less shrinkage in texture than UOD. Besides, instead of using hot water as pre-dewatering medium, HA-RF pre-treatment obtained better retention of water-soluble nutrient such as vitamin C and avoided generation of waste water. HA-RF is a energy-efficiency and eco-friendly method with lower energy consumption.

CONCLUSION

This study demonstrated that HA-RF heating was an effective blanching and pre-dewatering method for carrot cubes, and quality was well maintained. HA-RF heating may provide an alternative way for hot water blanching plus UOD pre-treatment as a simultaneous blanching and pre-dewatering method before final-stage drying for carrot cubes with high-quality.

REFERENCES

[1] Zhang, Z., Wang, J., Zhang, X., Shi, Q., Xin, L., & Fu, H., et al. (2018). Effects of radio frequency assisted blanching on polyphenol oxidase, weight loss, texture, color and microstructure of potato. *Food Chemistry, 248*, 173–182.

[2] Gong, C., Zhao, Y., Zhang, H., Yue, J., Miao, Y., & Jiao, S. (2019). Investigation of radio frequency heating as a dry-blanching method for carrot cubes. *Journal of Food Engineering. 245*, 53–56.

[3] Jiao, S., Zhu, D., Deng, Y., & Zhao, Y. (2016). Effects of hot air-assisted radio frequency heating on quality and shelf-life of roasted peanuts. *Food & Bioprocess Technology, 9(2)*, 308–319.

[4] Liao, M., Zhao, Y., Gong, C., Zhang, H., & Jiao, S. (2018). Effects of hot air-assisted radio frequency roasting on quality and antioxidant activity of cashew nut kernels. *LWT-Food Science and Technology, 93*, 274–280.

[5] Wu, B., Pan, Z., Qu, W., Wang, B., Wang, J., & Ma, H. (2014). Effect of simultaneous infrared dry-blanching and dehydration on quality characteristics of carrot slices. *LWT-Food Science and Technology, 57(1)*, 90–98.

Study of Radio Frequency Drying and Roasting of Shelled Peanuts

Su-Der Chen* and Chih-Yuan Cheng
National Ilan University, I-Lan City, Taiwan 26041

Keywords: radio-frequency, drying, roasting, peanut

INTRODUCTION

The freshly harvested shelled peanut (*Arachis hypogaea*) has about 40% moisture content, and it takes 7 to 10 days to reduce the moisture content to 15% by sun drying in order to avoid microorganism contamination during storage. Radio frequency (RF) and microwave (MW) drying can cause rapid friction of water molecules and ion vibration in food to generate heat energy; therefore, RF heating can rapidly achieve water evaporation in food to overcome the heat transfer resistance [1]. The drying time of 1.6 kg of in-shell walnuts reducing moisture content from 20% to 8% required 100 and 240 min by RF drying and only hot air drying, respectively [2]. Moreover, 45 min of hot air-assisted RF roasting at 110–130°C is feasible and efficient for obtaining high quality roasted salty peanuts [3]. The objectives of this study were using RF heating of fresh shelled peanuts for drying or direct roasting.

METHODOLOGY

The moisture content of 1 kg fresh shelled peanuts was reduced from 40% to 10% by drying for storage in the first drying part. A 5 kW, 40.68 MHz pilot-scale RF with hot-air drying system was used in this study (Figure 1a). A 1-3 kW microwave drying oven with three rotating drying trays and a 45℃, 6 kW cold-air drying oven were also used in this study for drying efficiency comparison (Figure 1b; 1c). The temperature of shelled peanuts was lower than 100°C during RF and MW drying. In the second roasting part, the temperature of the shelled peanut was above 120°C with only RF heating using three different electrode gaps. The surface temperature profiles and weight loss of 1 kg shelled peanuts during drying or roasting processes were measured at different time intervals, respectively.

Figure 1. (a) RF hot air heating equipment, (b) Microwave drying oven, (c) Cold air drying oven.

RESULTS

The average temperature profiles and drying curves of 1 kg shelled peanuts during RF, MW and cold air drying are shown in Figure 2. The drying times and total energy consumptions of RF and MW drying were much lower than cold air drying (Table 1). The temperature profiles and drying curves of 1 kg shelled peanuts by RF roasting with different gaps are shown in Figure 3, and the final roasting temperature distributions were uniform and above 120°C (Figure 4).

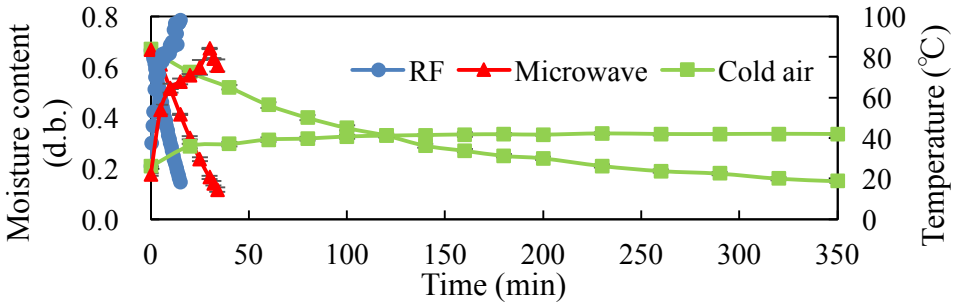

Figure 2. The temperature and drying curves of 1 kg shelled peanuts during cold air, MW and RF with gap of 17 cm drying.

Table 1 Effect of drying method on rate, time and energy consumption of 1 kg peanuts

Drying method	Linear regression equation	R^2	Rate (g/min)	Time (min)	Energy consumption (kWh)
RF	y = -21.80x + 1002	0.996	21.80	15	0.333
1 kW MW	y = -10.03x + 1004.4	0.996	10.03	34	0.56
2 kW MW	y = -21.61x + 1004.9	0.996	21.61	16	0.53
3 kW MW	y = -29.07x + 1000.5	0.978	29.07	12	0.60
Cold air	y = -0.813x + 926.75	0.872	0.813	350	21.29

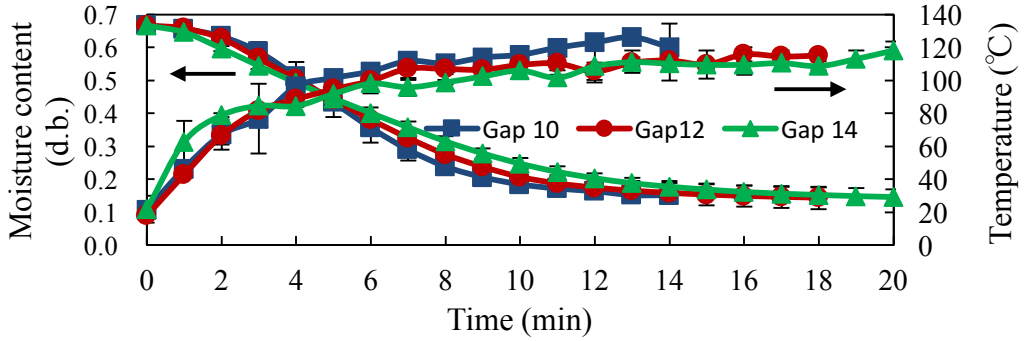

Figure 3. The temperature and drying curves of 1 kg shelled peanuts during RF directly roasting with different electrode gap.

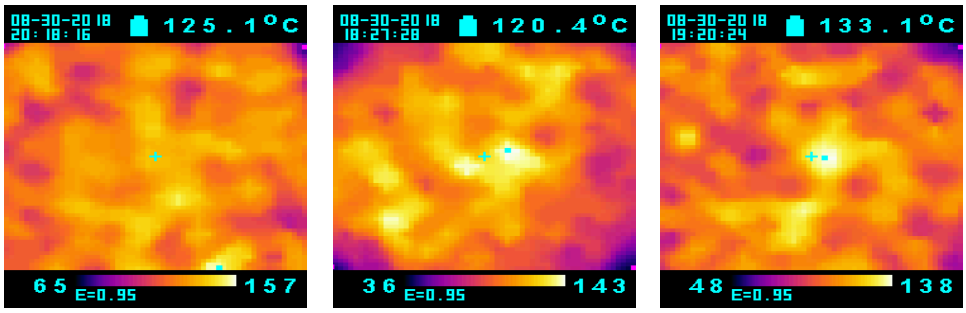

Figure 4. Surface temperature (top view) distributions of 1 kg shelled peanuts obtained by infrared thermal imaging after RF roasting at gap of 10, 12 and 14 cm.

DISCUSSION

The cold air drying of 1 kg fresh shelled peanuts took almost 6 hr to accomplish and the energy consumption was much higher than both RF and MW drying. The RF drying of peanuts appeared to follow a constant drying rate and obtained the shortest drying time and energy consumption. Increasing microwave power for drying peanuts obtained a shorter drying time. The RF direct roasting of fresh shelled peanuts quickly reached about 120℃ and only required 14~20 min depending on selected gaps. The temperature distributions of roasted peanuts were uniform.

CONCLUSION

Both RF and MW heating can rapidly achieve water evaporation in shelled peanuts to accelerate drying and use less energy than cold air drying. Both RF drying and direct roasting of 1 kg shelled peanuts were continuously processed. It took less than 20 min, which were affected by the gap distance between RF electrodes.

REFERENCES

[1] F. Marra, L. Zhang and J. G. Lyng, Radio frequency treatment of foods: Review of recent advances, *J. Food Eng.* vol. 91, no 4, pp.497-508, 2009.

[2] B. Zhang, A. Zheng, L. Zhou, Z. Huang and S. Wang, Developing hot air-assisted radio frequency drying protocols for in-shell walnuts. *Emir. J. Food Agr.*, vol. 28, no 7, pp. 459-467, 2016.

[3] S. Jiao, D., Zhu and Y. Zhao, Effects of hot air-assisted radio frequency heating on quality and shelf-life of roasted peanuts. *Food Bioprocessing Technol*, vol .9, pp. 308-319, 2016.

RF Drying of Insects as Foods and Feeds

G. Battaglia[1], F. Bressan[1], I. Capozzi[1], E. Gutseva[2] and T. Veccia[1]

[1]Officine di Cartigliano SpA, Cartigliano (Vicenza), Italy
[2]Entogourmet S.L., Lorca (Murcia), Spain

Keywords: RF drying, insects drying, cricket drying, entomophagy.

INTRODUCTION

Entomophagy is the practice of humans eating insects as food. It is widely used in many parts of the world, especially in some parts of Asia, Africa and Latin America [2]. In western countries entomophagy has caught the attention of media, research institutes, cooks, food industry, legislators, agricultural and food agencies. Insects also contribute to food and feed for livestock, replacing fish meal, soy and cereals in animal diets [1]. Rising incomes, especially in developing countries, are increasing the global food demand [5]. Per capita meat consumption in high-income countries is expected to increase by 9% by 2030 compared with the consumption of 86 kg/year in 2000. In China, an increase of almost 50% is expected. Consequently, this will also increase the demand for coarse grain as feed to livestock [6]. Feed conversion ratios (FCRs) are particularly important in animal production enterprises. From long-term statistics for the United States, the following FCRs were given: 2.5 for chicken, 5 for pork, and 10 for beef [3], while it is 1.7 for crickets (*Acheta domesticus*) [4].

The technology needed to produce protein flours from insects, as the raw material, is now developing. Many factors and processes influence the enrichment of insect protein, including the selection of species, variability of drying and comminution. Different pre-treatments (blanching, freezing and defatting) and drying methods (oven drying, freeze drying and fluidized bed drying) affect the results of the final product [7]. In this short paper a new kind of drying treatment, including RF (27 MHz) technology, is presented. It allows industrial-scale protein production from insects (crickets in this case), with reduced costs and time.

METHODOLOGY

A typical RF system consists of two main components: generator and applicator. The generator part is used to generate the radio frequency waves and the applicator part is where the material is placed and heated.

A granular solid product can be treated with RF by using two different applicator configurations, which mainly depend on the thickness of the product. The configuration

chosen, in order to dry the insects, is the so called "stray-field" system, since the product is treated in a layer of 1.5cm thickness.

A hot air blade is placed on the head of the machine in order to eliminate the excessive free water of the material coming from the blanching process. Four air extraction fans are placed on top of the machine in order to remove the moisture that comes from the drying process.

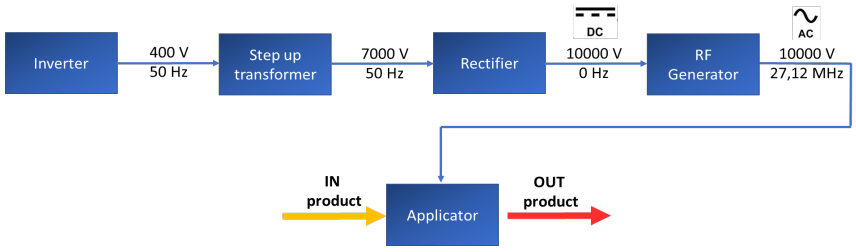

Figure 1 Schematic representation of the RF section

The RF tunnel machine, used for drying crickets, is equipped with two 45kW generators. The heating tunnel's dimensions are: length 6 m and width 3 m. The productivity is around 150-200 kg/h. The picture below shows the RF tunnel and the product at the outlet of the process.

Figure 2 – RF Dryer processing crickets

The crickets' moisture is measured with a Kern DBS-60 moisture analyzer settled at 120°C, and the protein content was determined by using a Kjeldahl MLAB015 spectrophotometer.

RESULTS

The RF dryer processing time was approximately 40 minutes and the maximum temperature of the product was 80°C (Table 1) . The product's outlet moisture was around 8% after starting from 60% inlet moisture content. Compared with the conventional hot air technology, the protein amount after RF drying process was 10% higher.

DISCUSSION

The drying process of crickets by using RF technology shows promising results compared with current technologies in terms of process time [8], moisture and protein

contents. Moreover, the appearance of this product, dried with RF, looks more natural, without any burned effect (Figure 3).

Table 1 Overview of drying methods

Method	Temperature [°C]	Time [h]
Freeze drying	-49	48
Oven drying	60	24
Oven drying without blanching	80	7
Oven drying without freezing	80	17
Fluidized bed drying	60	3
RF	80	0.5

Figure 3 Appereance of milled product after conventional tratment (left) vs RF treatment (right)

CONCLUSIONS

The RF technology represents a possible solution to satisfy the need for rapid industrial processing of insects for animal and human consumption, while still observing the requirements of moisture, and organoleptic and nutritional properties.

REFERENCES

[1] A. Van Huis, Potential of Insects as Food and Feed in Assuring Food Security, *The Annual Review of Entomology*, vol. 58, pp.563-583, 2013.

[2] FS. Bodenheimer, Insects as Human Food: A Chapter of the Ecology of Man, *The Hague: Junk*, p.352, 1951.

[3] V. Smil, Eating meat: evolution, patterns, and consequences, *Population and Development Review*, vol 28, pp599–639, 2002.

[4] BJ. Nakagaki, GR. deFoliar, Comparison of diets for mass-rearing *Acheta domesticus* (Orthoptera: Gryllidae) as a novelty food, and comparison of food conversion efficiency with values reported for livestock. *Journal of Economic Entomology. 84:891–96* 1991.

[5] S. Msangi, MW. Rosegrant, Feeding the future's changing diets: implications for agriculture markets, nutrition, and policy. *In 2020 Conference: Leveraging Agriculture for Improving Nutrition and Health, Washington, DC, International Food Policy Research Institute* 2011.

[6] R. Trostle, Global agricultural supply and demand: factors contributing to the recent increase in food commodity prices. *Econ. Res. Serv. Rep. WRS-0801, pp. 1–30. United States Department of Agriculture., Washington, DC. July 2008 rev*., 2008.

[7] H. Bruggen, H. Jahger, B.J. Purschke, Influence of different pre-treatments and drying methods on the dry fractionation behavior of mealworm larvae (*Tenebrio Molitor*), Institute of Food Science and Technology, Vienna, 2017.

[8] G.B. Awuah, H.S. Ramaswamy, J. Tang, Radio Frequency Heating in Food Processing. Principle and Applications, *CRC Press*, 2015.

Targeted Food Heating Using a Solid-State Microwave Oven

C.S. Hopper[1], G. Grimaldi[1], F. Marra[2], J. Prochowski[1], and M. Sclocchi[1]

[1]IBEX, ITW Food Equipment Group, Glenview, IL, USA
[2]University of Salerno, Department of Industrial Engineering, Italy

Keywords: solid-state, microwave oven, heating algorithm.

INTRODUCTION

Solid-state RF generators offer a great deal of control over the heating pattern within an oven cavity [1,2]. This applies to both single, continuous food loads as well as those comprised of multiple components, often with different physical properties. In this paper, we present simulated and experimental results which demonstrate the targeting of specific components using frequency and phase manipulation.

METHODOLOGY

To demonstrate the ability to manipulate the heating pattern in such a way as to target specific food items or components within a single sample, several complementary techniques were used. The food under consideration for this study was a multi-component pre-cooked sandwich (egg and cheese between bread), which is reheated from chilled (5 °C). Single sandwiches as well as batches of two were used. Since the frequency and phase have a strong influence on the heating pattern(s), that information, along with power data for each of the 4 sources, were recorded in real-time. Simultaneously, fiber optic probes are inserted into the various components of the sample under test to record the temperature response which corresponds to the field and power data. Samples are tested using 2450 MHz with no phase change, i.e. “magnetron mode” heating. Results are then collected using a proprietary targeting algorithm which uses the full-bandwidth and phase variability available. Finally, the temperature/time evolution from both sample populations are compared to determine the statistical significance of any observed differences. Figure 1 shows the experimental setup. The electromagnetic field distribution and resulting temperature profiles for given RF settings are also simulated using COMSOL Multiphysics RF and Thermal Modules [3] for comparison and additional understanding of the observed behavior.

RESULTS

The sandwiches investigated here are a particularly illustrative item since the individual components are layered and have different thermophysical and dielectric properties.

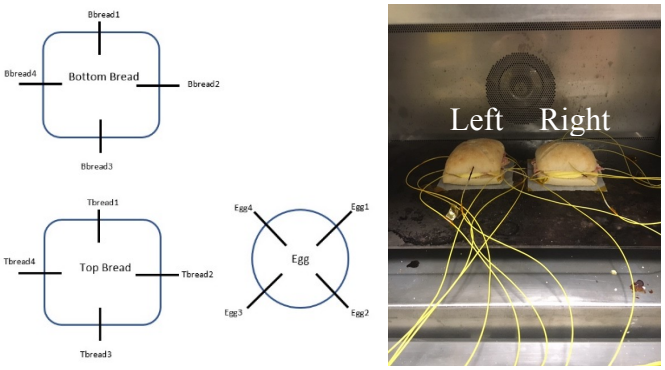

Figure 1. Example of experimental setup for temperature measurements of multi-sample, multi-component product. (a) Schematic of probe placement in a single sandwich and (b) two sandwiches placed in the cavity outfitted with fiber optic probes.

The first step in these experiments is to validate the consistency of the data measured for a given sample population. The variables used are forward power, frequency, and phase configuration. Several samples are heated with all variables fixed then tested for statistical significance. Samples for which all variables share the same value should be indistinguishable from each other (equal means). An optimization algorithm is then applied which is intended to target specific components of the sample(s).

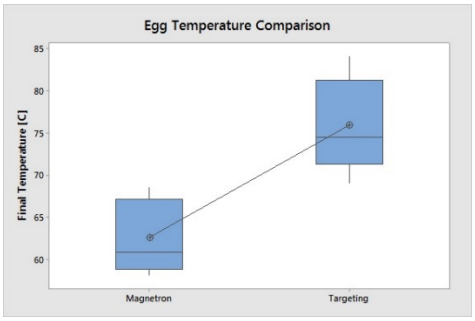

Figure 2. Boxplot of single-sandwich egg temperatures at the end of reheating.

In the single sandwich, the goal is to end with a higher temperature egg than is achieved using magnetron-type heating. For the two-sandwich batch, the objective is to heat the eggs more evenly than is accomplished with only a single frequency. Figure 2 shows the results from a set single-sandwich tests, where the temperature of the egg is significantly higher than without the targeting algorithm ($p<0.05$, $t=4.12$). The statistical analysis is done using Minitab 18 [4]. In Figure 3, the temperature data is shown for a two-batch sample using both magnetron-type heating and the targeting algorithm.

DISCUSSION

In the single-sandwich, the egg is heated significantly more when using an algorithm that is designed to specifically target the inner, denser core. Heating multiple sandwiches is more complicated and the optimization approach was somewhat different. In this case, time spent at a given frequency/phase configuration is weighted more heavily

to avoid thermal runaway while evenly distributing the energy delivered to the loads. An example of the simulated electric field distribution and power loss density for two frequency/phase configurations is shown in Fig. 4.

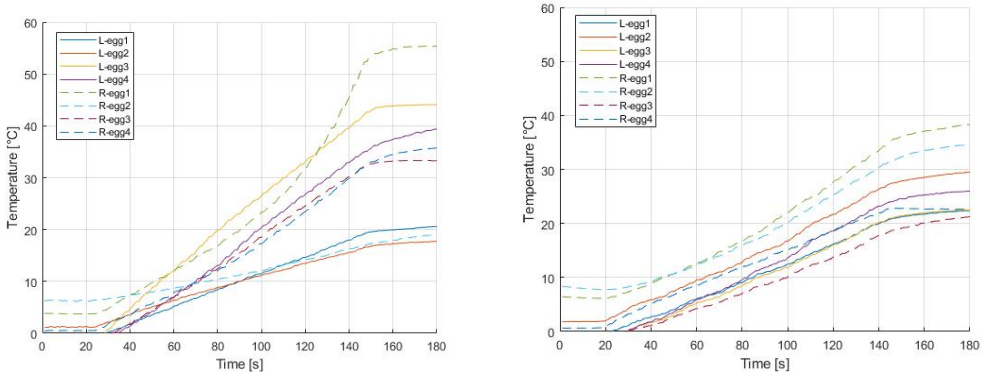

(a) (b)

Figure 3. (a) Magnetron-type heating of egg and (b) heating with targeting algorithm. L-egg and R-egg refer to the left and right sandwich, as shown in Figure 1.

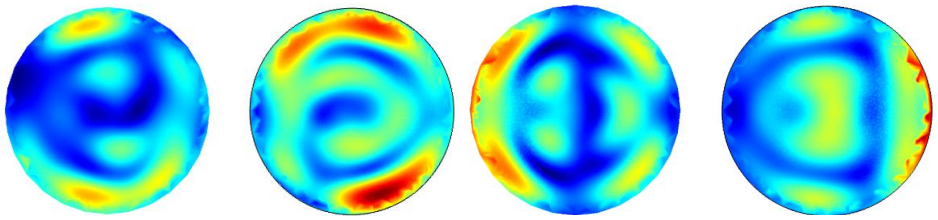

(a) (b)

Figure 4. (a) Electric field distribution in the right and left egg at f_1 and (b) Electric field distribution in the right and left egg at f_2. The power loss densities (from left to right) are 17W, 28W, 25W, and 26W.

CONCLUSION

Knowledge of the field distribution as well as an understanding of how to interpret the feedback delivered to the oven from the food allows for targeted heating algorithms to be written for a solid-state microwave oven. These algorithms have been demonstrated to improve efficiency and uniformity of both single- and multi-item cavity loads.

REFERENCES

[1] V.V. Yakovlev, Effect of frequency alteration regimes on the heating patterns in a solid-state-fed microwave cavity,*JMPEE*., vol. 52, no 1, pp.31-44, 2017.
[2] A. Wieckowski, P. Korpas, M. Krysicki, F. Doughiero, M. Bullo, C. Fager, *Efficiency Optimization for Phase Controlled Multi-Source Microwave Oven*, Proc. Intern. Conf. on Heating by Electromagnetic Sources (HES-13), pp. 207-213, Padua, Italy, 2013.
[3] COMSOL Multiphysics, version 5.4, COMSOL, Inc, www.comsol.com
[4] Minitab 18 Statistical Software, State College, PA: Minitab, Inc. www.minitab.com

The Evolution of Expert Cooking Intelligence

Steven J. Drucker

Droaster Laboratories LLC

Keywords: "Push button, get food", Smart appliance buying analytics, Mass customization, Future developments.

INTRODUCTION

How did Expert Cooking Intelligence's initial incarnations of "Make me a better cook" and "Ease and convenience" transform overnight into "Push button, get food"? When and how will smart appliance likeability, buzzworthy-ness, and value propositions become sufficiently compelling to overcome consumer buying objections? Fueled by crowd sourcing and Moore's Law, Expert Cooking Intelligence is exploding. Will newly empowered consumers' insistent demands for infinite mass customization impede, or accelerate, the evolution of Expert Cooking Intelligence based packaged foods, cooking appliances and perhaps even home cooking itself?

THE FIRST WAVE

Expert Cooking Intelligence emerged fully formed with the 1824 publication of America's first cookbook—"The Virginia Housewife". Its manifest was simple: "Make me a better cook". In a first, recipes of a scope and detail never before attempted were gathered into a single source. The cookbook's universal accessibility meant that every American household could aspire to the vision of "Make me a better cook".

THE SECOND WAVE

Expert Cooking Intelligence's second wave swept over consumers with the 1870 invention of the can opener, lifestyle changes coincident with the burgeoning industrial revolution and post-Civil War advances in canning technologies. This second incarnation, completely different in vision and manifest from that of "Make me a better cook", was irresistible—the timely and entirely welcome added value of "Ease and convenience". Packaged foods—from Campbell's Soup to Kellogg's Corn Flakes to Triscuits—built brand equities founded on "Ease and convenience".

A REVOLUTIONARY MIRACLE

The incorporation of packaged foods into recipes initiated the mixing and stirring together of "Make me a better cook" with "Ease and convenience". Frozen foods, however, pushed "Ease and Convenience" to the fore after World War II with the revolutionary miracle of heat and eat frozen TV dinners.

PUSH BUTTON, GET FOOD AND A SHOTGUN MARRIAGE

General Electric's 1967 incorporation of microprocessors into cooking appliances transformed "Ease and convenience" into its contemporary form—"Push button, get food". Following this overnight transformation, consumer demand for Expert Cooking Intelligence birthed the $15 Billion dollar microwave food industry, the $2 Billion microwave oven industry and the often awkward marriage between the two to which we are heir today.

SMART APPLIANCES, CONNECTING THE DOTS

Expert Cooking Intelligence's modern state is best understood with the aid of a finite linear continuum. The endpoints of the newly identified continuum are "Push button, get food" and "Make me a better cook". The ease and readiness with which microwave foods and ovens can be slotted along the continuum are set forth, from the marketplace persistence of microwave keypads with a plethora of buttons, to the nova like promise of meal kits, to the here and now of smart appliances. Smart appliance consumer purchasing intent and perceived value are positioned along the continuum—against a landscape of first time ever reported microwave oven industry sales analytics.

THE THIRD WAVE

The first and second wave linear continuum evolves from two to three dimensions. The newest incarnation transforms the continuum into a shape shifting space characterized by mass customization, from which emerge new, unexpected and uniquely synthesized developments in the future of Expert Cooking Intelligence.

Continuous Industrial-Scale Microwave-Assisted Extraction of High-Value Ingredients from Natural Biomass

Marilena Radoiu, Steven Splinter and Tomasz Popek

Radient Technologies Inc., Edmonton, Canada

Keywords: Microwave-assisted extraction, continuous processing, biomass, industrial scale.

INTRODUCTION

Extraction is a fundamental process for separation and recovery of bioactive compounds from plants. The exponentially increasing demand of herbal products and/or extracts for wider and safer applications, timely availability of high quality products with low cost of processing and higher yield are the needs of the growing herbal/nutraceutical medicine and food based industries. To meet these challenges, there is an increased demand for alternative and non-conventional extraction techniques.

An innovative technology for the continuous extraction of bioactive compounds from a wide range of biological materials has been developed, scaled up and successfully demonstrated at commercially-relevant scales. The technology, known as MAP™, or *Microwave-Assisted Process*, robustly transfers from laboratory to continuous, industrial scale operation. In wide-ranging trials, MAP™ has comprehensively demonstrated its ability to outperform many KPIs of conventional extraction processes, while offering biomass throughput, product consistency and low operational costs not attainable by other emerging technologies.

In this paper, the basis of the MAP™ technology will be described and select case studies presented.

METHODOLOGY

The continuous-flow extractor enabling MAP™ operates at 915 MHz; the extractor, designed for continuous processing of up to 200 kg/h of biomass material, is shown in Figure 1.

Verification of the mechanical integrity of the system was confirmed by flow testing of biomass / solvent slurries. Testing and verification of the efficiency of microwave energy transfer to the extractor cavity was completed at various microwave power settings using flowing water at 870 kg/h. The microwave energy transfer to the system was verified to be >95% in each case.

Figure 1: Continuous-Flow Industrial-Scale MAP™ Extractor

RESULTS

As an example of performance, continuous flow MAP™ extraction of the antioxidant SDG from flax biomass was performed using 70% ethanol / water as the solvent at two different conditions:

- 75 kg/h flax / 5 L/kg solvent / 15 kW microwave power / extractor residence time 24 min;
- 110 kg/h flax / 5 L/kg solvent / 20 kW microwave power / extractor residence time 16 min;

The industrial-scale conditions for these runs were determined by extrapolating from optimized conditions previously obtained from batch lab-scale MAP™ experiments. Figure 2 shows a comparison of the steady state recovery of SDG from flax obtained from lab experiments using single-stage conventional dispersed-phase mixing extraction, lab-scale MAP™ using the same solvent and solvent composition, and the results of the two industrial scale runs described above. From the figure, it is clear that scale-up was verified by obtaining identical results at two different flow rates and associated MAP™ energy densities. This confirmed that laboratory-scale MAP™ results can be successfully replicated at industrial scale and so verifies that the industrial-scale extractor performs as designed.

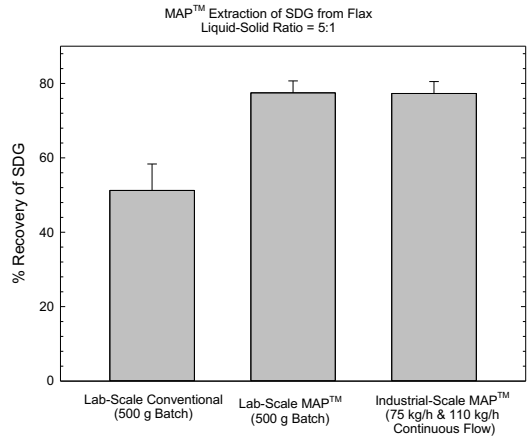

Figure 2: Comparison of conventional extraction, lab-scale MAP™ Extraction and industrial-scale MAP™ extraction of flax lignans (SDG) from flax biomass.

CONCLUSION

This work was focused on investigating the scaling-up of continuous flow process to industrial scales.

Based on laboratory experiments and their optimisation, a continuous flow extractor for industrial biomass extraction using MAP™ has been built and successfully demonstrated on various solvent – biomass matrices. The extractor comes with several benefits, including significantly increased flexibility with respect to operation:

- The contact time between the biomass and solvent before, during and after microwave treatment can be adjusted much more easily;

- It is possible to precisely control biomass residence time in the microwave zone and - if desired - separate the biomass from the solvent very quickly after treatment, or continue contact for any length of time at any temperature, depending on the desired outcome.

The extractor is also easily scalable. The continuous flow approach eliminates the requirement for having geometric similarity between scales (i.e the equipment shape and dimensions do not have to scale proportionately). Classically, even geometric similarity does not ensure thermal similarity in scaled systems – for example, heat transfer is an interface-controlled process and so the surface area relative to the volume is critical. As volumetric scale increases, the area relative to the volume decreases and the overall efficiency of heat transfer can decline considerably. There is no thermal inertia with microwaves, on the other hand. Since penetration depth is not an issue with the continuous flow design, the energy is deposited uniformly throughout the mixture resulting in rapid energy transfer and direct dielectric heating – hence the thermal inertia inherent to classical methods is not an issue.

Heat Transfer Analysis of Biomass and Solvent during Microwave Heating – A Modelling Approach

A. Taqi[1], J. Robinson[1], E. Farcot[2] and E. Binner[1]

[1]Faculty of Engineering, University of Nottingham, NG7 2RD, UK
[2] School of Mathematical Sciences, University of Nottingham, NG7 2RD, UK

Keywords: Biomass; Microwave; Heat Transfer; Chemical Potential

INTRODUCTION

Under experimental scales, it has been widely reported that microwave processing of biomass materials returns enhanced outcomes compared with conventional heating. These outcomes have been observed in a variety of applications, such as biomass extraction and pyrolysis. However, the microwave technology has not yet been implemented on industrial scales, due to the lack of fundamental understanding of the phenomena underpinning the action of microwaves. Such understanding is essential to predicting the outcomes of processing, and thereby enabling process scale-up and design. Recently, a novel mechanism (the chemical potential hypothesis) has been proposed [1], which could fundamentally distinguish between microwave processing and conventional heating in biomass-solvent systems. Nevertheless, this mechanism has not yet been subjected to testing, so as to understand whether it can occur in biomass-solvent systems subjected to microwave heating. Such an effort is essential to acquire an insight as to whether this mechanism should be further studied and understood. This communication aims to understand, from a thermal viewpoint, whether the chemical potential hypothesis can be inferred in biomass-solvent systems under microwave heating. The work uses computer modelling to simulate temperature developments in a hypothetical biomass-solvent system under microwave heating. If temperatures with sufficient magnitudes can be developed and sustained in the system, the hypothesis concerned can be inferred qualitatively.

MODEL ASSUMPTIONS AND DERIVATION OF EQUATIONS

The chemical potential is a hypothetical thermodynamic quantity that adjoins different driving forces of mass transfer into a single mathematical expression [2]. These driving forces include activity, pressure and temperature. The proposed hypothesis [1] constitutes that, in biomass-solvent systems subjected to microwave heating, a temperature gradient exists between the biomass material and the solvent phase. This acts as an additional driver for solvent mass transfer into the biomass, which induces cell pressures higher than those expected otherwise, causing cell rupture.

A heat transfer model has been developed, in which a biomass-solvent system with a given size (cellular scale) is subjected to microwave heating under variable parameters, including incident power, thermal conductivity and dielectric loss factor.

Equation 1 is the principal expression governing the microwave heat power input and conductive heat transfer. Furthermore, a few assumptions have been made regarding the system's geometry, the nature of the solvent and the propagation of microwaves. This is in order to simplify the problem and emphasise the outcomes in a clear manner.

$$\frac{dT}{dt} = \alpha\nabla^2 T + \frac{1}{\rho C_p}\dot{Q}_m$$

Equation 1. The principal equation governing heat. T is temperature, t is time, α is the heat transfer coefficient; ρ is density; C_p is the specific heat capacity; $\dot{Q}_m$ is the volumetric microwave power input.

RESULTS

Under microwave heating, temperature gradients are developed and sustained in biomass-solvent systems (Figure 1). At the cellular scale, these gradients are relatively small in magnitude.

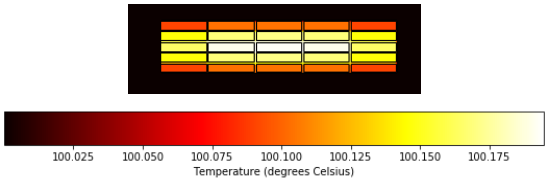

Figure 1. 2D map of the equilibrium temperature distribution of a biomass material with a surrounding solvent at given input microwave parameters. This has been obtained computationally.

DISCUSSION

While the temperature gradients developed are small, it has been stated that such magnitudes are sufficient to significantly alter the mass transfer patterns and bring about enhanced outcomes [1]. Therefore, from a thermal viewpoint the chemical potential mechanism is possible at the investigated scale. Further work will be carried out to assess the suitability of this hypothesis in a more comprehensive manner. This includes a quantitative analysis on how mass transfer patterns can alter.

CONCLUSION

Due to the development and sustaining of temperature gradients in biomass-solvent systems with microwave heating, it is possible for the chemical potential mechanism to take place.

REFERENCES

[1] C. S. Lee, E. Binner, C. Winkworth-Smith, R. John, R. Gomes, and J. Robinson, "Enhancing natural product extraction and mass transfer using selective microwave heating," *Chemical Engineering Science,* vol. 149, pp. 97-103, 2016.

[2] J. G. Wijmans and R. W. Baker, "The solution-diffusion model: a review," *Journal of membrane science,* vol. 107, no. 1-2, pp. 1-21, 1995.

Development and Scale-up of a Continuous Microwave-Assisted Extraction System on an Industrial Co-product

F. Arrutia, M.A. Calvo, M. Adam and E. Binner

Faculty of Engineering, The University of Nottingham, Nottingham, UK

Keywords: Microwave-assisted extraction, pectin extraction, waste management, functional carbohydrates.

INTRODUCTION

Thousands of tons of out of specification potatoes are produced every year. While the main part of potato's dry weight is starch, other components are also of interest for potential use as functional food products. Pectins have a structure divided into "smooth" and "hairy" regions. While those rich in smooth regions are valued for its hydrocolloid properties, hairy structures may constitute a promising source of prebiotics [1]. Potato pectins are highly branched and thus have poor gelling properties, but could be promising prebiotics. However, the current commercial pectin extraction process destroys the hairy regions, and therefore the inability to extract large quantities of hairy pectins is a barrier to progress in this area.

This study aimed to develop a novel, clean and scalable methodology to extract potato hairy pectin regions using Microwave-Assisted Extraction (MAE). In this first stage, an extraction process was developed and scaled-up through the construction of a pilot-plant continuous rig that allowed the production of gram quantities of extracts. Work is ongoing to develop methodologies to assess the prebiotic potential of these extracts.

METHODOLOGY

Laboratory-scale experiments allowed the selection of the main parameter's values to be used in the large-scale experiments. For the former, an Anton Paar Monowave 400 (St. Albans, UK) was employed as microwave equipment. Selection was based on the yield of extract obtained, calculated as:

Yield (%) = (Weight of dry extract)/(Weight of dry feed)×100%.

The final set-up of the pilot-plant scale rig is displayed in Figure 1.

Briefly, the complete extraction process consisted of a first enzymatic step to reduce starch content; then a microwave heating step; a pectin precipitation step; and a final centrifugation step to recover the extract.

In a first approach of analytical testing, the galacturonic acid (GalA) content of the extracts was measured as a screening method to quantify pectin, following the procedure developed by T. M. Filisetti-Cozzi and N. C. Carpita (1991) [2].

MAE results were compared with conventional extraction results (control).

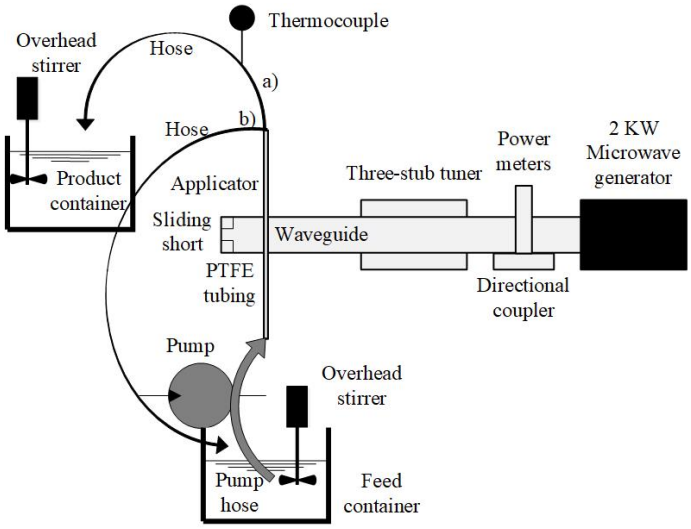

Figure 1. Schematic diagram of the pilot-plant scale microwave-assisted extraction rig. a) Single heating route. b) Full-recirculation route.

RESULTS

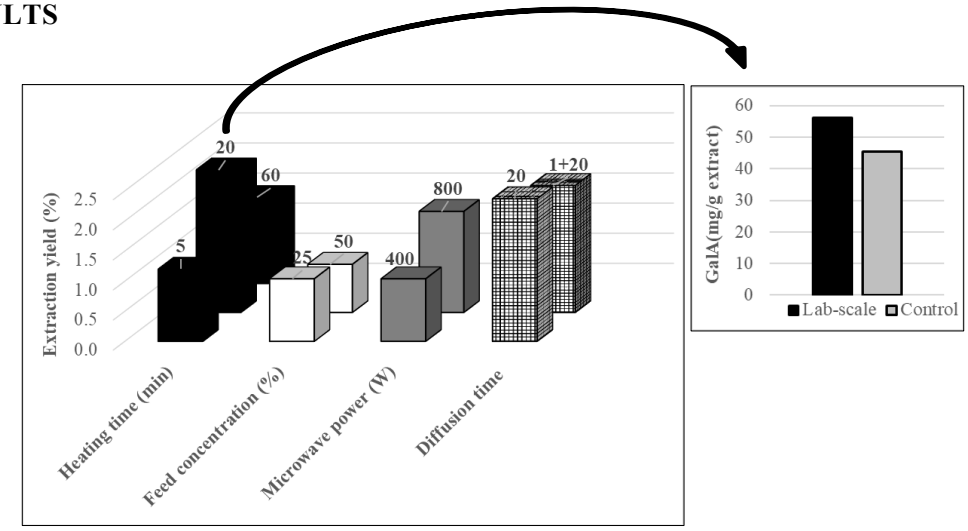

Figure 2. Yield of extract obtained for the different conditions assayed during laboratory-scale experiments.

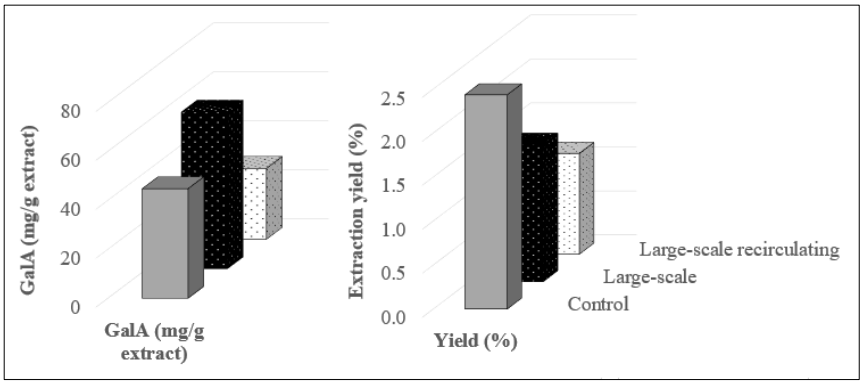

Figure 3. Yield of extract obtained for the different conditions assayed during pilot-plant scale experiments.

DISCUSSION

Figure 2 shows how intermediate heating times (20 min) worked better than shorter (5 min) or longer (60 min) treatments, highlighting the reduced processing times of microwave treatments compared to the standard conventional treatments (60 - 120 min). Higher powers yielded an increased amount of extract, and reduced as well the heating ramp. For diffusion time experiments, a reference treatment of 20 min was compared to an experiment in which the target temperature was applied for 1 min and then the solution was allowed to cool-down until a total time of 20 min elapsed. Small differences in yield were observed, further demonstrating microwaves as a fast treatment able to achieve same or even better results than conventional treatments. Extracts contained pectin, confirmed by the presence of GalA. Figure 3 displays the pilot-plant experiments, with which pectin-derived carbohydrates were as well obtained, although the yields were slightly lower than lab-scale. In this case, the recirculating treatment worked much worse than the single heating route, regarding both the yield and the GalA content obtained.

Therefore, short heating times are enough to obtain GalA contents higher than the control, as long as enough diffusion time is allowed and the feed concentration is not overloaded.

CONCLUSION

Overall, a pilot-plant scale continuous MAE rig was built and successfully employed in the extraction of potentially functional pectin-derived oligosaccharides from an industrial potato co-product.

REFERENCES

[1] J.-S. Yang, T.-H. Mu, and M.-M. Ma, Extraction, structure, and emulsifying properties of pectin from potato pulp. *Food. Chem*., vol. 244, pp.197-205, 2018.

[2] T.M. Filisetti-Cozzi and N.C. Carpita, Measurement of uronic acids without interference from neutral sugars. *Anal. Biochem*, vol. 197, no 1, pp.157-162, 1991.

Predictive Modeling of a MHz-driven Atmospheric-pressure Plasma Jet in Contact with Liquid: Current State and Perspectives

I. L. Semenov, K.-D. Weltmann

Leibniz Institute for Plasma Science and Technology, Greifswald, Germany

Keywords: atmospheric-pressure plasma jet, plasma-liquid interaction, biomedical and agriculture applications, predictive modeling.

INTRODUCTION

The interaction of atmospheric-pressure plasmas with liquids has become a topic of great interest in recent years. Plasma-activated liquids have gained increasing attention due to their potential applications in medicine, material synthesis, water purification and agriculture. At present, plasma jets, dielectric barrier (DBD) and corona discharges are the most common devices used for the generation of atmospheric-pressure plasmas. Plasma jets are usually operated with noble gases (argon or helium) in ambient air and generate highly reactive oxygen and nitrogen chemical species in a more controlled and repeatable manner than other plasma sources. Thus, the treatment of liquids by plasma jets provides an opportunity to tune the liquid chemical composition depending on applications. The choice of appropriate operating conditions is crucial in this case and is well supported by modeling studies. In this work, we demonstrate the results of predictive modeling for a MHz-driven atmospheric-pressure plasma jet [1] in contact with liquid. We provide an overview of recent results and discuss the future perspectives of our research on applications of the atmospheric-pressure plasma jets.

MODEL DESCRIPTION

The model of the plasma jet-liquid interaction describes the momentum, mass and heat transfer in the gas and liquid phases, generation of plasma discharge in the gas phase and the plasma-induced chemical processes in the plasma jet-liquid system. The governing equations of the model are solved numerically using the in-house code based on the finite-element method.

RESULTS & DISCUSSION

The developed numerical model is used to perform parametric studies and identify optimal operating conditions of the plasma jet interacting with water and phosphate-buffered saline. In particular, we discuss the effect of the jet operating frequency, operating gas composition, distance to the liquid and duration of plasma treatment. The obtained results demonstrate how the accumulation of the long-lived (H_2O_2, NO_2^-, NO_3^-, HNO_3, etc.) and short-lived (OH, O, NO, O_2^-, etc.) reactive species in the liquid can be mediated by changing the specific operating conditions of the plasma jet-liquid interaction.

CONCLUSION

The present work provides an overview of recent progress in the predictive modeling of the atmospheric-pressure plasma jets in contact with liquid for biomedical and agriculture applications. In addition, future perspectives of the application of atmospheric-pressure plasma jets and their modeling are discussed.

REFERENCES

[1] S. Reuter, Th. von Woedtke, K.-D. Weltmann, *J. Phys. D: Appl. Phys.* **51** 233001, 2018.

Applying 3D Scanning Method to Model the RF Heating Process for Irregular Shape Foods

Ruyi Zhang[1], Feng Li[1]and Yang Jiao[1]

[1] Research Center of Food Thermal Processing Technologies,
Shanghai Ocean University, Shanghai, China

Keywords: Radio frequency, 3D scanning, Computer simulation, Irregular shape.

INTRODUCTION

Radio frequency (RF) heating shows its advantages in food thermal processing with its characteristics of fast and volumetric heating. Sizes and shapes of food materials are critical influencing factors to its RF heating behavior [1]. COMSOL Multiphysics® is a commercial Finite Element Method (FEM) modeling package, which proved to be efficient in RF heating process modeling by many researches. However, many foods are of irregular complex geometries which cannot be described by the default options in the software. There are always discrepancies between a virtual shape and a real shape when depicting the food geometry, which influences the simulation accuracy during food processing.

As technology developed, the 3D scanning method was found to be capable of characterizing real geometry of various foods and to be imported into COMSOL Multiphysics® for simulating food processing [2]. In this study, we aimed to determine the simulation discrepancy between the real and virtual shape of potatoes in RF heating by applying the 3D scanning method. The thermophysical and dielectric properties were determined for RF heating simulation. RF heating experiments of the selected vegetables were conducted, and the temperature distributions obtained by experiment, regular-shape simulation and real-shape simulation within all vegetables were compared.

METHODOLOGY

Fresh potatoes were purchased from a local grocery store, rinsed, and dried with tissue paper. Imaging agent was sprayed on sample surfaces evenly. A high-resolution 3D scanner (Hualang sanwei, Guangzhou, China) was used to scan the samples from all angles. Then, the collected 3D data points were processed by the reverse-engineering method with a default software to obtain a solid surface.

Importing the generated geometry into COMSOL Multiphysics® (Figure 1a), a computer simulation process of RF heating was started by assigning physiochemical and dielectric properties of each domain, setting up initial and boundary conditions, meshing

the domains selecting of solvers, and solving the model. Parallelly, the virtual regular geometry, an ellipsoid, was created and the solutions were compared.

The experiments were conducted by using a 50 ohms 27 MHz RF heater (Sairem Labotron 12, France) under a setting power of 1 kW and an electrode gap of 11 cm to heat the sample. A fiber optic sensor was inserted into the potato sample to record the temperature-time history during the heating process (Figure 1b). After 40 min heating, the sample were taken out to obtain the surface temperature distribution with an infrared camera. The detailed simulation and experiment procedures could be found in a previous published work [1].

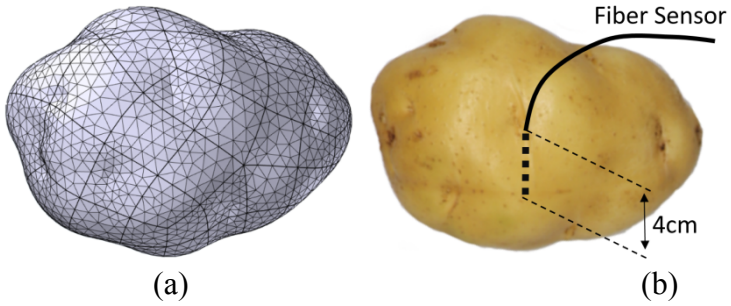

Figure 1. 3D scanned geometry and the real potato geometry with fiber sensor insertion location.

RESULTS

Figure 2 shows the heating profiles of potato heated by RF for 10, 20, 30 and 40 min experimentally, in real-shape simulation, and in regular-shape simulation, respectively.

The cold spot appeared at the thinnest portion of the potato sample, and hot spot was found in the top-middle section of the potato throughout the RF heating process. After 10 min RF heating, the top bump of the potato showed the highest temperature of 41.4 ºC and the lowest temperature showed at the right thinnest tip, which was 32.2 ºC. As heating time increased, the potato hot spot temperature increased to 48.5 ºC, 56.1 ºC and 60.5 ºC at 20, 30 and 40 min. Comparing the real-shape and regular-shape simulation with the experimental results, real-shape simulation results are much closer to the experimental results. The regular-shape simulation showed a relatively lower temperature in general. The intersecting surface temperature contour also showed the real-shape simulation could accurately predict the hot/cold spot location and temperature profile during RF heating.

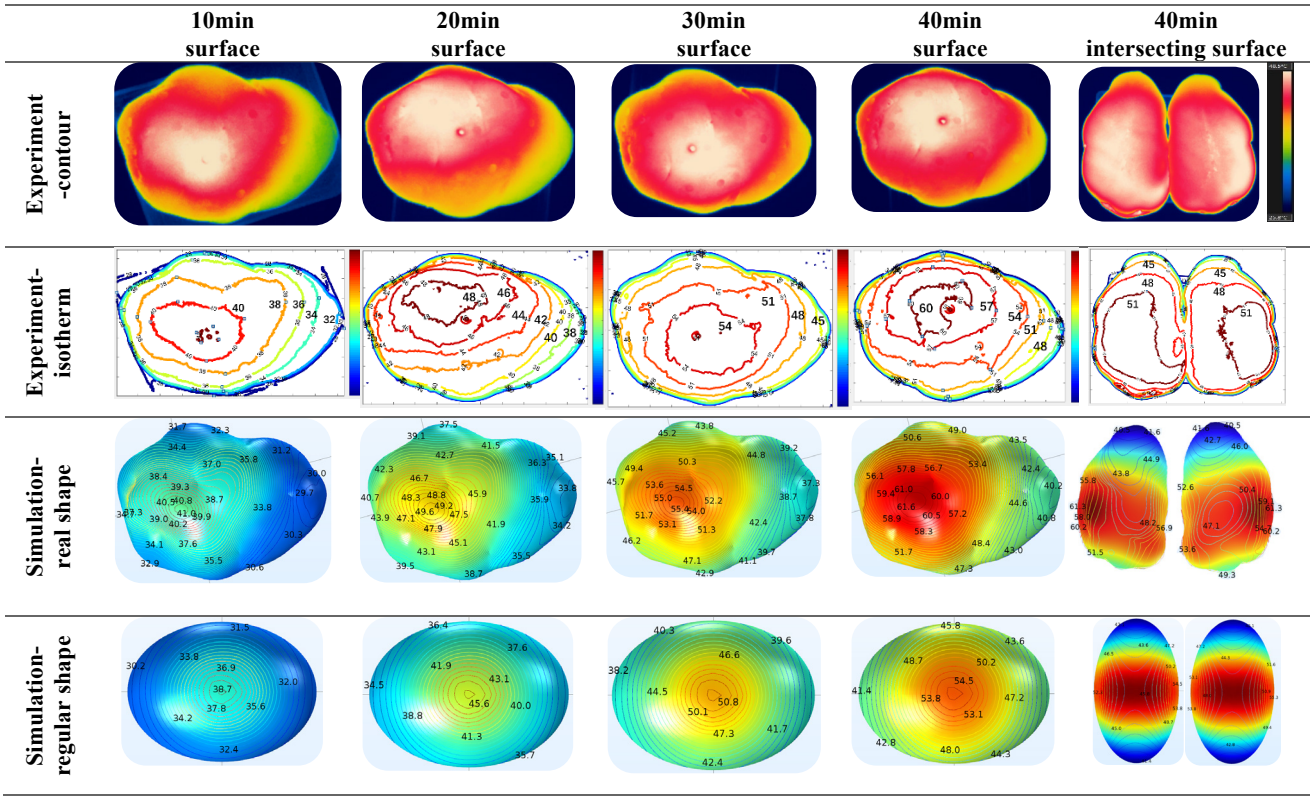

Figure 2. Simulated and experimental transient heat pattern of a potato with real and virtual shape during RF heating.

DISCUSSION

Real-shape simulated temperature results were similar to the experimental results at all time and locations within the potato geometry. Large temperature deviations were found between the regular-shape simulation and the experiment.

CONCLUSION

Using the 3D scanned geometry in simulating the RF heating process of an irregular-shape product is effective in accurately predicting the temperature distribution. The method can be applied to various loads with complex shapes in food industry.

REFERENCES

[1] Y. Li, F. Li, J. Tang, R. Zhang, Y. Wang, T. Koral, Y. Jiao. Radio frequency tempering uniformity investigation of frozen beef with various shapes and sizes. *Innov. Food Sci. and Emerg. Tech*. vol. 48, pp. 42-55, 2018.

[2] K.D. Kuffi, T. Defraeye, B.M. Nicolai, S.D. Smet, A. Geeraerd, P. Verboven. CFD modeling of industrial cooling of large beef carcasses. *Intl. J. of Refri,* vol. 69, pp. 324-339, 2016.

Transformation Optics for Computing Heating Process in Accordion Microwave Oven

Yuping Wu, Huacheng Zhu, Yang Yang, Kama Huang, Yi Zhang

(College of Electronics and Information Engineering, Sichuan University, Chengdu 610065, China)

Keywords: Heating uniformity, microwave heating, accordion microwave oven, portable, time-vary medium, transformation optics.

INTRODUCTION

Many households own domestic microwave ovens due to their convenience. [1] However, the microwave frequency and cavity dimensions produce standing waves. There are some drawbacks of microwave heating specifically in non-uniform heating which limit the development. [2] In order to improve the uniformity of the electromagnetic field in microwave multi-mode cavities, Plaza-Gonzalez et al. studied several kinds of mode stirrer configurations to change the electric field distribution and the mode of the electromagnetic field in multi-mode cavities. [3] The conventional domestic microwave ovens with fixed geometry is cumbersome and takes up space when not in use. In this paper, we present a novel accordion microwave oven which solves the moving boundary based on transformation optics. Transformation optics is proposed to solve the problem of the moving boundary during the model simulation. The accordion zone is replaced by a time-varying anisotropic layer on the basis of transformation optics, allowing the electromagnetic field inside the accordion microwave oven to be computed with consideration of the continuous motion of the moving boundary. The accuracy of this method is verified by comparing with the electric field distribution and the reflection coefficient of the port with the discrete position. By comparing with the COV (temperature coefficient of variation) of the heated material, it can be seen that the prosed method can greatly improve the uniformity of temperature distribution .

METHODOLOGY

A. The Theory of Transformation Optics Algorithms (TOA)

During the design of the accordion microwave oven and the optimization of the movement mode, the moving boundary of this system makes the calculation become more complex. In order to reduce the calculation size of this system. The coordinate transformation be used in this system. Firstly, the permittivity and permeability tensor of the time-variant medium are calculated by stretching the space with the theory of transformation optics. Generally, it is notable fact that Maxwell's equations are form-invariant under any coordinate transformations [1]. In order to simplify the computing, the

theory of transformation optics is applied to the coordinate.at first, we define a general coordinate transformation,

$$\vec{\mathbf{r}} \rightarrow \vec{\boldsymbol{r}}' = \boldsymbol{T}(\vec{\mathbf{r}})$$

Where $\vec{\boldsymbol{r}} = (\boldsymbol{x},\ \boldsymbol{y},\ \boldsymbol{z})$ and $\boldsymbol{r}' = (\boldsymbol{x}',\ \boldsymbol{y}',\ \boldsymbol{z}')$ are the vectors of position of the original and present coordinate system, respectively.

Maxwell equations remains form-invariant, even in different coordinate system. So the permittivity and permeability can be written as[4]:

$$\bar{\bar{\boldsymbol{\varepsilon}}} = \boldsymbol{\varepsilon}\bar{\bar{\boldsymbol{\Lambda}}}$$

$$\bar{\bar{\boldsymbol{\mu}}} = \boldsymbol{\mu}\bar{\bar{\boldsymbol{\Lambda}}}$$

$$\bar{\bar{\boldsymbol{\Lambda}}} = \left(\boldsymbol{det}\bar{\bar{\boldsymbol{J}}}\right) \cdot \left(\bar{\bar{\boldsymbol{J}}}^{\boldsymbol{T}} \cdot \bar{\bar{\boldsymbol{J}}}\right)^{-\mathbf{1}}$$

Where det denotes the determinant and $\bar{\bar{\boldsymbol{J}}}$is Jacobi's tensor, which is defined in Cartesian coordinates as:

$$\bar{\bar{\boldsymbol{J}}} = \frac{\boldsymbol{\partial}(\boldsymbol{x}', \boldsymbol{y}', \boldsymbol{z}')}{\boldsymbol{\partial}(\boldsymbol{x}, \boldsymbol{y}, \boldsymbol{z})} = \begin{bmatrix} \boldsymbol{\partial x'/\partial x} & \boldsymbol{\partial x'/\partial y} & \boldsymbol{\partial x'/\partial z} \\ \boldsymbol{\partial y'/\partial x} & \boldsymbol{\partial y'/\partial y} & \boldsymbol{\partial y'/\partial z} \\ \boldsymbol{\partial z'/\partial x} & \boldsymbol{\partial z'/\partial y} & \boldsymbol{\partial z'/\partial z} \end{bmatrix}$$

B. Model description

The microwave oven model used in this article consists of a multimode cavity containing a block of material,the input port is BJ22 waveguide, The waveguide is centered at the bottom of the cavity and connected to a microwave source. The field in the multimode cavity is excited by a transverse electric(TE) wave，which is a wave that has no electric field component in the direction of propagation. Other boundaries are assumed as perfect electric conductors (PEC). At the same time, the model is divided into several rectangle domains, three-dimensional(3D) swept meshes can be employed in a mesh building, as shown in Fig2(b).

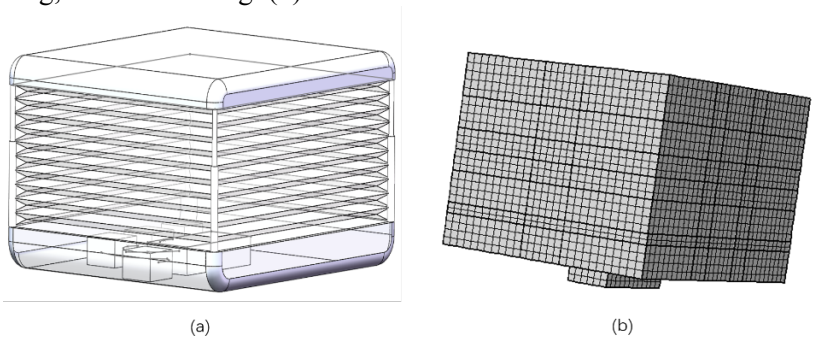

Fig.2. (a) an overall sketch of the accordion oven; (b) finite element mesh of the microwave cavity in this study.

RESULTS

To precisely compare the uniformity improvement of the accordion microwave oven, we need to quantify the heating results. One of the most efficient way to quantify the uniformity is to value the coefficient of variation (COV) .

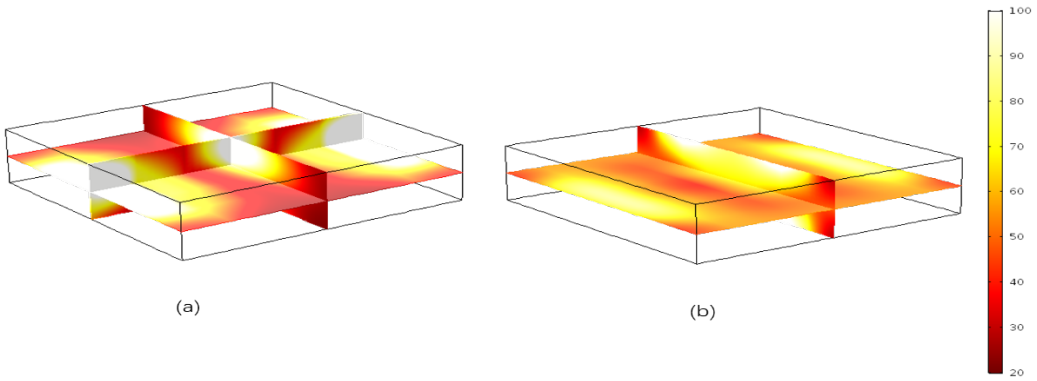

Fig.2.Spatial temperature profiles of potatoes heated by different methods (temperature unit: ℃): (a)heating with conventional microwave oven, COV=0.5413, T=59.1; (b) heating with accordion microwave oven based on transformation optics, COV=0.3120, T=63.33;

DISCUSSION

The COV is the ratio of the standard deviation to the mean. According to this method, a better uniformity of the heating results will have a lower COV. The COV of the potato in fixing heating is 0.5413 and the accordion heating is 0.3120 ,This can be considered as a (0.5413-0.3120)/0.5413 or 42.36 % increase in temperature uniformity.

CONCLUSION

In this study, we have proposed a new kind of method to solve the non-uniform heating problem of the microwave oven. Compared with the conventional microwave ovens, the proposed design can make a great contribution in the improvement of uniform temperature distribution,

REFERENCES

[1] Zhu H C , Liao Y H , Xiao W , et al. Transformation Optics for Computing Heating Process in Microwave Applicators With Moving Elements[J]. IEEE Transactions on Microwave Theory and Techniques, 2017:1-9.

[2] Vadivambal, R. , and D. S. Jayas . "Non-uniform Temperature Distribution During Microwave Heating of Food Materials—A Review." *Food and Bioprocess Technology* 3.2(2010):161-171.

[3] Plaza-Gonzalez P , Monzo-Cabrera J , Catala-Civera J M , et al. Effect of mode-stirrer configurations on dielectric heating performance in multimode microwave applicators[J]. IEEE Transactions on Microwave Theory and Techniques, 2005, 53(5):1699-1706.

[4] Ozgun O . Form Invariance of Maxwell's Equations: The Pathway to Novel Metamaterial Specifications for Electromagnetic Reshaping[J]. IEEE Antennas & Propagation Magazine, 2010, 52(3):51-65.

Measurement System to Determine Complex Dielectric Properties for Various Materials While RF Processing

Stephan Holtrup[1], Philipp Priester[1] and Klaus Werner[1]

[1]pinkRF, Nijmegen, Netherlands

Keywords: Solid state RF, dielectric measurement, microwave energy, RF heating, RF food processing, dielectric power measurement, TRL calibration.

INTRODUCTION

Dielectric properties are of major interest while processing materials with microwave energy. There is a lot of data available for different materials. One of the most investigated fluid materials with respect to the permittivity (ε_r), loss tangent ($\tan\delta$) and conductivity (σ) is water. Its complex permittivity can be modeled by Debye relation [1] and it is measured multiple times in different concentration with NaCl and at multiple temperatures. Water has a high permittivity change vs. frequency response and the losses are highly depending on the impurities of the water. Distilled water e.g. is nearly lossless while adding a small amount of salt to it forms a low conductivity medium that absorbs microwaves well. Salt is nearly always used in food and changes the material properties compared with the natural ingredients. Furthermore, a complete meal consists of various types of ingredients mixed together. Therefore, it is necessary to determine the material properties, not only for the individual ingredients, but also for the overall mixture. To measure the dielectric properties a setup is used, which is large enough to carry the overall mixture. Another impact on the dielectric properties is the microwave process itself. For example, while heating a meal water starts to boil, and the meal begins to dry. Lowering the water content also changes the dielectric properties. This results in the interest of performing the dielectric measurement while the material mixture is being treated with RF energy.

EXPERIMENTAL APARATUS

The measurement setup, shown in Figure 1, is built up with a microstrip line, including a container underneath the microstrip line for carrying the sample material or mixture. The fixture can be used to measure the complex dielectric properties of various mixtures, like processed food, or other liquids or solid compositions, which conform to the container's shape. While using the container underneath the microstrip line, RF power can be used to heat the dielectric and measurements of its complex permittivity can be done during the process. The container is open at the top for additional visual or IR sensing. The microwave power used in this experiment can be up to 250 W at 2400 to 2500 MHz, because this is a

commonly used ISM band. However, measurements at different frequencies are principally possible.

This test fixture is connected via standard N-Type cables and the RF connectors are then placed on the microstrip line via the mechanical mount. The coax to microstrip transition is corrected by the TRL-calibration performed with different calibration PCBs (thru, reflect and line) within a frequency range from 300 MHz to 2600 MHz. The sample material is then placed between a rugged microstrip line and ground. While the EM-wave is traveling along the microstrip line it interacts with the sample, which leads to changes in velocity and decreases in amplitude. This interaction can be measured by the S-Parameters, mainly S_{21}. In principal this measurement technique is based on the transmission line measurement technique. A detailed explanation can be found in [2].

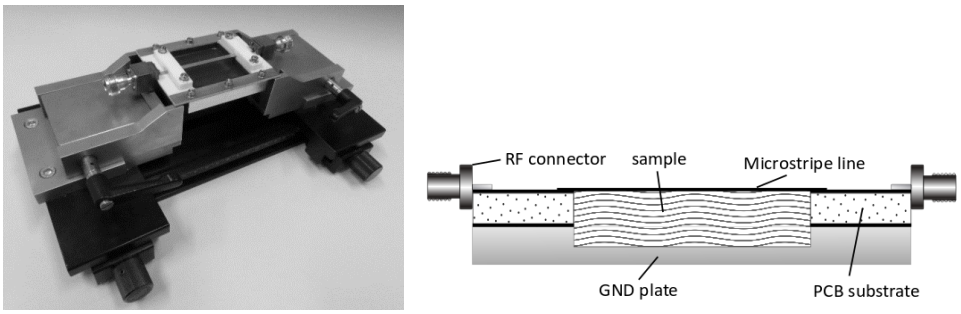

(a) (b)

Figure 1. Dielectric measurement system for large signal RF measurement. Picture of the fixture incl. mechanical mounts (a) and schematic cross section of the measurement setup (b).

RESULTS

Table 1 shows some example measurements, performed with this setup with small-signal-conditions, at an ambient temperature of 25 °C. Measurement results are in a good agreement with values taken from literature.

		Measurement			Literature		
Sample	f / MHz	ε'	ε''	tanδ	ε'	ε''	tanδ
Soja oil	2450	2.57	0.13	0.051	2.62	0.17	0.064
Saline (1%)	915	71.8	35.1	0.489	77.3	37.2	0.482
Salsa	2450	37.0	18.0	0.48	-	-	-

Table 1. Measured complex permittivity for different samples compared with literature values. Data for soja oil taken from [3] and for the saline solution (1.0% NaCl) taken from [4].

A large signal measurement with 2 W of RF power at 2450 MHz was performed for the salsa. The IR image was taken while the salsa was in steady state conditions. Figure 2 shows the IR image and the temperature profile along the microstrip line and from the hottest point close to the microstrip line across to the wall of the sample container. The measurement shows multiple effects. The salsa has a penetration depth of ca. 16 mm at

2450 MHz that prevents the RF from traveling through the entire sample container. Since the heat conductivity is present, the temperature decays more slowly compared with the exponential decay of the absorbed RF power along the microstrip line. The temperature drop at the beginning of the solid temperature line is because of the heat transfer into the wall of the sample container. The dashed line mainly shows the impact of the heat condition and the decay of the fringe field from the microstrip line, which decreases rapidly.

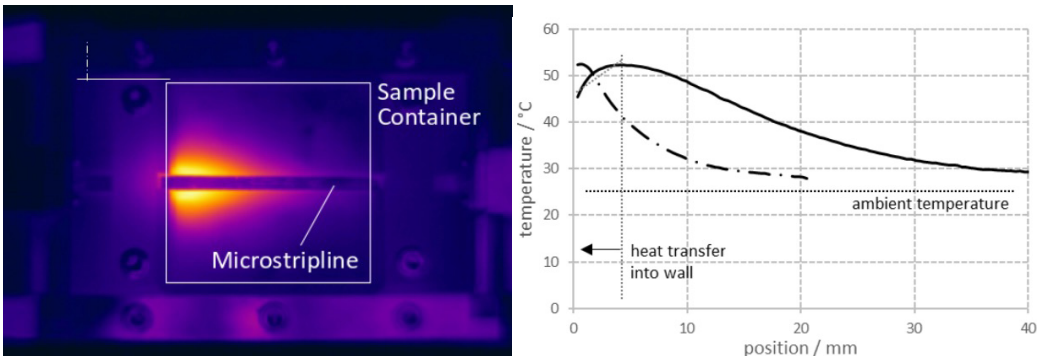

Figure 2. IR image (a) of salsa at 2W RF power at 2450 MHz in steady-state condition and the temperature profile (b) along the microstrip line (solid) and across to the wall (long dashed).

CONCLUSION

This test fixture is usable for complex permittivity measurements at different conditions. It can be used with a small or a large signal, and with or without additional heat sources to bring the material up to a homogeneous temperature. Additionally, it can also be used in a pulse mode (here a few seconds) to separate the relatively quick RF impact from the slow temperature effects, like heat conduction.

With this measurement system it is possible to gain the complex permittivity properties of various material compositions while processing with microwaves. Furthermore, this setup enables quick experimental evaluation of how the RF interacts with the sample material. This experimental data can be used to develop more accurate microwave heating applicators leading to a more efficient heating process.

REFERENCES

[1] S. Horikoshi, R. Schiffmann, J. Fukushima, N. Serpone, *Microwave Chemical and Materials Processing,* Springer, Singapore, 2018.

[2] V. Komarov, S. Wang, J. Tang, *Permittivity and Measurements, In Encyclopedia of RF and Microwave Engineering*, K. Chang (Ed.), 2005.

[3] M. Kent, *Electrical and Dielectric Properties of Food Materials*, COST 90bis Production, Science and Technology Publishers, Hornchurch, Essex, UK, 1987.

[4] J. N. Ikediala, J. Hansen, J. Tang, S. R. Drake, and S. Wang, *Development of saline-water-immersion technique with RF energy as a postharvest treatment against codling moth in cherries*, Postharvest Bio. Technol. 24:25–37, 2002.

Feasibility Study on Simultaneous Microwave Heating of Multiple Samples by Electromagnetic Coupling-Type Applicator

Tomohiko Mitani, Daichi Nishio and Naoki Shinohara

Kyoto University, Uji, Japan

Keywords: Microwave applicator, Electromagnetic coupling, Resonator, Simultaneous heating.

INTRODUCTION

A new type of microwave applicator using electromagnetic coupling is proposed in the present study. The electromagnetic coupling technologies have been recently studied and developed in the field of wireless power transfer [1]. Conventional single-mode applicators using waveguide cavity resonators and multi-mode applicators are basically surrounded and shielded by metal walls to prevent the microwave leakage. In case of batch treatment, these shielded applicators are needed to open and close the door or hatch in order to set up the samples. This effort could waste a significant amount of time particularly in microwave-assisted chemistry when one attempts to heat many samples of a small volume. Furthermore, unpredictable reflection in multi-mode applicators leads to low reproducibility of chemical processing by microwave heating. The proposed applicator contributes to solving these drawbacks. Moreover, it can provide an "open-space" design for microwave heating.

Previous work [2] verified that the proposed applicator could heat a liquid sample using 2.45 GHz microwave radiation. In this paper, we describe simultaneous microwave heating of multiple liquid samples using the electromagnetic coupling-type applicator.

METHODOLOGY

Schematic diagrams of the proposed applicators are shown in Fig. 1. These applicators were composed of two substrates (Nippon Pillar Packing, NPC-H260A, permittivity: 2.56, loss tangent: 0.0018, thickness: 1.6 mm) with half-wavelength rectangular resonators made of copper (thickness: 18 μm). Two liquid samples (4.3 ml ultrapure water) were poured into each glass test tube and set between two substrates. The 50 Ω input port was connected to the resonator on the primary substrate side. Regarding the secondary substrate, we investigated two cases: a single resonator was put facing the primary resonator as shown in Fig. 1(a), and double resonators and the primary resonator

were put in a triangular arrangement as shown in Fig. 1(b). The resonator size was 40 mm by 10 mm, and the target resonant frequency was 2.45 GHz. The distance between two substrates was 20 mm. The ground planes were placed on the back side of the resonators both on the primary and secondary substrates. When 2.45 GHz microwave is supplied from the input port to one of the resonators via a coaxial cable, an electromagnetic field is generated and coupled between the resonators and the liquid samples can be heated.

The proposed applicators were designed by using 3D electromagnetic simulator Ansoft HFSS. Impedance matching of the applicator can be realized by adjusting the resonator size and the distance between two resonators. After designing, demonstration experiments of simultaneous microwave heating were conducted. Temperature of each sample was measured by optical fiber thermometer during microwave heating.

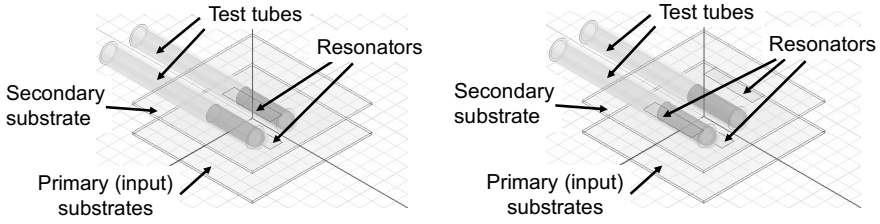

(a) (b)

Figure 1. Schematic diagrams of the proposed microwave applicators using electromagnetic coupling: single resonator (a) and double resonators (b) on the secondary substrate side.

RESULTS

Simulated results of electric field in the cross section of the proposed microwave applicators are shown in Fig. 2. It is observed that electric field was coupled between two substrates and was intensified in the liquid samples in both applicator configurations. Microwave absorption rate, which can be derived from the total absorbed power in two liquid samples divided by the input power, was 13.4% ~ 68.6% in the case of applicator with a single resonator, and 51.9% ~ 86.1% in the case of applicator with double resonators. Microwave leakage outside the applicator with double resonators was calculated to be 1.6% ~ 3.7%, which was half of the single resonator case: 3.3% ~8.0%. The microwave absorption rate and microwave leakage were dependent on the sample temperature, i.e. the sample permittivity.

Measured results of temperature variations of two liquid samples by microwave heating are shown in Fig. 3. Only the microwave applicator with double resonators was used in the experiments. The operating frequency was 2.45 GHz and the microwave output power was 10W; three trials were conducted in total.

DISCUSSION

As seen from simulation results, the performance of microwave applicator with double resonators were superior to that with a single resonator, in the light of microwave absorption rate and microwave leakage outside the applicator. The measured results shown in Fig. 3 prove that the proposed microwave applicator could heat two liquid samples

simultaneously and their heating rates showed almost the same trends. The measured temperature difference between two samples was 3.2 K at most.

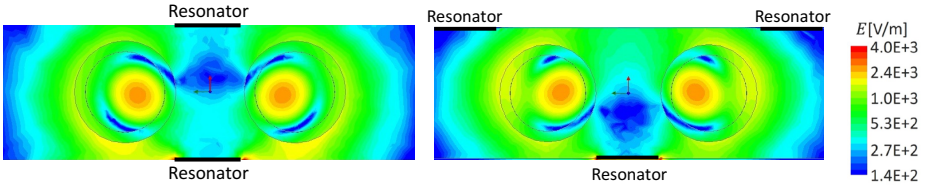

(a) (b)

Figure 2. Simulated results of electric field in the cross section of proposed microwave applicators: single resonator (a) and double resonators (b) on the secondary substrate side.

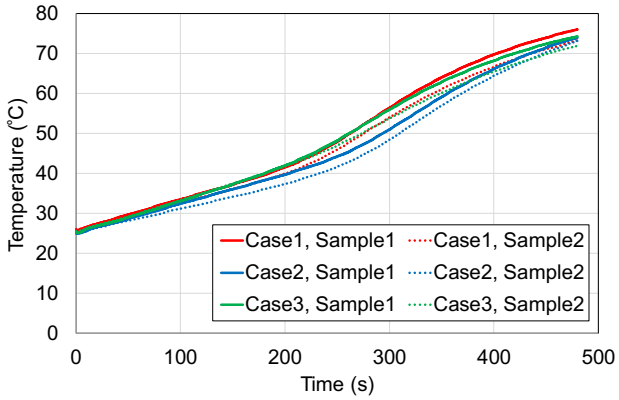

Figure 3. Measured results of temperature variations of liquid samples (ultrapure water) by the proposed microwave applicator using double resonators on the secondary substrate side.

CONCLUSION

A microwave applicator using electromagnetic coupling was successfully developed and simultaneous microwave heating of two liquid samples was realized with features of low microwave leakage. As a future work, we will expand the applicator area for simultaneous microwave heating of a large number of samples.

ACKNOWLEDGMENT

This work was supported by JSPS Kakenhi Grant Number 18K04263. Experiments were conducted thanks to collaborative research program: Microwave Energy Transmission Laboratory (METLAB), Research Institute for Sustainable Humanosphere, Kyoto University.

REFERENCES

[1] A. Kurs, A. Karalis, R. Moffatt, J. D. Jonnopoulos, P. Fisher, and M. Soljacic, Wireless Power Transfer via Strongly Coupled Magnetic Resonances, *Science*, vol. 317, pp.83-86, Jul. 2007.

[2] T. Mitani, D. Nishio, and N. Shinohara, Feasibility Study on a Microwave Heating Applicator Using Electromagnetic Coupling, *Proc. Asia-Pacific Microwave Conference (APMC) 2018,* Kyoto, Japan, Nov. 2018, FR1-103-3.

Test Set for Dielectric Measurements of Double Layer Laminates

V. Ramopoulos[1], S. Soldatov[1], G. Link[1] and J. Jelonnek[1,2]

[1]IHM, IHE[2], Karlsruhe Institute of Technology (KIT), 76131Karlsruhe, Germany

Keywords: Dielectric heating, dielectric measurements, mode, selectivity.

INTRODUCTION

Different types of synthetic leather are widely used as decorative materials for surface coating in the automobile industry. Hot melt bonding is the usual method to fix the decorative material (the decorative leather) to the substrate (typically polymer blend material) surface. The hot melt adhesive is located between the coating and the substrate surface. For some sorts of hot melts, a temperature of about 80 °C is enough to get them sticky. Microwave heating is a flexible, less time consuming and more energy efficient heating method as compared with conventional heating methods [1]. This is because of the volumetric and selective heating characteristics of the microwave heating. Particularly, the selectivity of microwave absorption, according to the loss factor of materials, allows a unique temperature distribution, which is not possible if using conventional heating methods. However, successful microwave heating of a coating-adhesive-substrate sandwich structure requires a detailed knowledge of the dielectric properties of the materials used. The measurements setup presented here allows the precise dielectric characterization of synthetic leather with and without glue. In this connection the synthetic leather is point wise coated with glue (see [1]). Figure 1 shows the developed measurements setup. Additionally, the full-wave 3D electromagnetic model of the experimental setup was developed to explore the influence of the adhesive, covering the wrong side of the coating, on the total permittivity.

METHODOLOGY

For the design of an appropriate test set, the cavity perturbation method was chosen. Since the synthetic leather has a relatively low dielectric loss factor [1], a cavity with a quality (Q-) factor above 1000 is required. At this place, a cylindrical cavity, which contains an equatorial split [2-3], is used. This enables measurements of flat samples positioned parallel to the cavity ends that occupy all the cavity cross-section. The cavity design allows the excitation of the TE_{111}- mode at 2.45 GHz and provides an unloaded Q-factor of about 12000. The TE_{111} –mode is chosen, because it provides a maximum electric field in the cavity center [4]. At the same time, the wall currents are parallel to the sample and cavity cut. Thus, a perturbation oriented along the cavity radius will not cut the surface currents. It minimizes the change of the electric field profile inside the cavity compared with an unsplit resonator. A small lab jack with a micrometer screw in combination with

an appropriate cavity holder is used to enable the precise adjustment of the distance between both resonator parts.

The calibration of the system requires the full-wave 3D electromagnetic field simulation. Here CST Microwave Studio is used. The calibration was made for a full range of the expected dielectric properties and thicknesses of the coating material, from 0.5 mm up to 2 mm.

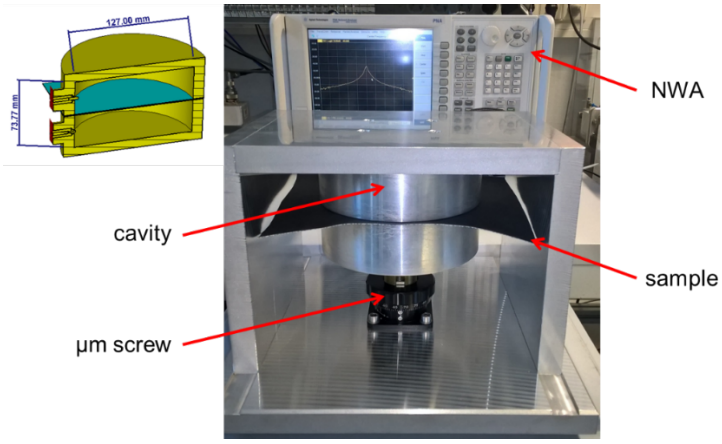

Figure 1. Measurement setup.

RESULTS

Two successive measurements were done for the dielectric characterization of the double layer material. In the first measurement the dielectric properties of the synthetic leather without glue was characterized. The leather thickness was estimated to be about 1 mm (± 0.05 mm). The corresponding dielectric properties of the measured leather samples (both with and without an adhesive layer), which are different in color, are presented in Table 1 (Synthetic leather (gray), synthetic leather (beige) and synthetic leather (black)).

Table 1. Measured dielectric properties

Material	ϵ'	$tan\delta$
Synthetic leather gray	1.87	0.020
Synthetic leather beige	1.88	0.021
Synthetic leather black	1.89	0.021
Synthetic leather black + Glue 1 with 2% carbon	2.05	0.050
Synthetic leather black + Glue 2 with 2% carbon	2.07	0.053
Synthetic leather black + Glue 1 with 4% carbon	2.13	0.068
Synthetic leather black + Glue 2 with 4% carbon	2.11	0.075
Glue 1 with 2% carbon	8.04	0.391
Glue 2 with 2% carbon	9.04	0.388
Glue 1 with 4% carbon	12.05	0.437
Glue 2 with 4% carbon	11.04	0.534

Moreover, the effective permittivity of the black synthetic leather, covered by different kinds of glue, was measured (Table 1, Synthetic leather black + Glue 1 with 2% carbon, Synthetic leather black + Glue 2 with 2% carbon, Synthetic leather black + Glue 1 with 4% carbon and Synthetic leather black + Glue 2 with 4% carbon). The adhesive mass fraction was estimated to be about 3.2 weight percent. For the further processing, and by using the density of the glue, the dot-wise adhesive volume was approximated by a homogeneous layer with an effective thickness of 0.08 mm. Based on the known effective glue thickness, the dielectric properties of the glue are estimated with the post processing tool 'Extract Material Properties from S-Parameters' in CST Microwave Studio (see Table 1, glue 1 and glue 2 with 2% and 4 weight% carbon blend, respectively). The accuracy of the estimated properties strongly correlates to the sample thickness. An estimated uncertainty in the calculated effective glue thickness of ± 12 % leads to a measurement error of ± 12 % for the permittivity and ± 15 % for the loss factor of the glue, respectively.

CONCLUSION

In the present work, a test set for dielectric characterization of thin multilayer materials at 2.45 GHz was designed. This design is based on a TE_{111} cylindrical resonator with an equatorial slit. The full wave numerical simulations enabled the calibration of the measuring system in the full range of dielectric properties of the investigated materials. The dielectric properties obtained for synthetic leather agree well with the data measured with the cavity perturbation approach in a TE_{104} cavity reported in [1]. However, the hot melt permittivity evaluated with CST post-processing routine results in values which are a factor of 4 higher as compared with the ones reported in [1]. This may be explained by the different preparation methods of the measured samples. In [1], the sample was a compact from dried adhesive powder that typically never reaches full density, therefore permittivity is underestimated. Here errors occurred due to assumption of an effective glue layer.

ACKNOWLEDGEMENT

This research and development project is funded by the German Federal Ministry of Economic Affairs and Energy (BMWi) within the 6. Energy Research Program (funding number 03ET1576A) and managed by the Project Management Jülich (PTJ)

REFERENCES

[1] S. Soldatov, J. Meiser, B. Lepers, G. Link and John Jelonnek. Microwave assisted bonding of synthetic leather to plastic substrates. In 3rd Global Congress on Microwave Energy Applications. Cartagena, Spain, 25-29 July 2016

[2] Michael D Janezic, Edward F Kuester, and JB Jarvis. Broadband complex permittivity measurements of dielectric substrates using a split-cylinder resonator. In Microwave Symposium Digest, 2004 IEEE MTT-S International, volume 3, pages 1817-1820. IEEE, 2004.

[3] Ali, Mohd. Tarmizi, M. K. M. Salleh and Md. Mahfudz Md. Zan. Air-Filled Circular Cross Sectional Cavity for Microwave Non-Destructive Testing. In International Journal of Mechanical and Mechatronics Engineering Vol:2, No:6, 2008.

[4] A. Nesbitt, P. Navabpour, B. Degamber, C. Nightingale, T. Mann, G. Fernado, R. J. Day, "Development of a microwave calorimeter for simultaneous thermal analysis infrared spectroscopy and dielectric measurements IOP Publishing Ltd", pp. 2313-2325, 2004.

RF Power Substrates Applied for RF Energy

J.H. Berkel

Multek technologies, Zhuhai, China

Keywords: Power amplifier, RF cooking, heating and drying, RF power module, Solid State, Pallet heatsink.

INTRODUCTION

Given today's requirements for electronic products in 5G communications, RF energy, wearables, Internet of things (IoT), autonomous driving and other applications, the printed circuit boards (PCBs) and their respective substrate materials play a critical role for the fabrication, reliability, and cost of these electronics. This statement is particularly true for the PCBs for RF Energy applications. Very high power levels of RF next to large heat fluxes due to losses in the amplifier structures and (in-) compatibilities with automated assembly and test machines have made the used PCBs and hence the RF amplifier an expensive component. A fact that the former RF Energy Alliance has tried to alleviate since the manufacturing cost levels of the older technologies have prevented any significant uptake of the solid state RF Energy technology into commercial or even white-goods applications.

In the meantime, recently developed PCB technologies have changed this picture drastically.

This paper focuses on RF power amplifier modules manufacturing. Thanks to newly available PCB technologies, we can now realize large scale applications with innovative designed, engineered and manufactured applications. Integration of functionality and volume manufacturing approaches are becoming possible now. These approaches contribute significantly to the development of these markets. This paper is showing the details on how these technologies work.

TECHNOLOGY BACKGROUND

When starting with the design of a new discrete power transistor applications, typically a so-called reference design done by the original transistor component company along with application notes are issued to potential customers.

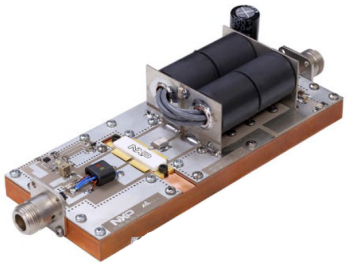

Figure 1: Typical "old style" reference design of a low frequency, high power single amplifier stage

These reference designs are quite bulky, heavy, and not suitable for large scale manufacturing. (see figure 1) Many manual steps and tuning of the amplifier stages are

required. Also, the single layer RF laminate on a massive copper heatsink did not provide for design flexibility or integration of additional functions. As stated, this technology does not lead to industrializing new products repeatability, at reasonable costs.

By working with all the partners in the supply chain a completely different approach was developed to meet the needs of the potential customers.

Patented

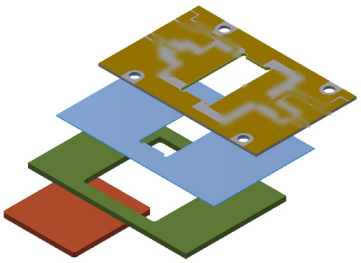

Figure 2: Basic elements of the new PCB technology: Different FR4 layers with high design freedom combined with a RF laminate and embedded copper coins for the thermal management.

The technology is explained together with the requirements of the power transistor circuitry and other components embedded in the PCB stack and/or present on the top layer of the board. The technology "ingredients" include:

- Various materials (like FR4, copper, RF laminate, pre-preg) used and combined into hybrid structures to enable an optimal combination of RF performance at low cost.
- Embedded heat removal elements (copper coins) integrated into the stack to enable heat spreading and removal along with flush mounting onto heatsink bodies.
- An overall material stack that provides mechanical robustness and testability of the module without further mechanical carriers (like the former copper or aluminum backing)

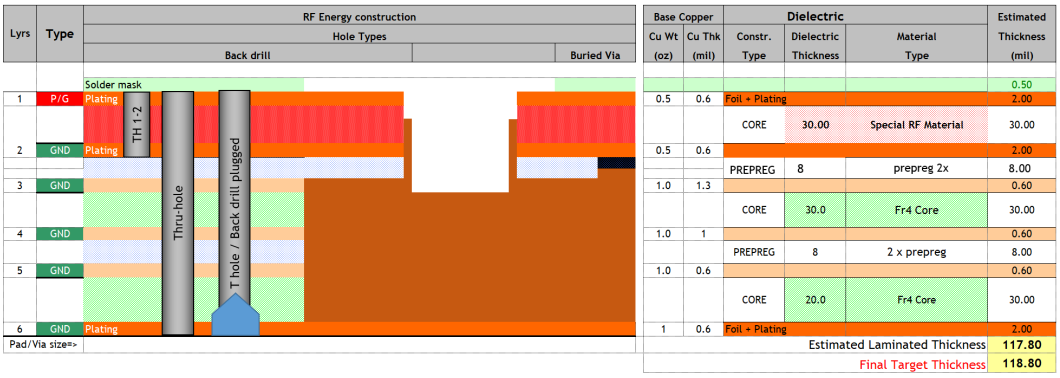

Figure 3: Build-up example with the different layers, connections, heat body, etc.

- Various shapes and sizes of heat removal elements to cater to different dissipation scenarios
- Different means to cater for high output power challenges and the prevention of transitions in the RF signal path
- Freedom to design embedded shapes for heat removal or additional functionality
- Manufacturing procedures and materials compliant with automated, high volume manufacturing and testing
- The definition and specialized care for critical dimensions and other critical design input parameters

RESULTS

Major RF component manufacturers have successfully adopted these technologies enabling the growth in RF Energy devices. This technology is part of the next generation RF power amplifier modules, at the same time drastically improving the "readiness" of the modules. Additionally, implementation of this technology resolves RF power difficulties, and the application of the modules makes it much easier to handle over single RF power transistors.

In short, the new technology and its integrated concepts yield power amplifier module solutions, which support the successful combination of RF properties with integrated heat removal methods. See, e.g., a launched product example below.

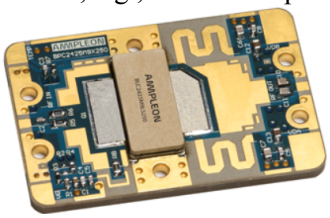

Figure 4: 250W, 2.45GHz RF power amplifier module built using the new technology. (courtesy Ampleon)

Furthermore, the method allows, in parallel, a route to bare die applications which is another break-through process. That is, the traditional transistor package vanishes. Instead, a multi-component, multi-stage amplifier can be embedded directly on the copper coin using semiconductor chips attachment and direct wire bonding.

RF power transistor engineers need to re-think their current design strategies to make use of the new possibilities of this technology optimally.

CONCLUSION

This development is a significant step forward for RF Energy applications. RF cooking and related industrial applications have adopted this technology by driving smaller and more cost-effective RF designs. This technology enables smaller amplifier modules, more functional integration, helping launch new intriguing solid-state RF Energy applications and appliances.

The first signs are there after many years of promises.

REFERENCES

[1] Keith Nelson, Quan Li, Lu Li and Mahesh Shah, Solder reflow attach method for high power RF devices in air cavity packages, Freescale/NXP semiconductor application note AN1908 Rev. 1 2/2011.
[2] Mustafa Konca and Steven J. Miller, LDMOS power amplifier design, Worcester Polytechnic Institute, Apr 2008.
[3] K. Werner, Design Challenges of SS-PAs for RF Energy Applications, IMPI's 50th Symposium
[4] Barry Manz, RF Energy is finally cooking, Microwaves & Radio Frequency. Dec 18, 2017.
[5] M. DeVincentis, G. Hollingsworth, R. Gilliard, "Long life solid-state RF powered light sources for projection display and general lighting applications", Microwave Symposium Digest, 2008 IEEE MTT-S International, June 2008: 1497 – 1500

Measurement of Graphene Films Based on Near-field Scanning Microwave Microscopy

ZhiLiao Du[1], Zhe Wu[1], Kun Peng[1], WeiWei Gan[1], BaoQing Zeng[2]

[1]School of Physics, University of Electronic Science and Technology of China, Chengdu, China
[2]School of Electronic Science and Engineering (National Exemplary School of Microelectronics), University of Electronic Science and Technology of China, Chengdu, China

Keywords: Graphene, Electromagnetic properties, Near-field, Microwave microscopy.

INTRODUCTION

In 1928, Synge first suggested the viability of near-field microscopy and in 1962 Soohoo demonstrated near-field microscopy at microwave frequencies. Near-field scanning microwave microscope (NSMM) operates like scanning probe microscopy. The general principle applied in NSMM is electromagnetic resonance perturbation. The measurement data is acquired in the form of a shift in resonant frequency and a quality factor change when the resonator and probe tip is held above a sample that perturb the electrical interaction between the probe tip and the sample in the microwave near-field region. These perturbations change the amplitude of the reflected signal S11 and shift the resonant frequency f_r. Using a simulation model to simulate the tip-sample interaction, the measurement data can be used to reveal material properties of interest which are not measured directly, such as the dielectric constant, conductivity, permeability [1] and other properties [2] of the sample under test. The NSMM [3] can provide a non-destructive method to distinguish the local electromagnetic properties of the sample rapidly [4]. In this manuscript, a characterization method for graphene films is described based on the NSMM under different annealing temperatures. By adopting NSMM with λ/4 coaxial cavity, when the probe is located close to the sample, we could figure out the samples high frequency electromagnetic characters according to the electromagnetic response in near-field area.

EXPERIMENTAL APPARATUS AND PROCEDURE

Graphene films were prepared by oxidation-reduction method, and graphene oxide films were annealed in Ar at different temperatures of 350°C, 550°C, 650°C and 800°C for 1 h to obtain graphene. Figure 1 shows the NSMM setup composed of a high quality (Q) factor λ/4 resonator, axial-rotation stabilizer, x-y motor, piezoelectric motor at z direction, vector network analyzer (VNA) (Agilent Technologies E5062A), lens, charge-coupled device (CCD) and a monitor. The graphene sample was placed on the flat platform which

was on top of the x-y motors. NSMM images can be collected and the diagram with the varying distance between the tip and the sample was drawn by MATLAB.

RESULTS AND DISCUSSION

Fig.2(a)-(c) show the measured results of frequency shift Δf_r ($\Delta f_r = |f_r - f_{r0}|$,where f_r is the resonant frequency which can be determined by $w_r = 2\pi f_r = 1/\sqrt{LC}$), S11 (reflection signal)and Q factor (Q factor is physically defined as the ratio of the energy stored in the resonator to the energy dissipated per cycle) of graphene films at different annealing temperatures with varying tip-sample distances. The Cr film (100nm thick) produced by sputtering was measured as the reference film also shown in Fig. 2.

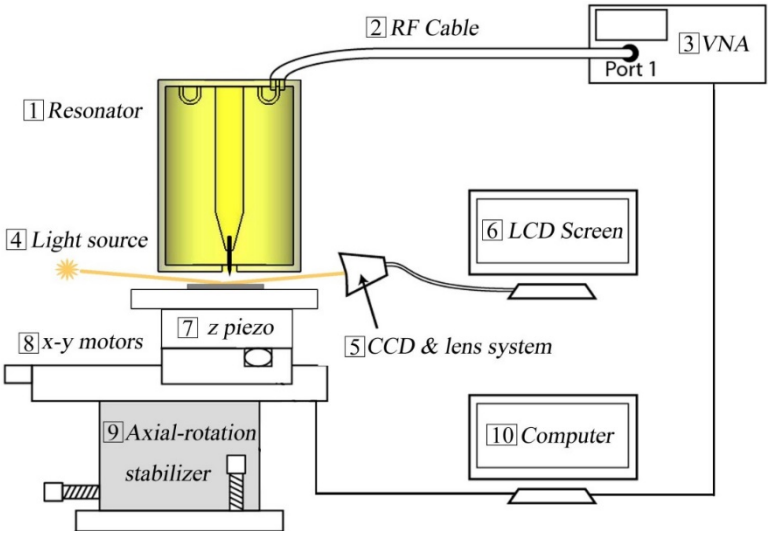

Fig. 1. The schematic of NSMM setup

In Fig.2 (a), frequency offset of the resonator decreases with the increase of tip-sample distance. The testing curves of graphene samples annealed at 800 °C are almost coincident with the Cr film. The curves of graphene sample after annealing at 650°C and the Cr film present a little deviation. However, the test results for annealing temperature of 350°C and 500°C have large difference with the results of Cr film. As shown in Fig.2 (b) and Fig.2 (c), the S11 amplitude decreases and the quality (Q) factor increases for the graphene films, as tip-sample distance increases. The dependence of the Q factor and the tip-sample distance for the graphene films after annealing at 800℃present nonlinear which is similar to the curve of the Cr film.

The graphene films prepared after the annealing temperature of 800℃have better conductivity than samples after annealing at other temperatures. The dielectric constant and the resistivity of graphene samples annealed at 800°C are similar to the metal Cr film, while the annealing temperatures of 350℃, 550℃and 650℃are not high enough to produce the graphene film with metallic character.

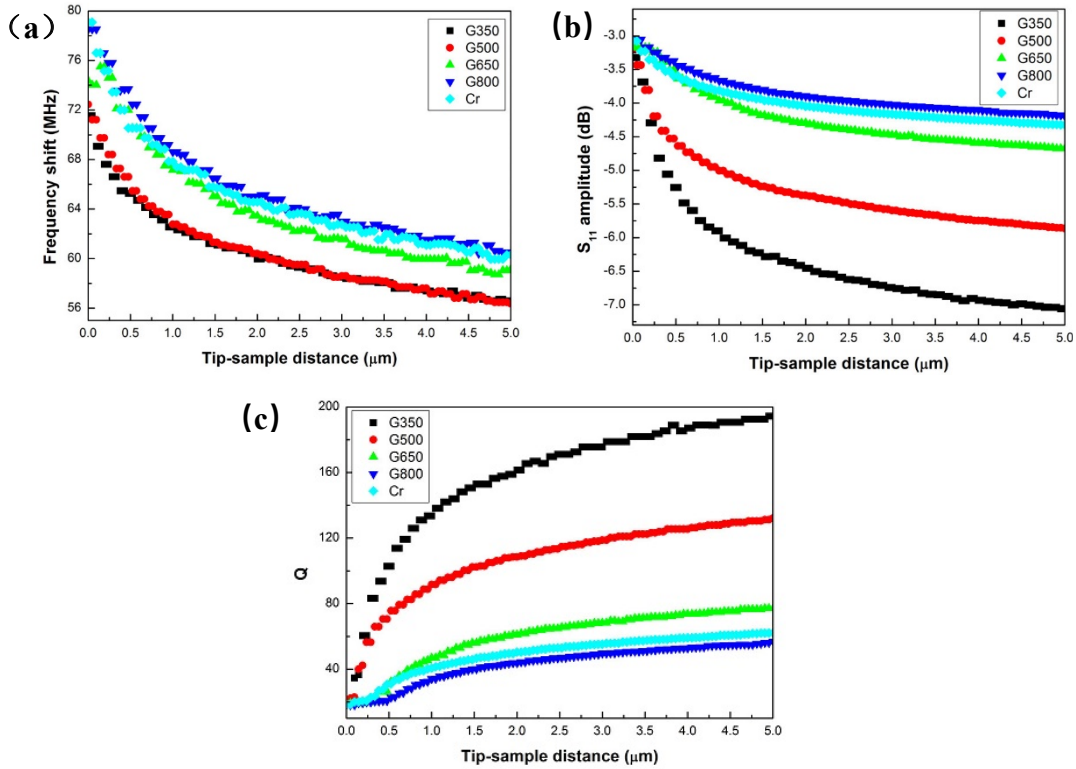

Fig. 2. (a)The frequency shift, (b) the S11 amplitude, and (c) the Q factor of graphene films at different annealing temperatures. Cr film was also measured as a reference.

CONCLUSION

The NSMM can measure the electromagnetic properties and distinguish the quality for the graphene films prepared after different annealing temperatures. The results and images obtained demonstrate that NSMM can be employed in thin film analysis for characterization of local electrical property of materials. This method can also apply for defect detection non-destructively which may help to improve the quality of graphene and improve the graphene manufacture and applications business.

REFERENCES

[1] K.P. Gaikovich,A.I. Smirnov and D.V. Yanin, et al., Near-field resonance microwave tomography and holography, *Radiophysics and Quantum Electronics.*, Vol. 60, No.9, Feb.2018.

[2] Z.Wu, W.Q.Sun and T.Feng, Imaging of soft material with carbon nanotube tip using near-fiel d scanning microwave microscopy, Ulamicroscopy., vol.148, pp.75-80, Jan.2015.

[3] Z.Wu, A.D.Souza and B.Peng, Measurement of high frequency conductivity of oxide-doped anti-ferromagnetic thin film with a near-field scanning microwave microscope, *AIP Advances*, vol.4, issue.4, Apr.2014.

[4] S. Stankovich, D.A. Dikin and R.D.Piner, et al., Synthesis of graphene-based nanosheets via chemical reduction of exfoliated graphite oxide, Carbon, vol.45, issue.no.7, pp.1558-1565.Jun.2007.

Fundamental Principles of Microwave Ovens: Requirements to Achieve Accurate Results and the Presentation Thereof

Robert F. Schiffmann
R.F. Schiffmann Associates, Inc, New York, USA

Keywords: Microwave ovens; test procedures; achieving statistical reproducibility; pre-warming ovens; non-uniformity problems; physical descriptions.

INTRODUCTION

When performing experiments, a fundamental requirement is to overcome as many, or preferably all, of the artifacts that are present in the experimental design and equipment. Experimenting with microwave ovens is especially difficult given the large number of such artifacts, including variability in performance between ovens, as well as such things in any single oven as the existence of "hot" and "cold" spots; in some cases the change in output power, resulting from heating of components; heating of the turntable and structure; and more. All of these can be considered to be artifacts of a particular oven and, in order to achieve statistically reliable results, need to be overcome or eliminated.

PART 1: PERFORMANCE REQUIREMENTS

Here are the steps suggested in order to take control of the artifacts and ensure the reliability of the results.

- IEC 60705 test
  - Should be run daily
  - First on a cold (not used for 8 or more hours)
  - Repeat on oven warmed for 20 minutes
  - If no change – daily tests may be run on cold oven
  - If change of 10% or more, tests must be rum on pre-warmed ovens
- Location of hot/cold spots
  - Especially important when testing small-size samples
  - All tests must be performed in exactly the same location

- Turntable warming
  - Glass turntables tend to become warm or hot during tests
  - If so, turntable should be cooled in room temperature water & thoroughly dried between tests.
  - If no turntable, then the floor must be cooled between tests.
- Temperature measurement
  - Temperature probe(s) must be located in exactly the same position for each test
  - May need to glue or otherwise fasten probe(s) to sample holder between tests.
  - Interior of oven must be maintained at room temperature
- Time
  - Time between tests must be rigidly measured and maintained
- Temperature
  - Sample temperature must be controlled so all samples start at the same temperature
  - Interior of oven must be maintained at room temperature

PART 2: PUBLICATION REQUIREMENTS

The purpose of publishing experimental results is not simply to provide those results to a large audience, but also to give the audience an opportunity to confirm or refute those results, and so, an accurate description of the experimental equipment and procedure is required. It is not sufficient to simply give the name of the manufacturer of the microwave oven, the model number, and it's suppose it output power as provided by the manufacturer. Among the other data that should be provided are:

- a physical description of the oven,
- cavity dimensions,
- material from which the cavity is made,
- whether or not there is turntable or mode-stirrer;
- location of the launch,
- IEC 60705 data expressing actual output power,
- data indicating power output after 20 mintes of use, i.e. warmed oven
- Heating pattern in oven, i.e. hot/cold spots
- Location of samples

COMMENT:

None of the above is exhaustive, but should be considered merely a guideline to be adjusted for specific circumstances. But, at the least, all of these suggestions should be seriously considered when designing and performing microwave oven tests, and the publication thereof.

The Influence of Microwave Soil Treatment and Biochar Application on the Toxicity of Arsenic in Rice (*Oryza sativa* L.)

Humayun Kabir, Graham Brodie, Dorin Gupta and Alexis Pang

The University of Melbourne, Dookie, Australia

Keywords: Microwave, Soil heating, Arsenic toxicity, Remediation, Biochar, Rice yield

INTRODUCTION

Rice, which is the most widely grown staple food for more than half of the world's population (>3.5 billion), has a higher arsenic (As) accumulation capacity than other cereals. Arsenic is considered a class 1 carcinogen. A considerable amount of As (0.01 – 2.05 μg g^{-1}) has already been reported in rice throughout the world [1]. Remediation of this devastating toxic heavy metal is important and urgent for food quality and safety. Different remediation technologies, such as vitrification, electrokinetic treatment, soil flushing and solidification, ion exchange, ultrafiltration, phytoremediation etc. [2] to avoid As pollution, have already been introduced but none of these methods satisfies the full-scale remediation requirements due to the processes being ineffective, costly or taking too long with usage restricted to smaller-scale operations with lower efficiency [2]. Microwave (MW) assisted pyrolysis is currently being used for waste treatment [3]. Additionally, biochar (BC) created via pyrolysis process has been used effectively for adsorbing soil heavy metals. MW treatment of soil has also shown many beneficial effects on rice crop growth. Therefore, the application of MW soil treatment, along with the incorporation of BC, may be of interest for As remediation.

METHODOLOY

A three factorial, completely randomized block designed glasshouse pot experiment was conducted with four replicates of each treatment combination at the Dookie Campus (36°24′ S, 145°43′ E) of the University of Melbourne, Australia. The soil classified as clay, was collected from a crop paddock of the Dookie farm at a depth of 0 -15 cm. Unperforated plastic pots (27 cm diameter) were filled with 8.5kg soil. These pots were treated with five levels of As (0, 20, 40, 60 and 80 mg kg^{-1} soil) as aqueous solution and three level of BC (0, 31.08 g and 62.16 g/pot) prior to the application of three levels of MW energy (0, 127.06 and 254.12 kJ kg^{-1} soil). A 6 kW

MW chamber consisting of 6 magnetron (1 kW each), with the frequency of 2.45 GHz, was used for 0, 3 and 6 minutes to achieve soil temperatures of approximately 0, 60 and 90ºC respectively [4]. Biochar was prepared from saw dust using microwave assist pyrolysis process. Twelve seeds of the 'YRM 70' rice variety were sown in each pot in February 2018. Fertilizers were applied according to practies. Different growth parameters such as plant height, tiller number, leaf chlorophyll concent, plant vigor, and biomass yield were measured during the growing period and the final dry biomass and grain yield were measured at crop maturity.

RESULTS

The results showed that, the MW soil treatment had a significantly beneficial effect on plant height, leaf chlorophyll content (SPAD value), tiller number/plant, and grain yield/pot, even at the higher rate (80 mg kg^{-1}) of As application (Figure 1). Six minute MW (MW-2) treatment showed significant increase in plant growth and grain yield/pot compared to the MW 3 minutes (MW-1) and control treatment. Whereas, the single effect of BC-1 (31.08 g/pot) on the plant growth and grain yield/pot, was better than the BC-2 (62.16 g/pot) at lower As levels (20 and 40 mg kg^{-1} soil), but there was no significant effect of BC treatments at higher As levels (60 and 80 mg kg^{-1} soil). However, in terms of combined effect, the highest grain yield was observed in MW-2 and BC-1 treatmentat 20 mg kg^{-1} soil As,whereas, 17.85% increased grain yield was recorded in combination of BC-2 and MW-2 treatment.

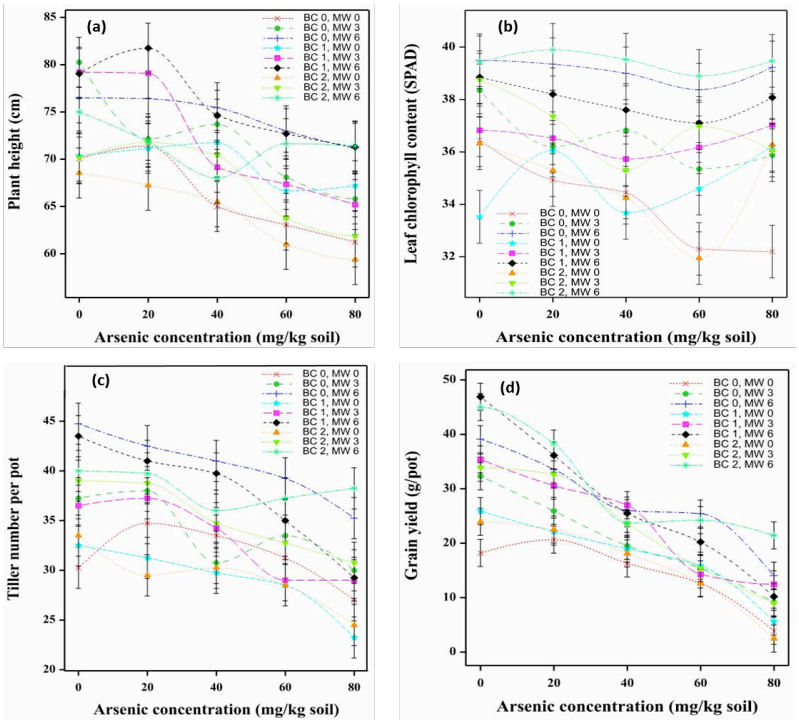

Figure 1. Effect of Microwave soil treatment and Biochar application in As contaminated soil on rice crop (a) plant height at maximum tillering, (b) leaf chlorophyll content as SPAD value, (c) tiller number at maximum tillering/pot, and (d) grain yield/pot

whereas, single MW-2 and combination with BC-2 reveal better at higher As levels. Furthermore, at highest As level, yield reduction was 78.57% compare to control

DISCUSSION

The overall results from the experiment indicates that, the microwave (MW) soil treatment, at a frequency of 2.45 GHz, had a significantly beneficial effect on rice plants' growth and grain yield, even at higher rates of arsenic (As) application. The possible reason for higher plant growth and grain yield is due to increased soil fertility based on MW treatment led more nutrients and organic carbon release from dead microorganisms (4). This could futher be explained through availability of higher amounts of substrate in the soil and ultimately enhanced microbial activity for better utilisation of nutrients [5]. Furthermore, MW soil irradiation enhanced the soil organic matter humification, increasing the macromolecular organic substances with higher numbers of functional groups and synthesis of organometallic and coordination compounds [6], which possibly reduced the bioavailability of As. BC is a carbon rich material, which has potential to adsorb As because of its high microporosity, surface area and surface functional groups, created at the time of high temperature pyrolysis process. Therefore, the combined effect of MW and BC application showed significant As adsorption in the soil and reduced the As toxicity in rice plant.

CONCLUSION

Microwave (MW) soil treatment along with biochar (BC) application has the potential to reduce the arsenic (As) toxicity in rice plant. For better understanding and explanation, further validation experiments, soil humification after MW treatment and As adsorption capacity of BC used in this experiment is needed.

REFERENCES

1. Williams, P., et al., *Variation in arsenic speciation and concentration in paddy rice related to dietary exposure.* Environmental Science & Technology, 2005. **39**(15): p. 5531-5540.
2. Lim, K., M. Shukor, and H. Wasoh, *Physical, chemical, and biological methods for the removal of arsenic compounds.* BioMed research international, 2014. **2014**.
3. Dauerman, L., et al. *Microwave treatment of hazardous wastes: feasibility studies*. in *Microwave Conference, 1992. APMC 92. 1992 Asia-Pacific*. 1992. IEEE.
4. Brodie, G., *An assessment of microwave soil pasteurization for killing seeds and weeds.* Plant Protection Quarterly, 2007. **22**(4): p. 143.
5. Zhou, B.W., et al., *Effect of microwave irradiation on cellular disintegration of Gram positive and negative cells.* Applied Microbiology and Biotechnology, 2010. **87**(2): p. 765-770.
6. Kim, M.C. and H.S. Kim, *Artificial and enhanced humification of soil organic matter using microwave irradiation.* Environmental Science and Pollution Research, 2013. **20**(4): p. 2362-2371.

Dual-Frequency Microwave Oven

Hong Zhao, Xiaoyun Li and Wenjie Fu

School of Electronic Science and Engineering, University of Electronic Science and Technology of China, Chengdu, China

Keywords: Microwave oven; dual-frequency; 2450MHz; 915MHz

INTRODUCTION

Comparing with the traditional heating, the microwave heating is directly heated to the food itself and it does not require heat conduction. The microwave heating has the advantages of rapid heating, high efficiency, energy saving, and can maintain the original taste and nutrients of the food well due to short cooking time [1-3]. Nowadays, the microwave oven has become a very popular kitchen appliances around the world.

In microwave oven, the oven cavity acts a multi-mode microwave resonator, the microwave field is excited in the oven cavity. However, due to the boundary conditions and resonance characteristics, the microwave field is not uniform in the cavity. Thus, the food heating uniformity is still a terrible problem for microwave oven. Several methods have been proposed and adopted in microwave productions. One of them is adopting two 2450 MHz magnetrons, but when two magnetron operation simultaneously, they will disturb each other, even damage the magnetron. In this research, a dual-frequency microwave oven which adopts both 2450 MHz and 915 MHz is proposed and built up. Through adopting filter, the disturbance between two microwave generators are solved. Moreover, the different field distribution can be excited in microwave oven at different frequency, the electromagnetic simulations and initial experiment results show that this method is potential to improve the microwave heating uniformity.

METHODOLOY

The dual-frequency microwave oven is based on a flatbed microwave oven (Midea X7-321D, Guangdong, China), which cavity size is 430mm × 290mm × 275mm. The 2450 MHz microwave is input into cavity from magnetron by rectangle waveguide and flat antenna. A solid-state microwave generator (Wattsine WSPS-915-1000DF, Chengdu, China) is used to generate 915 MHz microwave, which maximum output power is 1000W. The 915 MHz microwave is input into cavity by coaxial cable and 'I' shape antenna. The 2450 MHz waveguide can be operated as a high-pass filter, and protect the magnetron disturbed by 915 MHz microwave energy. To protect 915 MHz microwave generator, a coaxial low-pass filter is designed and manufactured, which is assembled between the antenna and coaxial cable. To measure heating uniformity, humidity sensitive papers was used in experiments, which was kept at a moisture content of about 20% to 25%, adhered to the mica board, and supported by a PTFE tube bracket in the cavity. In this experiment, the humidity sensitive paper was heated by 2450MHz alone, 915MHz alone and

2450MHz+915MHz mixing heating. At different microwave frequencies and the same power, the experiment was carried out for the same time. The respective temperature distribution maps were recorded by thermal imager (FLUKE Ti32, USA), and compared with the field distribution maps.

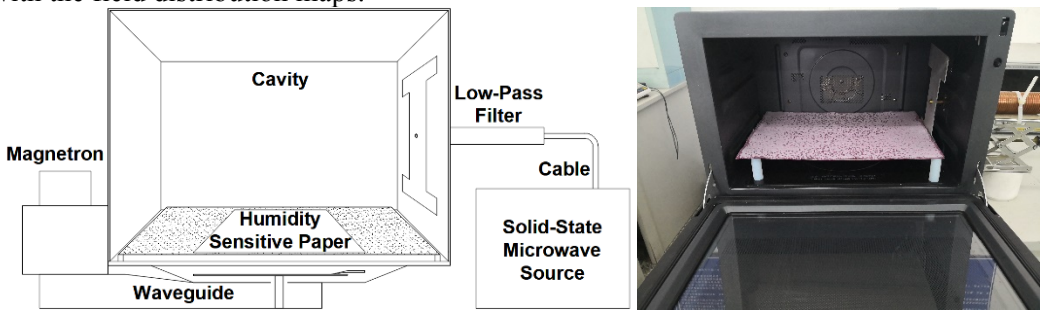

(a) (b)

Figure 1. (a) Schematic diagram and (b) photo of the dual frequency microwave oven experiments.

ELECTROMAGNETIC SIMULATIONS

The 3D electromagnetic (EM) simulation software HFSS is used to simulate the field distribution in microwave oven cavity. Figure 2(a) is the electric field distribution excited by 2450 MHz microwave, and Figure 2(b) is the electric field distribution excited by 950 MHz microwave. The results show that both 2450 MHz and 915 MHz microwaves can be inputted into Midea X7-321D cavity. The electric field distributions of 2450 MHz and 915 MHz are sufficiently different. By adjusting the power of 2450 MHz and 915 MHz microwave, the heating uniformity in microwave oven would be improved.

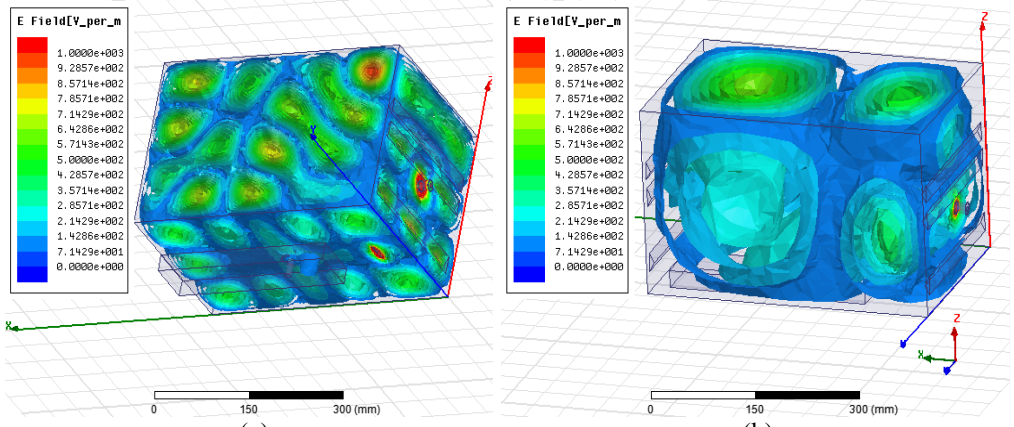

(a) (b)

Figure 2. Electric field distribution of (a) 2450 MHz and (b) 915 MHz microwave excited in microwave oven by HFSS simulation.

EXPERIMENTAL RESULTS

The experimental results are presented in Figure 3. Figure 3(a) is the thermal image of humidity sensitive paper heated 30 second at 300W, 2450 MHz microwave. Figure 3(b) is the thermal image of humidity sensitive paper heated 30 second at 300W, 915 MHz

microwave. Figure 3(c) is the thermal image of humidity sensitive paper heated 30 second at 300W, 2450 MHz mixed 300W, 915 MHz microwave.

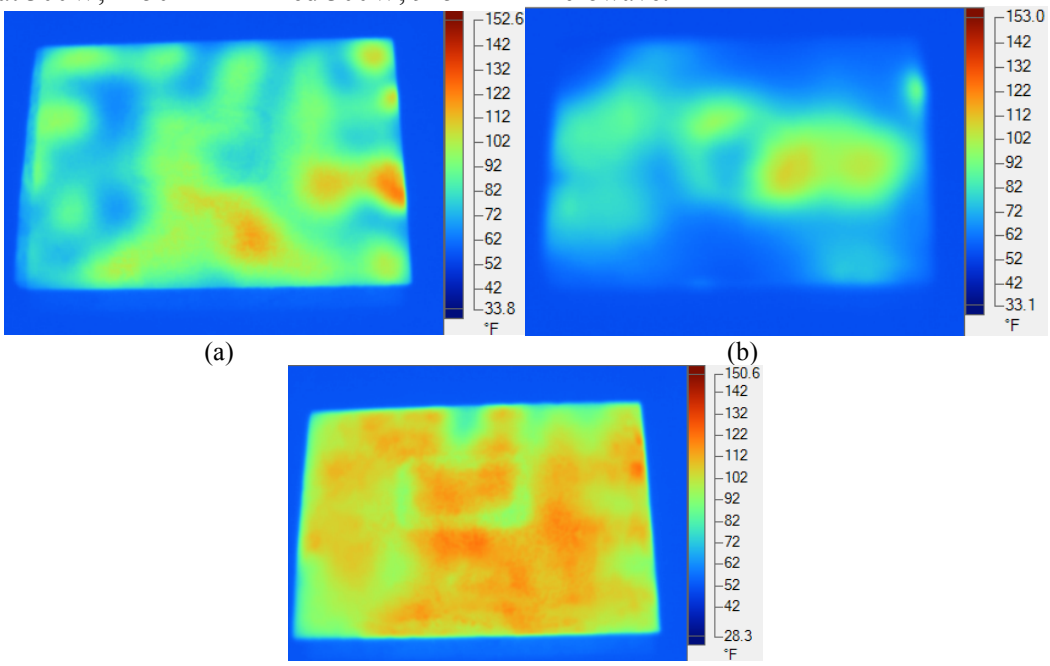

Figure 3. Thermal images of humidity sensitive paper after microwave heating at (a) 300W, 2450 MHz, (b) 300W, 915 MHz, and (c) 300W, 2450 MHz mixed 300W, 915 MHz.

DISCUSSION

The experiment results show that at different frequency, the excited field distribution is different in microwave oven. Through adjusting the powers of two different microwave generators, the heating uniformity can be improved.

CONCLUSION

When microwave oven cavity is large enough, both 915 MHz and 2450 MHz microwave filed can be excited in oven cavity. Because the frequencies of two microwave generators are different, the disturbance between two sources can be solved by filters. Thus, this method would be a practicable approach for microwave oven to improve heating uniformity.

REFERENCES

[1] Wang Chunxia, Zhou Guoyan. Influence of Microwave Heating on Quality Characteristics of Frozen Steamed Breads, J. Food Science, 2013,34(3):11-15
[2] Wang Shaolin. Microwave heating principle and its application, J. Physical, 1997(4).
[3] Guo Jianzhong, Hao Yushu. Application and development of microwave energy in food industry, J. Guangzhou Chemical, 2000,28(4)：40-41

Investigation of the Microwave Dielectric Properties of Various Zeolite Catalysts for Pyrolysis and Gasification Upconversion

Pranjali D. Muley[1]*, Cosmin Marculescu[2] and Dorin Boldor[1]
[1]Department of Biological & Agricultural Engineering, Louisiana State University and Agricultural Center, Baton Rouge, LA, USA 70803
[2]University Politechnica of Bucharest, Romania

Keywords: Dielectric properties, catalytic upconversion, microwave pyrolysis.

INTRODUCTION

Thermo-catalytic upgrading of pyrolysis and gasification products is crucial to obtain high value products from biomass conversion. Zeolite supported catalyst is the most abundantly used upgrading catalyst, both in petroleum and biofuel industry, due to its high thermal stability, carbon oxide affinity and large surface area [3]. Zeolite catalyst, impregnated with metals, can be effectively used to improve product quality for both pyrolysis and gasification products. To increase the process efficiency and obtain a uniform temperature distribution within the catalyst bed, microwave heating can be employed [2]. Knowledge of microwave dielectric properties of materials can aid in understanding the attenuation of microwave energy through the material during processing, thus, dielectric properties play a major role in microwave reactor design. This, the catalyst's dielectric properties were measured.

METHODOLOGY

The dielectric properties (dielectric constant ε' and dielectric loss ε") of various HZSM5-Zeolite powders, impregnated with various metals including (Fe2+. Fe3+. Cobalt, Molybdenum, and Nickle, and Clinoptilolite), were measured using a vector network analyzer and a transmission line method with a coaxial cell using EpsiMu dielectric kit. The data was collected in the frequency range of 154 MHz to 4.5 GHz. The EpsiMu dielectric kit consisted of a 6mm OD and 144 mm long coaxial cell. The powdered catalyst samples were thoroughly packed inside the cell (figure 1). All measurements were taken at room temperature. All measurements were taken in triplicates to insure repeatability. After collection of data, the dielectric properties data were processed in the associated EpsiMu software.

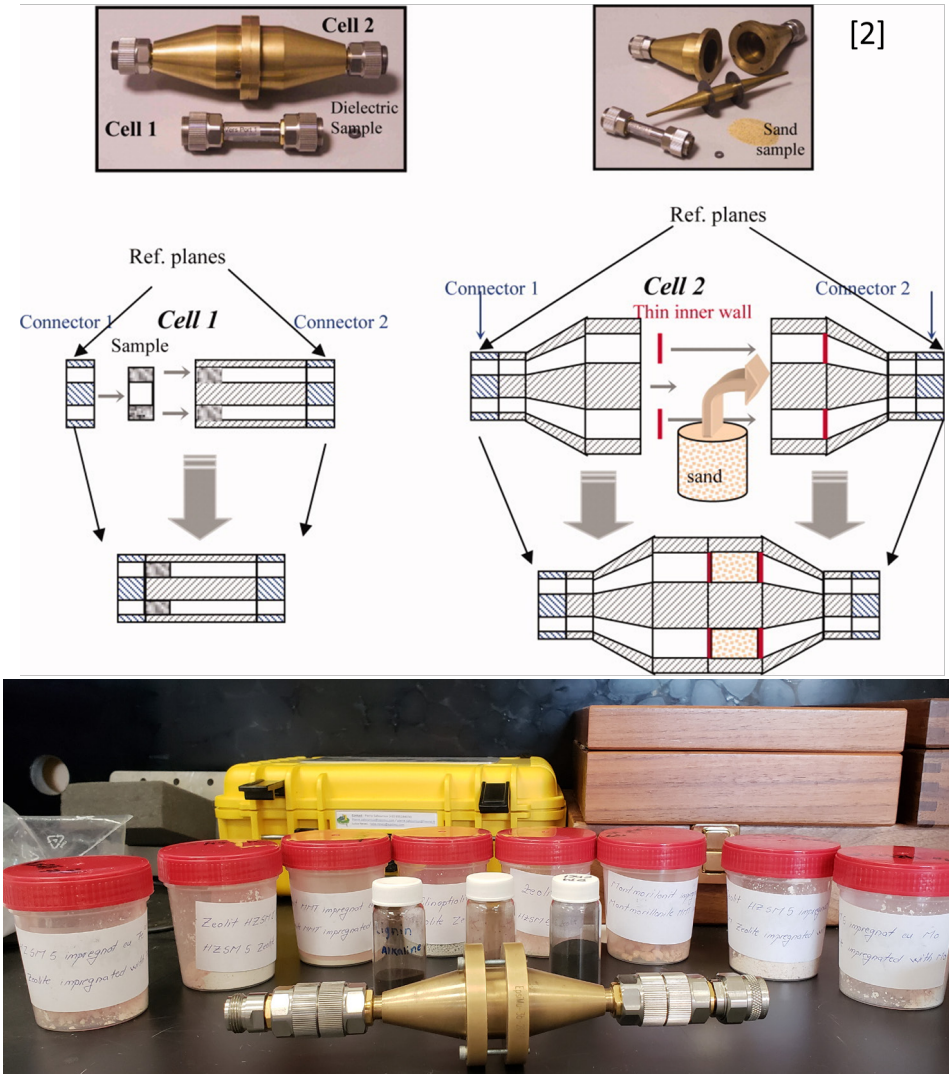

Figure 1. Schematic diagram for EpsiMu cell with sample

RESULTS

Results indicate that the microwave dielectric properties, in almost all cases, depend significantly on frequency. Both dielectric loss and dielectric constant decreased with frequency. All catalysts were good microwave absorbers, making them suitable for microwave-based biofuel upgrading (Figure 2). Dielectric properties were plotted at two allowed IMS frequencies; 915 MHz and 2450 MHz. The dielectric constant values for all catalysts ranged between 1.5 and 2.0 whereas the dielectric loss values ranged from 0.04 to 0.14. HZSM5-Mo had the highest dielectric loss value.

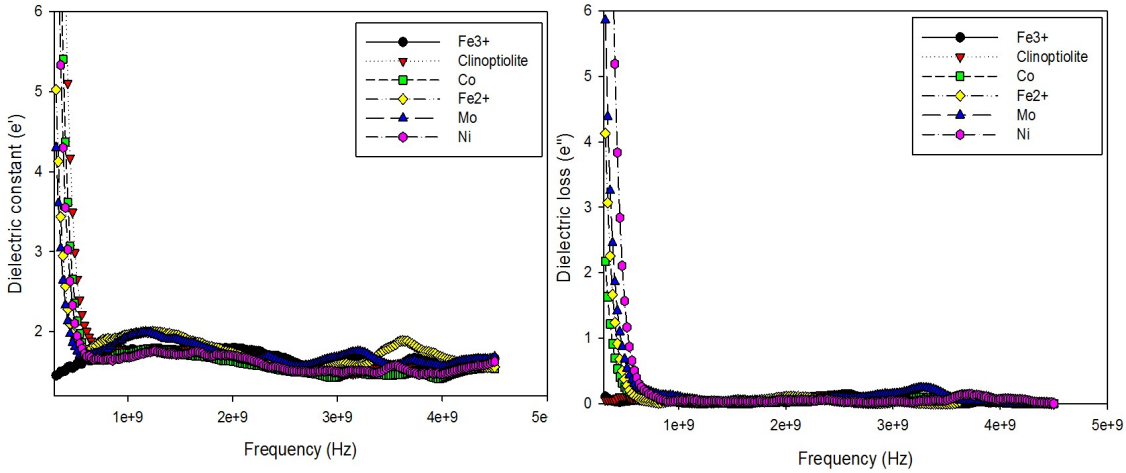

Figure 2. Dielectric constant and loss values of various metal impregnated zeolite catalysts

DISCUSSION

The dielectric properties of metal impregnated HZSM5 catalyst did not vary significantly with metal type. All catalysts showed a decrease in dielectric constant and loss values as the frequency increased. Moderate loss values for all catalyst types indicate that the material is lossy and can be readily heated in a microwave cavity. Based on the dielectric loss values, the material has higher loss values at 2450 MHz compared to 915 MHz frequency, hence they can be more effectively heated at 2450 MHz.

CONCLUSION

We successfully measured the dielectric properties of various metal impregnated zeolite catalysts using EpsiMu dielectric kit at different frequencies. The dielectric properties decreased with frequency. All catalyst types showed high microwave absorbency and can be heated using a microwave reactor for thermo-catalytic cracking of biomass pyrolysis vapors.

REFERENCES

[1] State, Razvan Nicolae, et al. "A Review of Catalysts Used in Microwave Assisted Pyrolysis and Gasification." *Bioresource Technology* (2019).

[2] Microwave and Optical Technology Letters, Volume: 52, Issue: 12, Pages: 2643-2648, First published: 22 September 2010, DOI: (10.1002/mop.25570)

[3] Jwa, E., et al. "Plasma-assisted catalytic methanation of CO and CO2 over Ni–zeolite catalysts." *Fuel processing technology* 108 (2013): 89-93.

Drying Kinetics and Quality Characteristics of Pre-osmosed Carrot Cubes during Hot Air-assisted Radio Frequency Heating

Chuting Gong[1], Yanyun Zhao[2], Yubin Miao[3], Hangjin Zhang[1], Jin Yue[1], Shunshan Jiao[1*]

[1]SJTU-OSU Innovation Center for Environmental Sustainability and Food Control, Key Laboratory of Urban Agriculture, Ministry of Agriculture, School of Agriculture and Biology, Shanghai Jiao Tong University, 800 Dongchuan Rd., Shanghai 200240, China

[2]Department of Food Science and Technology, 100 Wiegand Hall, Oregon State University, OR, USA

[3]School of Mechanical Engineering, Shanghai Jiao Tong University, 800 Dongchuan Rd., Shanghai 200240, China

Keywords: Radio frequency (RF), Drying, Quality, Carrots, Drying kinetics

INTRODUCTION

Fresh fruits and vegetables of high moisture content decay easily, and dehydration is a common method for long-term preservation. Conventional dehydration generally uses hot air which requires long drying time and high energy consumption. Radio frequency (RF) heating had been proposed and investigated as a final-stage dehydration method recently. Hot air-assisted radio frequency heating (HA-RF) was used as second-stage drying method for mangoes, following conventional steam blanching and hot-air pre-dewatering. Sample quality was better than hot-air drying and comparable to vacuum drying [1]. Besides, HA-RF was investigated for nut drying and showed great potential as a rapid, uniform and fine quality drying method [2-3]. This study investigated HA-RF as a final-stage drying method following RF dry-blanching and osmotic pre-dewatering. HA-RF drying protocol was determined, and associated quality changes (texture, vitamin C, color, etc.) were evaluated by comparing with conventional hot-air drying. Besides, the suitability of commonly used thin-layer drying models was evaluated for the drying process, and the logarithmic model was more suitable for HA-RF drying.

METHODOLOGY

RF heating unit (12 kW, 27.12 MHz) was used in this study. Carrot cubes (5.0× 5.0×5.0 mm^3, 500 g) were first RF dry-blanched and osmotically pre-dewatered, then placed in a polypropylene container, the sample thickness was 4.0 cm and treated by HA-

RF heating with electrode gap of 6.0-7.0 cm and 60℃ hot air. Temperature profile was recorded by fiber optic sensors and temperature uniformity index (TUI) was used for evaluating heating uniformity, Vitamin C content was determined by 2,6-dichloroindophenol method, sample color and texture were measured by chromascope and texture analyzer, respectively. Drying kinetics were mathematically described by ten thin-layer drying models. Data were analyzed by analysis of variance (ANOVA) and tested at significant level of 0.05.

RESULTS

Larger electrode gap showed lower TUI value, drying rate and water diffusivity. And the time required for HA-RF to achieve final moisture content less than 10.0% was 235- 260 min while it was 660 min for conventional hot-air drying. As for the quality, a_w reduced to less than 0.5 after both drying methods. Hardness and springiness of carrot cubes decreased after HA-RF and was relatively higher than conventional method. Higher redness which is preferred was obtained after HA-RF treated at 6.0-6.5 cm electrode gap. Vc content of samples after conventional method was significantly lower than those after HA-RF. Besides, the drying kinetics of pre-osmosed carrot cubes were described well by logarithmic model.

Table 1. HA-RF drying characteristics of pre-osmosed carrot cubes

Electrode gap	Drying time (min)	Moisture content(w.b.%)	TUI	Drying rate ($g/ kg^{-1} min^{-1}$)	D_{ef} ($\times 10^{-8} m^2/s$)
6.0 cm	235	9.89 ± 0.13^{a}	0.05 ± 0.01^{a}	1.32 ± 0.04^{a}	7.70 ± 0.13^{a}
6.5 cm	250	9.82 ± 0.12^{a}	0.03 ± 0.01^{b}	1.24 ± 0.02^{b}	7.39 ± 0.21^{a}
7.0 cm	260	9.66 ± 0.17^{a}	0.03 ± 0.01^{b}	1.20 ± 0.02^{c}	6.48 ± 0.13^{c}

Table 2. The water activity, vitamin C content, texture and color (redness) of pre-osmosed carrot cubes after conventional hot air drying and HA-RF drying.

Treatments	a_w	Hardness	Springiness	a* (redness)	Vc content (%)
Fresh	0.940 ± 0.04^{a}	48.75 ± 2.17^{a}	0.58 ± 0.04^{c}	29.56 ± 0.44^{b}	100.00 ± 0.00^{a}
Conventional method (70 □, 660 min)	0.496 ± 0.04^{b}	23.80 ± 2.11^{d}	0.51 ± 0.07^{d}	28.67 ± 0.44^{c}	27.13 ± 1.96^{c}
HA-RF (6.0 cm, 235 min)	0.400 ± 0.04^{d}	30.19 ± 2.15^{bc}	0.63 ± 0.05^{b}	30.62 ± 0.90^{b}	29.19 ± 1.96^{c}
HA-RF (6.5 cm, 250 min)	0.412 ± 0.03^{c}	31.02 ± 2.07^{b}	0.77 ± 0.06^{a}	34.03 ± 0.28^{a}	45.95 ± 4.68^{b}
HA-RF (7.0 cm, 260 min)	0.409 ± 0.04^{cd}	29.14 ± 1.13^{c}	0.79 ± 0.06^{a}	29.42 ± 0.18^{b}	46.44 ± 1.96^{b}

The superscripts in the same column with different alphabet are significantly different ($p<0.05$)

Table 3. Carrot cubes thin-layer drying model and parameters (R^2, RMSE and SEM values) during HA-RF drying

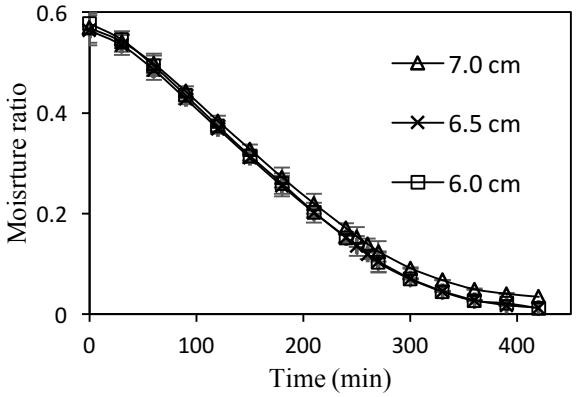

Fig.1. Moisture ratio of pre-osmosed carrot cubes during HA-RF heating at different electrode gaps (6.0-7.0 cm).

DISCUSSION

The results indicated that electrode gap of 6.5 cm provided fine heating uniformity, acceptable drying rate and water diffusivity. Owing to rapid and volumetric heating characteristics of RF heating, pre-osmosed carrot cubes after HA-RF drying had expected redness, higher hardness and Vc retention. And drying time was reduced by 50% when comparing with conventional method. Besides, a constant-rate drying period was the main stage of HA-RF treatment and a logarithmic model was more suitable for HA-RF drying.

CONCLUSION

This study demonstrated that HA-RF is a rapid and efficient heating method. And it showed great potential in providing a uniform and high-quality final-stage drying method for pre-osmosed carrot cubes.

REFERENCES

[1] Zhang, H., Gong, C., Wang, X., Liao, M., Yue, J. & Jiao, S. (2019). Application of hot air-assisted radio frequency as second stage drying method for mango slices. *Journal of Food Process Engineering*, DOI: 10.1111/jfpe.12974.

[2] Wang, Y., Zhang, L., Johnson, J., Gao, M., Tang, J., Powers, J. & Wang, S. (2014). Developing hot air-assisted radio frequency drying for in-shell macadamia nuts. *Food and Bioprocess Technology*, 7(1), 278-288.

[3] Jiao, S., Zhu, D., Deng, Y., & Zhao, Y. (2016). Effects of hot air-assisted radio frequency heating on quality and shelf-life of roasted peanuts. *Food and Bioprocess Technology, 9(2)*, 308–319.

Computational Procedure for Quantitative Characterization of Uniformity of High Frequency Heating

Petra Kumi and Vadim V. Yakovlev

Center for Industrial Mathematics and Statistics, Department of Mathematical Sciences, Worcester Polytechnic Institute, Worcester, MA, USA

Keywords: Dissipated power, FDTD, heating patterns, temperature, uniformity metrics.

INTRODUCTION

For many years, heating uniformity has been a prevalent topic in research on the effects of electromagnetic (EM) thermal processing. With the appearance of special means for visualization of heating patterns such as IR cameras capturing distribution of heat on the surface, or modeling tools capable of simulating 3D fields inside the objects, the task of pattern characterization has become relevant. However, it is usually handled via visual inspection leading to a qualitative conclusion. Review of computations aiming to characterize the phenomenon in quantitative terms (see, e.g., [1]-[5]) do not suggest an existence of a commonly accepted metric for heat patterns induced by high frequency EM treatment.

In this paper, we propose an approach that allows one to numerically characterize the level of uniformity of high frequency heating by evaluating the distributions of dissipated power and temperature. We report on the development of a computational tool, which (*i*) visualizes 2D or 3D matrices representing the patterns, (*ii*) analyzes their structures using a special standard-deviation-based metrics, and (*iii*) identifies the heat distribution characterized by the best uniformity.

METHODOLOGY

The developed computational procedure quantifies uniformity of high frequency EM heating by processing the patterns (matrices) produced by numerical simulation of the scenario in question; to this end, we employ the Finite Difference Time Domain (FDTD) solver *QuickWave* [6]. EM computation outputs distributions of dissipated power P_d, whereas the coupled EM-thermal simulation results in fields of temperature T.

The metric of uniformity of dissipated power is introduced, following [1]-[5], as

$$\lambda_P = \frac{\sigma}{\mu}, \tag{1}$$

where σ is standard deviation of P_d data points from the average value and μ is the mean of P_d. Computational experiments with 2D matrices show that lower λ_P values correspond to better uniformity, and multiple smaller "peaks" in the pattern/matrix seem to have a bigger effect in increasing λ_P than a single high peak.

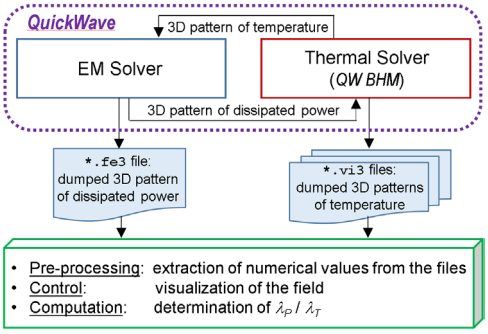

Figure 1. Operations of the computational procedure and its association with *QuickWave*.

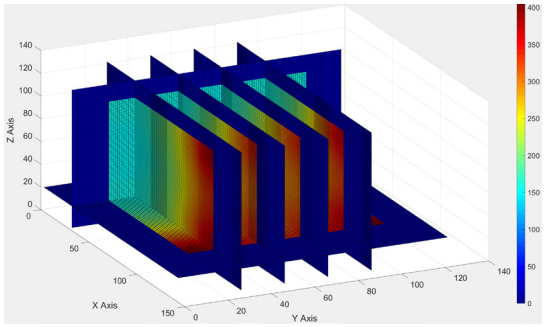

Figure 2. Visualization of a temperature pattern in a rectangular sample of a ceramic material at a particular time of the heating process.

In an iterative simulation of the EM-thermal coupled phenomenon, the EM process happening on a nanosecond scale is assumed to occur instantly, whereas heat diffusion is considered as taking place on the scale of real time (seconds). Temperature field is computed after each iteration, and a series of temperature patterns represents evolution of temperature distribution in the course of thermal processing. Hence n temperature patterns should be used to characterize the process. Accordingly, we define the metric of temperature uniformity in the microwave heating process as:

$$\lambda_T = \frac{\sum_{i=1}^{n} \frac{\sigma_i}{\mu_i}}{n}, \tag{2}$$

where σ_i and μ_i represent, respectively, standard deviations and the means of temperature data points after every ith heating time step; all heating time steps are assumed to be equal.

The procedure is implemented in *MATLAB*; it extracts the required data from `*.fe3` and `*.vi3` files (containing P_d and T fields, respectively) dumped from *QuickWave*, visualizes (to better control the process) the patterns in 2D or 3D, and calculates $\lambda_{P,T}$. The flow-chart in Figure 1 provides some details on functionality of the developed computational tool. Downloaded numerical data can be visualized using various means of the *MATLAB* graphics system. One example of possible 3D visualization of a temperature pattern is shown in Figure 2.

RESULTS AND DISCUSSION

The procedure was tested with several computational projects involving EM and coupled (EM-thermal) simulations. In this summary, we report its use in virtual experimentation with microwave heating of a SiC fabric as a part of microwave-assisted chemical vapor infiltration. A coupled model of the process carried out in SAIREM Labotron HTE M30KB CL PRO system uses temperature-dependent EM and thermal material parameters of a stacked SiC plies and simulates evolution of the temperature field induced at resonant and non-resonant frequencies.

Figure 3 shows how two typical heating processes in the system evolve. When the processed SiC disk is heated at a resonant frequency, thermal runaway quickly develops: after reaching 636 ºC for the first 19 s, maximum temperature increases by 420ºC for the

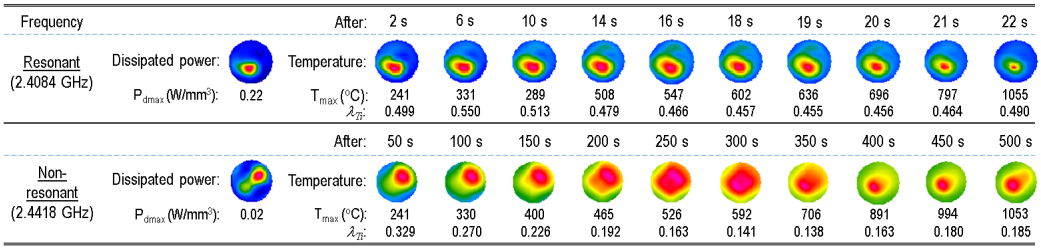

Figure 3. Non-normalized temperature patterns on the top of a 55×8 mm disk of stacked SiC fabric plies heated in SAIREM Labotron (power 1.1 kW); patterns at resonant and non-resonant frequencies are computed with 1 and 5 s heating time steps, respectively. Individual metrics (λ_{Ti}) and maximum temperature (T_{max}) are shown along with corresponding patterns of dissipated power.

last 3 s. The process is quick; high values of λ_T (0.51) and λ_{Ti} (in Figure 3) reflect significant non-uniformity of the heating process. In contrast, when heating at a non-resonant frequency, due to low energy coupling, the heating process is much slower (1053°C is now reached for 500 s instead of 22 s), and the metric of uniformity is lower (λ_T = 0.21) going to lowest values in the second half of the process due to the effect of thermal conductivity.

CONCLUSION

Two metrics for quantitative characterization of uniformity of heating of materials by high frequency EM waves have been introduced. The developed computational procedure dealing with simulated data on dissipated power and temperature distributions quantitatively characterizes the levels of uniformity of those patterns. In the computational study of high temperature microwave processing of SiC fabric plies, the procedure was been used to track and analyze evolution of temperature field and proved to be a helpful CAD tool. It can be also easily adapted to work with data from IR cameras.

ACKNOWLEDGMENT

The work was supported by the AFRL (via Leidos, Inc.) (Grant No P010200226) and the 2018 WPI Summer Undergraduate Research Fellowship (SURF).

REFERENCES

[1] S.J. Wang, K. Luechapattanaporn, and J. Tang, Experimental methods for evaluating heating uniformity in radio frequency systems, *Biosystems Eng. J.,* vol. 100, pp. 58-65, 2008.

[2] L. Pan, S. Jiao, L. Gautz, K. Tu, and S. Wang, Coffee bean heating uniformity and quality as influenced by radio frequency treatments for postharvest disinfectations, *Amer. Soc. of Agricult. & Bio Eng.,* vol. 55, pp. 2293-2300, 2012.

[3] S. Ozturk, F. Kong, R.K. Singh, J.D. Kuzy, and C. Li, Radio frequency heating of corn flour: heating rate and uniformity, *Innovative Food Science & Emerging Technologies,* vol. 44, pp. 191-201, 2017.

[4] H. Zhu, J. He, T. Hong, Q. Yang, Y. Wu, Y. Yang, and K. Huang, A rotary radiation structure for microwave heating uniformity improvement, *Applied Thermal Engng*, vol. 141, pp. 648-658, 2018.

[5] E.M. Moon and V.V. Yakovlev, Computer-aided design of a dielectric insert supporting uniformity of fast microwave heating, *COMPEL*, DOI 10.1108/COMPEL-06-2017-0266, 2017.

[6] *QuickWave*, 1998-2019, QWED Sp. z o.o., www.qwed.com.pl.

Comparison of Thawing Performance of Cycled and Inverter Microwave Heating

Jiajia Chen, Nathaly Vargas

Department of Food Science, University of Tennessee-Knoxville, Knoxville, TN, USA
Keywords: microwave heating, cycled, inverter, modeling, heating uniformity.

INTRODUCTION

Traditional microwave ovens use cycled power supply to control the power level, in which magnetron delivers full power for a period of time followed by no power for the rest of the cycle. On the other hand, inverter power supply employs a constant lower power level with magnetron always on. The inverter heating, a relatively new approach in microwave, was purposely developed to improve the heating uniformity and efficiency, as reported from Panasonic [1]. Theoretically, cycled heating and inverter heating should deliver similar time-averaged power in the time scale of one cycle. Chen et al. [2] evaluated the thawing performance differences (temperature, heating uniformity, and color change) between cycled and inverter heating using multiphysics based computer simulation models. The results showed that there was no significant difference between the two heating approaches on the thawing performance, which is opposite to the statement from the companies using the inverter technology, such as Panasonic. In Chen's research, the conclusion was made from a specific condition: a tylose cube (50 mm) was used as a model food to be heated in the oven for about 2 minutes without rotation. This condition was different from the typical scenario of using a microwave oven to thaw a real product, in terms of the product shape, size and rotation. Therefore, the thawing performance comparison of cycled and inverter microwave heating should be evaluated comprehensively at conditions that are close to real-life heating process.

METHODOLOGY

Multiphysics models based on finite element method were used to compare the thawing performance between the cycled and inverter microwave heating. In the cycled heating, the magnetron was set as on for 10 seconds with full power (1200 W) followed by off time of 10 seconds (0 W power), and repeated for 6 minutes; while in the inverter heating, the magnetron was set on for the whole 6 minutes heating process with 50% power (600 W), as shown in Figure. 1. A tray of frozen mashed potatoes of commercial size and shape (550 g, rectangular shape) was used as a model food and heated in both above-mentioned cases. The rotation of the mashed potato in the oven was also considered in the models.

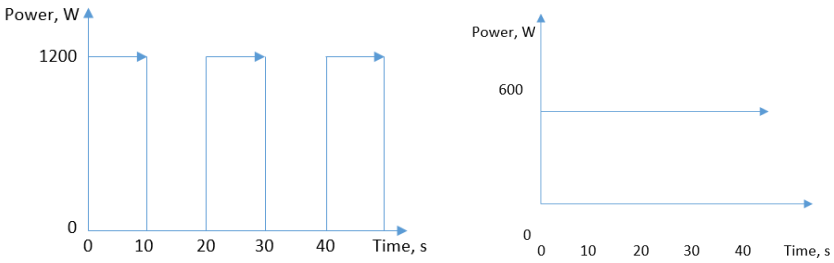

(a) Cycled heating approach (b) Inverter heating approach

Figure 1. Power output from cycled (a) and inverter (b) power supplies.

A geometric model was developed for a domestic microwave oven (Model no: NN-SN766S; Panasonic Corporation, Shanghai, China) rated at 1200W, as shown in Figure 2. The governing equations consisting of Maxwell's equations, heat transfer equation, convective heat transfer boundary condition, and perfect electric conductor boundary condition were set up in the models.

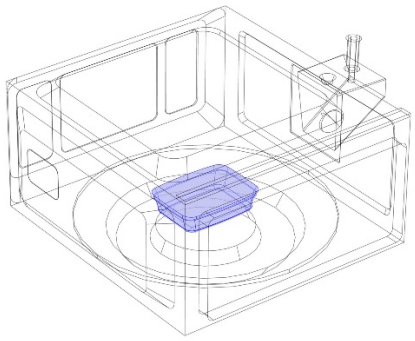

Figure. 2. Geometric model of microwave oven and food product.

RESULTS

After six minutes' thawing process, the (a) average temperature and (b) temperature standard deviation throughout the whole food product were calculated and shown in Figure 3. The average temperature of the inverter heating process increased continuously; while the cycled heating approach showed zig-zag temperature change, where the temperature increased when the power was on while slightly decreasing when the power was off. The temperature standard deviation of the inverter heating approach was maintained at a low constant level during the first 2 minutes of heating and then showed a liner increase. The temperature standard deviation of the cycled heating approach behaved the same way during the first 2 minutes and then showed zig-zag increase and decrease trend.

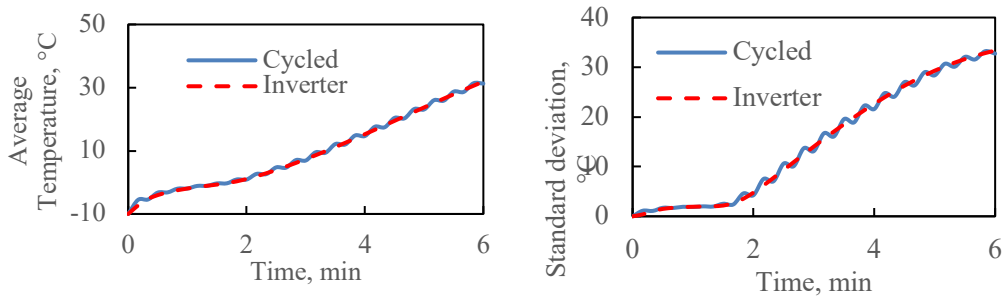

(a) Average temperature (b) Standard deviation

Figure 3. Comparison of thawing performances between cycled and inverter heating

DISCUSSION

The continuous increase of the average temperature using inverter heating approach was attributed to the continuous microwave power output provided by the inverter power supply in the oven. The zig-zag temperature change was attributed to the pulsed microwave power output delivered to the food product. When the power was off, the food product lost thermal energy to the ambient and caused a slight temperature drop, which was clearly observed at higher temperatures. The power on-off cycle also caused the zig-zag change of the temperature standard deviation. When the power was off, the temperature could equilibrate in the food product and decreased the standard deviation value.

However, the cycled and inverter heating approaches did not show significant difference on average temperature and standard deviation. This result is valid for this product shape and size. More food shapes and sizes will be evaluated to fully understand the difference between inverter and cycled microwave heating process. The comprehensive results will be discussed during the conference presentation.

CONCLUSION

For 550 g mashed potato sample of rectangular shape evaluated in this study, no considerable differences between the inverter and cycled heating approaches were found. More food product conditions will be evaluated and discussed.

REFERENCES

[1] Panasonic services company, 2009. Technical Guide – Microwave ovens with inverters. http://educypedia.karadimov.info/library/Inverter.pdf

[2] Chen, F., Warning, A. D., Datta, A. K., & Chen, X. (2016). Thawing in a microwave cavity: Comprehensive understanding of inverter and cycled heating. Journal of Food Engineering, 180, 87-100.

Study of the Heating Characteristic of a Cylindrical Microwave Heating Cavity

Yingying Chen[1,2] and Donglei Luan[1,2]

[1] Engineering Research Center of Food Thermal Processing Technology,
Shanghai Ocean University, Shanghai 201306, China
[2] College of Food Science and Technology,
Shanghai Ocean University, Shanghai 201306, China

Keywords: Microwave oven, cylindrical cavity, heat characteristic, temperature distribution

INTRODUCTION

Domestic microwave oven has been an essential appliance in the kitchens worldwide. It provides rapid and convenient heating for food stuffs. But the major drawback of microwave heating is non-uniform heating. The non-uniform heating within a domestic microwave oven was due to the uneven electric field distribution within the cavity. There are many factors that may affect that distribution, such as shape and size of the cavity, position of the microwave port, frequency [1], and presence of the food load. Several methods such as turntable [2] and mode stirrer are utilized to improve heating uniformity. However, the improvement level was limited by their theory: continuously changing the relative position of food and electric field.

Compared with traditional rectangular shape of domestic microwave oven, cylindrical microwave heating cavity was very few in practical application. Theoretically, cylindrical cavity could improve the heating stability and uniformity of food with different electric field mode from rectangular cavity because there are only two dimension parameters of a cylindrical cavity. The objective of this study was to investigate the heating characteristics of a cylindrical heating cavity that could provide another option for heating uniformity improvement of microwave oven.

METHODOLOGY

In this study, a cylindrical microwave heating cavity was studied to reveal its heating characteristics. A commercial domestic microwave oven was used to provide the microwave source. A metallic cylindrical cavity was put inside the microwave oven and covered the wall with port to form an cylindrical microwave heating cavity. Figure 1 shows the microwave oven and the cylindrical cavity. The door was closed to prevent microwave

(a) (b)

Figure 1. Microwave oven and the cylindrical cavity.

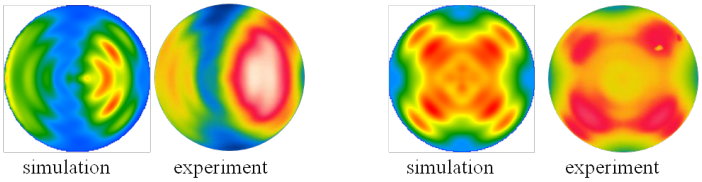

Figure 2. Heating pattern results of for simulation and experiment of food A: stationary; B: 90° rotation.

leakage. A computer simulation model was developed to assist the study. The model was built based on the commercial software of QuickWave. A finite difference time-domain (FDTD) was utilized to solve the coupled Maxwell and heat transfer equations. The frequency of the microwave oven and the oven with cylindrical cavity were measured by A 2650A spectrum analyzer and a matched M401 antenna (B&K Precision, Yorba Linda, CA, USA).

RESULTS

Results showed that the heating pattern obtained from simulation agreed well with the experimental results that derived from infrared thermal camera and chemical marker method (Figure 2). The position and size of microwave source port significantly affect the overall heating pattern. The presence of glass table and its height could affect the overall heating pattern. The effect of varying frequency had little influence on heaing pattern.

DISCUSSION

Varying frequencies had no effect on heating pattern which proved its heating stability. For exclusive microwave oven which requires high uniformity and stability, a cylindrical heating cavity was recommended.

CONCLUSION

Cylindrical microwave heating cavity provided a better option for microwave oven design with good stability and it have potential to obtain better heating uniformity.

REFERENCES

[1] D. Luan, J. Tang, P.D. Pedrow, F., Liu F, and Z. Tang, Analysis of electric field distribution within a microwave assisted thermal sterilization (MATS) system by computer simulation, *J. Food Eng*., vol. 188, pp. 87-97, 2016.

[2] S. Geedipalli, V. Rakesh, A. Datta, Modeling the heating uniformity contributed by a rotating turntable in microwave ovens, *J. Food Eng*., vol. 82, no 3, pp. 359-368, 2007.

CW Magnetron Based Mode Control using Machine Controllable Perturbations

Gregory J. Durnan[1]

[1]Kent State University, Kent, OH, USA

Keywords: Perturbation Methods, Wideband Log Periodic Antennas, Machine Control.

INTRODUCTION

For the last decade makers of LDMOS and more latterly GaN transistor devices have attempted to replace the use of magnetrons in consumer ovens with solid state solutions. This typically has involved removing the magnetron and replacing it with a micro controlled frequency synthesizer with feedback mechanisms to monitor return loss and RF power levels. In order to use these devices successfully and ensure reliable measurement systems, circulators are generally necessary to keep them functioning at an efficient impedance matching point.

As one can imagine this adds considerable complexity to an existing system that is relatively simple in its present magnetron form. Of course, the payoff is that if done correctly mode monitoring and position control can be achieved so that the cooking quality can be improved [1]. Present magnetron systems have no such feature to allow profile-based cooking due to the perceived shortcomings of these low-cost devices. Quotations from typical component sources show that Magnetrons in the 700 Watt to 1200-Watt range typically can be obtained in quantity from US$1 to US$3. These are prices solid state transistors will not match in the foreseeable future. As such it merits looking at whether it is possible to achieve improved results from these low-cost magnetron devices.

METHODOLOGY

There are two initial problems that appear to affect the controllability of Magnetrons in low cost cooking solutions. The first is the frequency stability of the output of a Magnetron. What is found and presented in this paper is that much can be done to improve this situation simply by operating a Full wave rectification power system. The poor quality of the current half wave voltage doubling system exacerbates the poor frequency spectrum of the Magnetron output leading to a somewhat broad spectrum from 2400MHz to 2480MHz, and apparently no control (Figure 1). Solidifying the frequency output via a filtered and stabilized supply was found to provide a stable frequency source [2]. The filtered and stabilized supply added an extra 3 high voltage capacitors and diodes

to the system to provide full wave rectification. As such, by using additional existing components the increase in cost was less than $10 at volume.

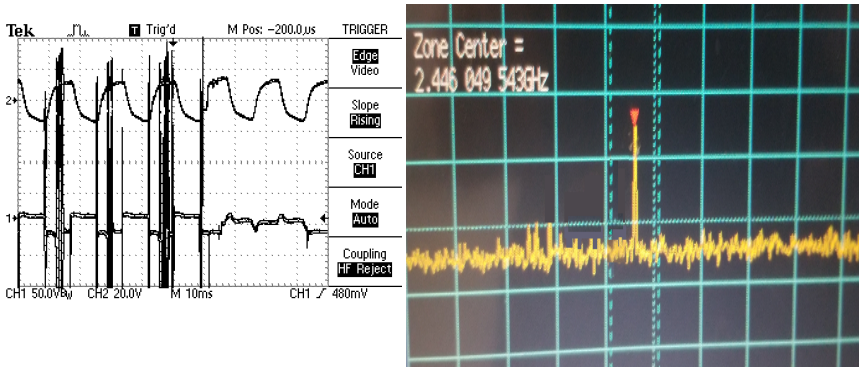

Figure 1. a). The current and voltage waveforms from the doubling circuit of a typical consumer microwave, leading to poor spectral performance of the Magnetron. b). The improved spectral performance after enhancing the magnetron supply via active feedback.

Load pulling was then used via a method of perturbations in order to load pull the frequency of the stabilized magnetron. This method of perturbation was implemented using a stepper motor controlled wideband circularly polarized log periodic device. By having a Raspberry PI based control system scan the frequency space no solid-state phase control or arrays are necessary. This simplifies potential systems considerably. We also achieve approximately a 40MHz frequency pull of the magnetron as we perturb the cavity space and hence the VSWR presented to the magnetron - this was repeated with a 500 mL water load as well as in the empty cavity. Control of the log periodic device allowed us to "pull the VSWR" under a number of loading conditions. As such we actively load pull the magnetron as seen in a typical Rieke diagram (Figure 2) [3].

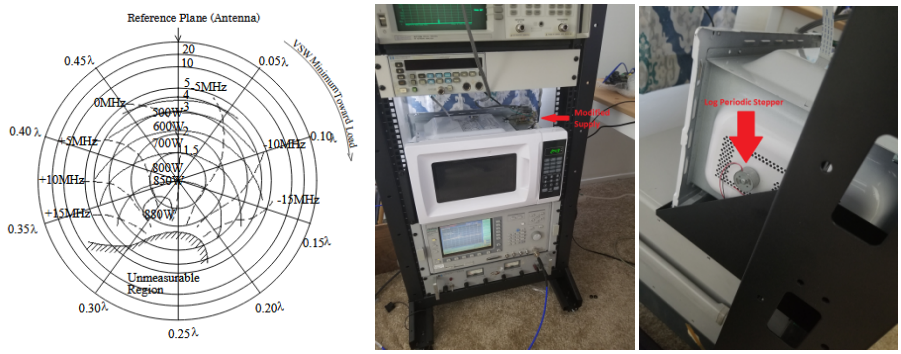

Figure2.a). The Rieke diagram showing frequency pull possibilities for a 2M229consumer magnetron. b). The system setup and c). the stepper motor for rotating the circular Log Periodic.

DISCUSSION

In practice we find that although limited by a reduced frequency pull, we still have access to sufficient intrinsic modes within the cavity to monitor and lock onto via IR

sensors. This had previously been done by the Author using Flir Cameras [1], however the NOIR has also provided satisfactory results - but it is still subject to ongoing refinement. In this case we have found that unlike previous systems, the Raspberry PI foundation has made available a common Camera module with the IR filter (the NoIR Camera) removed such that it provides sensitivity in this spectrum. As a result, we find we have a solution at a much-reduced cost over both FLIR and similar modules.

Figure3. a).The Raspberry PI NoIR Camera, at under $30 provides a lower cost alternative to a FLIR and is noted by its black silkscreen, and b). The camera in-situ atop the oven cavity during testing.

CONCLUSION

Using a controllable perturbation device (in the form of a machine rotatable log periodic structure) in conjunction with mode monitoring and improved power supply performance we are able to show that many of the shortcomings of a consumer grade microwave oven can be improved. We used the log periodic structure to provide a wideband, circularly polarized option for perturbation. Like all antenna's we were also able to mismatch it to provide the VSWR we required. In addition, by maintaining the cost structure via the reuse as far as possible and the minimal addition of expensive hardware necessary for solid state devices we are able to show that cost considerations can also be improved.

REFERENCES

[1] G. J. Durnan, Mode Fitting and Evenness Studies in Loaded Microwave Cavities, *Proc. 52nd IMPI Microwave Power Symp., Long Beach, CA, June 2018*.

[2] M. Neubauer, R.P. Johnson, and M. Popovic, Phase and Frequency Locked Magnetrons for SRF Sources. United States: N. p., 2014. Web. doi:10.2172/1156596.

[3] Toshiba Hokuto, Magnetrons for Microwave Ovens, Retrieved from http://www.hokuto.co.jp/eng/products/magnetron/pdf/brochure.pdf

Untraditional Thermal Convection in Liquid by Microwave Heating

PeiYang Zhao, WeiWei Gan, Jing Zhao, Xuan Chai, BaoQing Zeng and Zhe Wu

University of Electronic Science and Technology of China, Chengdu, China

Keywords: Microwave heating; Convection; liquid; temperature distribution.

INTRODUCTION

When heating water, milk, etc. in a microwave oven, it is often found that the temperature of the top of the liquid in the cup is higher than the temperature at the bottom. However, this phenomenon does not occur in the conventional heating method. Continuous flow microwave heating was successfully simulated by using a COMSOL Multiphysics software package by iterative coupling of high-frequency electromagnetism, fluid flow and heat transfer for Newtonian as well as non-Newtonian fluids[1]. In this paper, the reasons for the above phenomena are explained through multi-physical field coupling simulation, and the accuracy of simulation results is verified through experiments to some extent.

SIMULATION AND EXPERIMENTAL

Firstly, the physical model is simplified in the multi-physical field simulation software. The electric field distribution in the microwave oven and the temperature distribution of water in the glass cup are simulated and calculated. Then the experiment was carried out. The microwave power was set to 1000w, and the temperature distribution of water was detected by infrared thermal imager after 90 seconds of heating. Then use a more accurate probe thermometer to measure the temperature at the top and bottom of the water.

$$\nabla \times \mu_r^{-1}\left(\nabla \times \vec{E}\right) - k^2(\varepsilon' - j\varepsilon'')\vec{E} = 0 \qquad (1)$$ Maxwell equation

$$\rho C_p \frac{\partial T}{\partial t} = k\nabla^2 T + P_v \qquad (2)$$ Heat equation

$$\rho \frac{\mathrm{d}v}{dt} = -\nabla p + p\vec{F} + \mu\Delta v \qquad (3)$$ Navier-Stokes equation

RESULTS

The stratification of water temperature can be clearly seen from the photographs taken by the infrared thermal imager. With a more accurate probe thermometer, the temperature at the top of water is 64.7℃, the bottom of water is 54.4℃, and the temperature difference is 10.3 ℃.

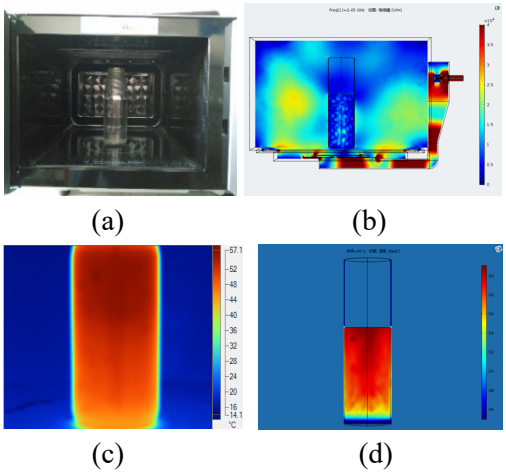

Figer1. Microwave oven and water for heating in a glass cup(a); Electric field distribution in microwave oven(b); Water temperature distribution images by infrared thermal imager (c); Temperature distribution in coupled simulation of multi-physical field of water(d)

DISCUSSION

It can be seen from the electric field distribution in the microwave oven that the heat source is simultaneously distributed in various regions of the water. Therefore, the top and bottom of the water are simultaneously heated. The water at the bottom is heated and its density becomes smaller and flows upward, while the water at the top is also heated.

CONCLUSION

The heat source of traditional heating is at the bottom of water. For example, when water is heated on a stove, hot water from the bottom of the pan rises, displacing the colder denser liquid, which falls. After heating has stopped, mixing and conduction from this natural convection eventually result in a nearly homogeneous density, and even temperature[2].When water and other liquids are heated in a microwave oven, since the bottom and the top of the water are simultaneously heated, The temperature of the bottom water rises, the density becomes smaller, and the flow upwards, and the top water is still in the state of being heated. There is only one-way convection in water. Untraditional heat convection causes the phenomenon that the water temperature at the top is higher than that at the bottom.

REFERENCES

[1] Salvi D, Boldor D, Aita G M, et al. COMSOL Multiphysics model for continuous flow microwave heating of liquids[J]. Journal of Food Engineering, 2011, 104(3):422-429.
[2] You D . An Overview of Heat Transfer Correlations for Supercritical CO2 Cooling in Macro-channels[J]. 2017.

Deactivation of Polyphenol Oxidase Enzymes in Apple Pomace at Point of Source

M.A. Calvo, F. Arrutia and E. Binner

Faculty of Engineering, University of Nottingham, Nottingham, UK

Keywords: Microwave-assisted extraction, apple pomace, waste management, browning.

INTRODUCTION

Apple pomace is the main processing by-product of juicing, where despite the optimization of industrial techniques, 4.2 Mt of apple pomace are produced yearly worldwide [1]. This waste stream could be suitable for human consumption as a dietary fiber. However, a major barrier to its upgrading is the rapid browning it undergoes after juicing. Browning occurs as a result of the oxidation of phenolic compounds present in the apple's tissue to quinones, which eventually polymerize into melanin due to the action of the enzyme polyphenol oxidase (PPO). Thermal treatments can inactivate PPO and halt the browning but damage the food quality. The fast and volumetric heating characteristic of microwaves can provide a flash treatment minimizing food quality alterations.

The aim of this project was to investigate whether PPO present in apple pomace could be deactivated using microwave energy, in order to delay browning for as long as possible. For that, a pilot-plant microwave-processing rig was developed and assessed.

METHODOLOGY

Apples were manually sliced and mashed. Vacuum filtering separated the pomace from the juice. The former was diluted 1:2 (w/v) with tap water prior to heating treatments. Small-scale heating trials were performed in a Miniflow 200 W generator working at 2450 MHz, while large-scale experiments were performed using a pilot-plant continuous rig built and commissioned for the purpose (Figure 1). The treated pomace was collected into a jacketed tank and promptly cooled down to room temperature. Afterwards, the cooled pomace was vacuum filtered using a cheesecloth for dewatering.

The browning of the treated and untreated pomace was monitored quantitatively, by measuring its CIELab colour parameters across time with a Lovibond LC 100 Spectrocolorimeter (Amesbury, UK).

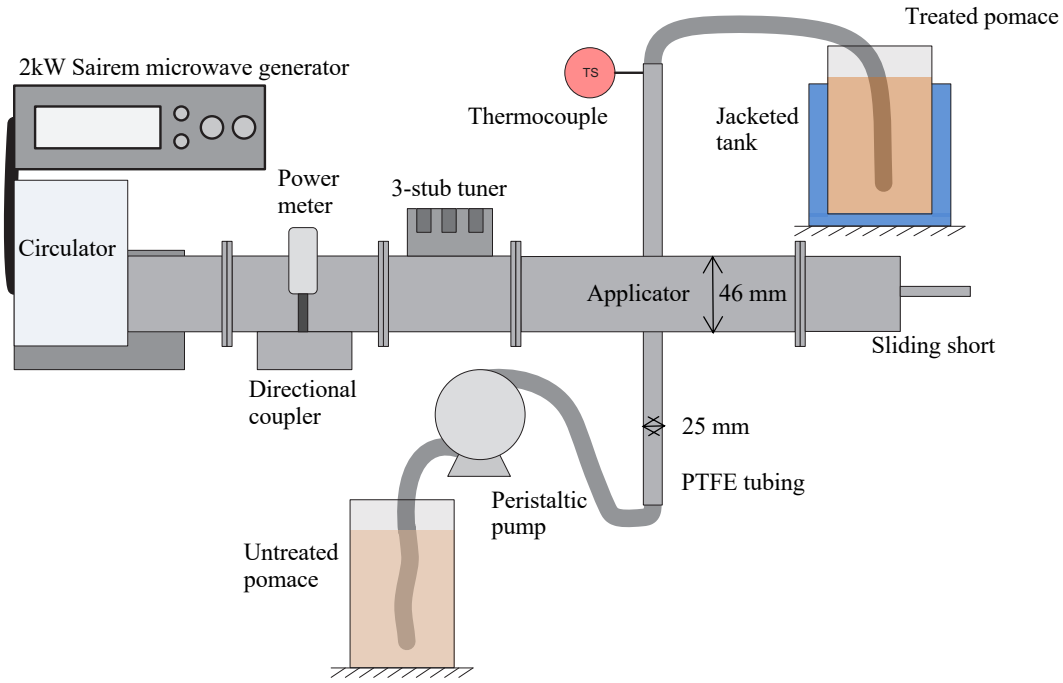

Figure 1. Schematic diagram of the pilot-plant scale continuous microwave-processing rig.

RESULTS

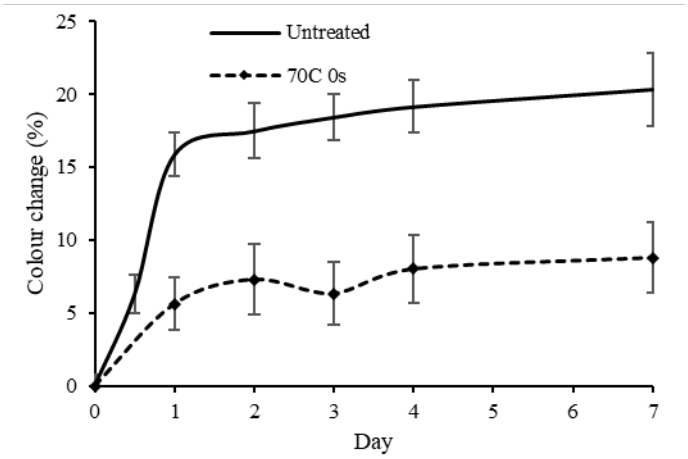

Figure 2. Average colour change of heated and raw apple pomace across time.

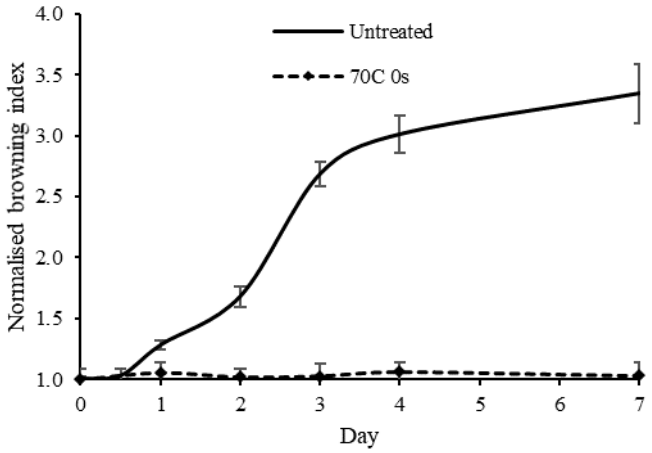

Figure 3. Normalised browning index of heated and raw apple pomace across time.

DISCUSSION

As clearly shown in Figure 2, the color change was halved when compared to the untreated sample. In the case of the browning index (Figure 3), the measured values were also stabilized and tended to cluster closer to browning levels of 1.1. Still, the error bars of both sets of data overlap each other.

CONCLUSION

A portable microwave system for the on-site continuous inactivation of PPO enzymes has been developed. Overall, flash treatments of <3 s at 70 ºC virtually halt the apple pomace browning for at least a week. In that time, untreated specimens browning increased more than threefold.

REFERENCES

[1] V. Oreopoulou and C. Tzia, *Utilization of by-products and treatment of waste in the food industry,* Springer, Boston, MA, 2007.